

**DEFORMATION ACROSS THE SAN ANDREAS FAULT
NEAR PARKFIELD, CALIFORNIA**

by
Brett Baker

A thesis submitted to the
Department of Geology and Geophysics and
the Graduate School of the University of Wyoming
in Partial Fulfillment of Requirements for the Degree of

MASTER OF SCIENCE
in
GEOLOGY

Laramie, Wyoming
April, 1993

TO THE OFFICE OF THE GRADUATE SCHOOL:

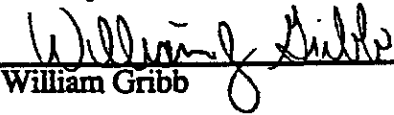
The members of the committee approve the thesis of Brett Baker
presented on April 15, 1993.



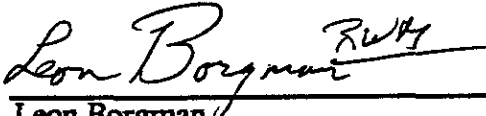
Ronald Marrs, Chairman



Charles Angevine

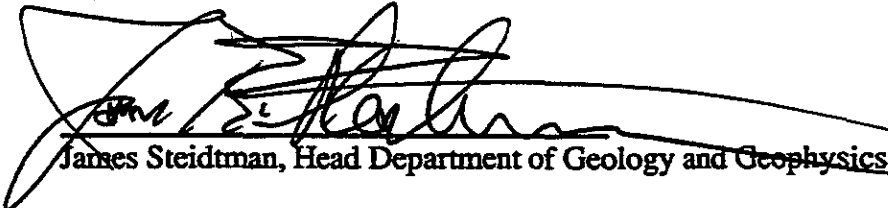


William Gribb



Leon Borgman

Approved:



James Steidtman, Head Department of Geology and Geophysics

Thomas G. Dunn, Dean of Graduate Studies and Research

Baker, Brett, Deformation Across the San Andreas Fault Near Parkfield, California,

M.S., Department of Geology and Geophysics, April, 1993.

Repeated surveys of 22 fault-crossing alinement arrays between 1983 and 1992 along the 40-km-long Parkfield segment of the San Andreas fault have determined deformation patterns, creep rates, and fault-zone widths. Deformation patterns fall naturally into two distinct classes. The Type I pattern occurs at 6 arrays and is defined by rigid-block motion outside of the fault zone with homogeneous right-lateral shear within the fault zone. The Type II pattern occurs at 4 arrays which exhibit motion in a left-lateral sense as one approaches the fault zone and homogeneous right-lateral shear across the fault zone. Type III pattern includes 7 arrays that do not fulfill the requirements of either Type I or Type II.

Type I deformation indicates that the earth moves as rigid blocks separated by a narrow zone of weak material that deforms by homogenous simple shear. Type II pattern suggests the alinement array was initially surveyed after a strain event and before the strain release, or that the array crosses a shallow asperity.

Creep rates (determined from alinement arrays) decrease along the Parkfield fault segment from a maximum of 15.2 mm/yr at the northwest end of the segment to <1 mm/yr in the southeast end of the segment in southern Cholame Valley. These rates are slightly higher than those recorded by creepmeters in that same area. At sites where the rates do not agree, the disagreement is probably due to non-tectonic movement of the alinement array monuments or creepmeter piers or by Type II deformation where the maximum offset is in the center of the array.

Fault zones vary from 10 meters to over 30 meters wide. The narrower fault zones tend to undergo Type I deformation, while the wider zones fall into deformation Types II and III.

DEDICATION

In memory of Edith Breniman, a saint, whose grace through life I could never hope to emulate, and Sandy Burford, a friend, whose drive, dedication, faith, strength and perseverance gave me perspective.

ACKNOWLEDGEMENTS

This study would never have been completed if it weren't for the people of Parkfield, who have made the many scientists that invade their homes welcome. From the USGS, I would like to thank Kate Breckenridge, Beth Brown, Sandy Burford, Robert Burford, Mark Harris, Ron Jenkins, and Scott Nelson for their assistance in the field and the office. Rich Liecchi kindly helped drill holes for the monuments. Jim Lienkaemper listened to my off-the-cuff ideas. Robert Simpson, is appreciated for his ever present smile and willingness to help even when he had no time. He kindly took time to edit the thesis and made many valuable suggestions. Robert and Trudy Wallace, I thank for their words of wisdom and friendship even though my dog left fleas throughout their home. My advisor Ron Marrs for his many editorial improvements of the thesis and encouragement along the way.

I especially thank James F. Wilmesher and Jon Galehouse. Jim's presence in the field turned tedious surveying tasks into enjoyable trips to the country, and made long days and difficult situations much more tolerable. Jon got me interested in both geology and neotectonics during my first semester of undergraduate school. He hired me as a research assistant in 1984, the year I completed my first alignment array survey. Jon also showed me how to use my elbows on the basketball court-a valuable skill.

TABLE OF CONTENTS

SECTION	PAGE
I Introduction	1
II General Geology	6
III Description of Alinement Arrays	9
IV Measurement Procedure	11
V Methods of Calculating Displacement.	15
VI Precision of Measurements	15
VII Site Characteristics.	19
VII Patterns of Deformation.	20
VII Deformation Mechanisms	31
VIII Seismicity	35
IX Comparison of Alinement Array and Creepmeter Creep Rates. .	36
X Nontectonic Displacement of Monuments	39
XI New Survey Techniques.	38
XII Conclusions	44
References Cited.	46
Appendix A: Site Descriptions, Maps and Data Plots.	50

LIST OF TABLES

	Page #
Table 1. Alinement Array Data for the Central San Andreas Fault.	5
Table 2. Comparison of True Angle and Deflection Values with Mean Values Obtained from Three Sets of Eccentric Centers	8
Table 3. Site Characteristics	19
Table 4. <i>F</i> and t-tests on Creep Rate Distributions between Deformation Patterns I, II, II in Figure 13.	27
Table 5. <i>F</i> and t-tests on Creep Rate and Fault Distributions in Boxes 1 and 2 of Figure 14.	29
Table 6. Alinement Array Creep Rates and Deformation Patterns	30

LIST OF FIGURES

	Page #
Figure 1. Shaded Relief Map of the Parkfield-Cholame Valley	3
Figure 2. Geologic Map of the Parkfield-Cholame Valley Area.	7
Figure 3. Map View of an Alinement Array	10
Figure 4. Cross Section of Typical Monument.	12
Figure 5. Sketch of the Deflection Target.	14
Figure 6. Test of Survey Repeatability	16
Figure 7. Biased Angle Measurements.	17
Figure 8. Deformation Patterns I through III	21
Figure 9. Spatial Distribution of Deformation Patterns	22
Figure 10. Example of Deformation Pattern I.	24
Figure 11. Example of Deformation Pattern II	25
Figure 12. Example of Deformation Pattern III.	26
Figure 13. Plot of Creep Rate vs Deformation Pattern Type	27
Figure 14. Comparison of Fault Width and Creep Rates.	28
Figure 15. Deformation Mechanisms	31
Figure 16. Possible Explanation for Type II Deformation	32
Figure 17. Location of Creeping and Locked Areas of the SAF.	34
Figure 18. Plot of Seismicity and Surface Creep Rates.	35
Figure 19. Block Diagrams of a Subsurface Monument.	39

LIST OF FIGURES (cont.)

Figure 20. New Monument and Target	41
Figure 21. Proposed Field Procedure.	42
Figure 22. XMM4 Site Description	53
Figure 23. XMM4 Site Map.	54
Figure 24. XMM4 Data Plots.	55
Figure 25. MDR4 Site Description.	56
Figure 26. MDR4 Site Map.	57
Figure 27. MDR4 Data Plots.	58
Figure 28. VAR4 Site Description.	59
Figure 29. VAR4 Site Map.	60
Figure 30. VAR4 Data Plots.	61
Figure 31. PKW4 Site Description.	62
Figure 32. PKW4 Site Map.	63
Figure 33. PKW4 Data Plots.	64
Figure 34. XPN4 Site Description.	65
Figure 35. PKN4 Site Description	66
Figure 36. XPN4 Site Map.	67
Figure 37. PKN4 Site Map.	68
Figure 38. PKN4 and XPN4 Data Plots.. . . .	69
Figure 39. PKF4 Site Description.	70
Figure 40. PKF4 Site Map.	71

LIST OF FIGURES (cont.)

Figure 41. PKF4 Data Plots	72
Figure 42. TAY4 Site Description	73
Figure 43. TAY4 Site Map	74
Figure 44. TAY4 Data Plots.....	75
Figure 45. RCW6 Site Description	76
Figure 46. RCW6 Site Map.	77
Figure 47. RCW6 Data Plots.	78
Figure 48. XDR5 Site Description	79
Figure 49. XDR5 Site Map	80
Figure 50. XDR5 Data Plots	81
Figure 51. HST4 Site Description.	82
Figure 52. HST4 Site Map	83
Figure 53. HST4 Data Plots	84
Figure 54. HSW4 Site Description	85
Figure 55. HSW4 Site Map.	86
Figure 56. HSW4 Data Plots.	87
Figure 57. WKR4 Site Description	88
Figure 58. WKR4 Site Map.	89
Figure 59. WKR4 Data Plot	90
Figure 60. KEN5 Site Description.....	91
Figure 61. KEN5 Site Map	92
Figure 62. KEN5 Data Plots	93
Figure 63. HAR4 Site Description	94

LIST OF FIGURES (cont.)

Figure 64. HAR4 Site Map	95
Figure 65. HAR4 Data Plots	96
Figure 66. CRR4 Site Description	97
Figure 67. CRR4 Site Map	98
Figure 68. CRR4 Data Plots	99
Figure 69. GHG4 Site Description	100
Figure 70. GHG4 Site Map	101
Figure 71. GHG4 Data Plot	102
Figure 72. PGH4 Site Description	103
Figure 73. PGH4 Site Map	104
Figure 74. PGH4 Data Plots	105
Figure 75. XWT4 Site Description	106
Figure 76. XWT4 Site Map	107
Figure 77. XWT4 Data Plots	108
Figure 78. H464 Site Description	109
Figure 79. H464 Site Map	110
Figure 80. H464 Data Plots	111
Figure 81. X464 Site Description	112
Figure 82. X464 Site Map	113
Figure 83. X464 Data Plots	114
Figure 84. PPP4 Site Description	115
Figure 85. PPP4 Site Map	116
Figure 86. PPP4 Data Plots	117

Introduction

The San Andreas transform fault system (SAF) is the main boundary between the North American and Pacific lithospheric plates. In central California, the long-term slip rate is $\approx 35 \text{ mm yr}^{-1}$ (Prescott, Lisowski and Savage, 1981; Sieh and Jahns, 1984). Plate motion models (Argus and Gordon, 1990; DeMets et al., 1990) indicate that the total Pacific-North America motion is $48 \pm 1 \text{ mm yr}^{-1}$ at 36°N in central California. The remaining 13 mm yr^{-1} of motion is dispersed across the area between the SAF and the eastern boundary of the Basin and Range Province. Evidence of this deformation can be found in folding and faulting throughout this region. In the central California area, about 65% of the relative movement between the two plates occurs as right-lateral strike slip motion on the SAF. This motion occurs as movement during earthquakes and as aseismic slip, which is also called fault creep (Wesson, 1988). Fault creep was first measured in the 1960's (in California) by Steinbrugge et al., (1960) and Tocher, (1960). There have been several cases in California in which the rate of fault creep changed noticeably just before local earthquakes (Burford, 1988; Simpson et al., 1988; Mavko, et al., 1985; Nason, 1973; Allen and Smith, 1966). One of these examples occurred prior to the Parkfield 1966 earthquake (Brown, et al., 1967). Two weeks before the earthquake, fresh en echelon cracks were observed in soil 1.5 km southeast of Parkfield, and nine hours before the main earthquake an irrigation pipeline (crossing the fault) broke. These suggest substantial fault creep before the earthquake, and thus, fault creep measurements may prove valuable in earthquake prediction.

Fault creep can be determined by measuring the opening of cracks and offsets of man-made features such as curbs, fences, and buildings that cross faults (Wesson, 1988). It can also be measured very accurately by periodic surveys of alinement arrays (sets of survey monuments that cross the fault) and periodic or continuous measurements using

creepmeters (wire or rod extensometers stretched 10-30 meters across the fault). Fault slip occurs as both event slip and interseismic slip (Lienkaemper and Prescott, 1989). Event slip is the combination of coseismic and rapid preseismic and postseismic slip.

The Parkfield, California, segment of the SAF (Fig. 1), is the most densely instrumented fault segment in the world. Since 1985, the U. S. Geological Survey (USGS) and the California Division of Mines and Geology (CDMG) have been operating the Parkfield Earthquake Prediction Experiment along the Parkfield segment of the SAF. Changes in physical characteristics of the Parkfield segment (such as fault creep, seismicity, microseismicity, strain, geochemical measurements, water well levels, magnetic field intensities, et cetera) are being measured round the clock. Hopefully, changes in physical characteristics measured by these instruments will allow the USGS to issue a short term warning of an impending earthquake. Benefits already include an improved understanding of the relationships between such characteristics as rainfall, fault creep, water level changes, strain, potential fields, seismicity, microseismicity, and geochemistry.

Creepmeters gather real-time measurements of aseismic and seismic slip in the Parkfield area. There have been four different types of creepmeters used. These are described more fully by Duffield and Burford (1973), Nason et al. (1974), and Goultz and Gilman (1978). The configuration presently in favor at the USGS consists of an invar wire stretched between an instrument pier and an anchor pier 20 to 36 meters apart across an active fault (Schulz, 1989; Schulz, et al., 1982; Schulz and Burford, 1977). Generally, before a creepmeter is installed, an alinement array is used to accurately determine the location of the active slip zone. The creepmeter wire typically crosses the fault at an angle of 30-45°. Depending on the orientation of the two piers relative to the fault, the creepmeter will measure either extension or contraction of the piers with movement of the fault. Because the wire is held taut over a rocker arm by a weight at the instrument pier, creepmeters can record either right-lateral or left-lateral motion independent of their orientations to the fault. When the fault slips, the wire is pulled through a splicer block and a displacement transducer. Slip is measured mechanically via a micrometer on the splicer block and electronically by the transducer. The transducer sends the reading to the data collection platform

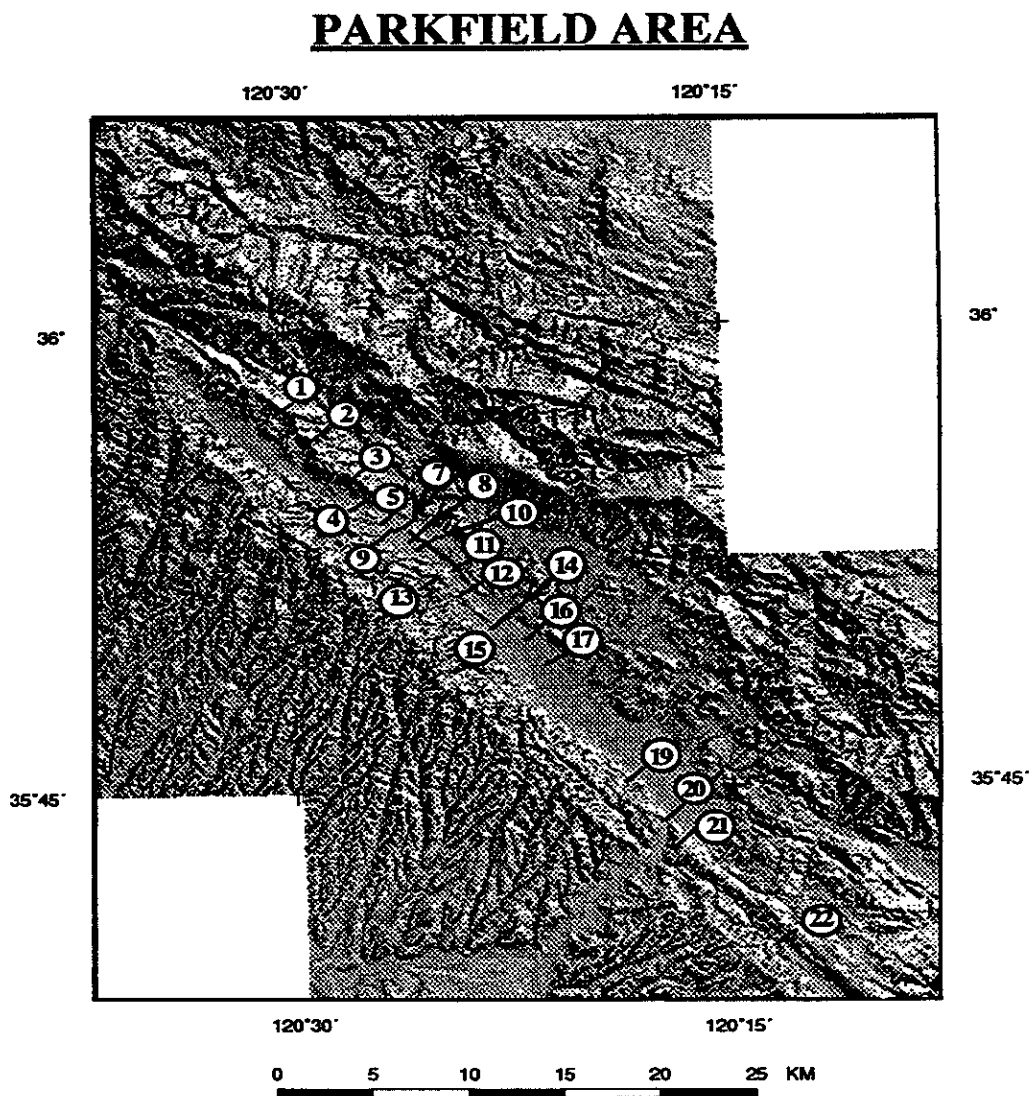


Figure 1. Shaded Relief Map of the Parkfield-Cholame Valley Area. Alinement array site numbers correspond with the array numbers in Table 1. Arrays 6 and 18 are nearly coincident with arrays 5 and 17 respectively. Arrays 4, 8, 12 and 15 lie on the Southwest Fracture Zone.

(DCP) then to a GOES satellite which relays the signals to computers at Menlo Park. A computer algorithm then automatically converts the signal into millimeters of offset and determines whether or not it exceeds predetermined alert thresholds. If a threshold is exceeded, the computer activates a beeper system and scientists are quickly notified.

The Parkfield segment last ruptured in a M 6 earthquake on June 27, 1966. Lindh and Boore (1981) reported that the 1966 Parkfield earthquake nucleated beneath a 5° bend in the fault trace at the NW end of the rupture zone (on Middle Mountain) and that the dynamic rupture was arrested at its southeast end by a 1-km-wide right step in the fault trace in the Cholame Valley, just south of Gold Hill. Thus, these two geometric features (the bend and the right step) were used to define the Parkfield segment. Bakun and McEvelly (1979, 1984) and Bakun and Lindh (1985) commented that the 1966 Parkfield event was the sixth in a series of similar events that had previously ruptured the Parkfield segment in 1857, 1881, 1901, 1922, and 1934. These earthquakes all had similar magnitudes, epicenters, seismic moments, rupture areas, and southeast direction of rupture expansion. Based on the history of recurrence (at intervals of 22 ± 5 years), the next M 6 Parkfield earthquake was assigned a 95% probability of occurring in the 10 year window from January 1983 to January 1993.

Tocher (Tocher et al., 1968; Tocher 1969) established five prototype alignment arrays (each 300-meters long) between Harris Ranch and Bitterwater Valley on the SAF. These operated from 1963 to 1967. Detection of aseismic slip drew interest in determining the local amount of slip, the width of the fault zones and the pattern of near-field deformation. The USGS first began monitoring fault creep with alignment arrays in 1966 at a site in the southern Cholame Valley area (Burford and Harsh, 1980). Since its inception in 1966, the USGS network of arrays has been expanded to include sites scattered from Mendocino to El Centro near the Mexican border (Wilmesher and Baker, 1987). There have been long periods when no surveys were conducted and other periods with frequent repetition of surveys. Figure 1 shows the locations of the 22 alignment arrays on the Parkfield segment of the SAF. Table 1 provides general information about the arrays.

Table 1. Alinement Array Data for the Central San Andreas Fault.

#	Site Code	Site Name	Latitude	Longitude	First Survey	Last Survey	# of surveys
1	XMM4 ^a	Middle Mountain	35° 57.5'	120° 30.1'	29-Apr-84	8-Aug-91	14
2	MDR4 ^a	Middle Ridge	35° 56.6'	120° 29.1'	9-May-79	20-Nov-91	11
3	VAR4 ^a	Varian Ranch	35° 55.3'	120° 27.7'	15-May-86	4-Apr-91	13
4	PKW4 ^{ab}	Parkfield Kester	35° 54.4'	120° 27.6'	7-Feb-85	24-Jul-91	18
5	XPN4 ^a	Parkfield North	35° 54.0'	120° 26.5'	27-Dec-84	21-Aug-91	14
6	PKN4 ^a	Parkfield New	35° 54.0'	120° 26.5'	8-Jan-88	7-Aug-91	7
7	PKF4	Parkfield Bridge	35° 53.7'	120° 26.0'	19-May-83	25-Jul-91	18
8	TAY4 ^a	Taylor Ranch	35° 53.4'	120° 25.6'	28-Aug-84	25-Jul-91	22
9	RCW6 ^b	Ranchita Cyn. Rd.	35° 53.1'	120° 26.5'	19-Nov-86	21-Aug-91	13
10	XDR5	Durham Ranch	35° 53.1'	120° 25.3'	7-Jun-84	22-Apr-87	10
11	HST4	Hearst North	35° 52.4'	120° 24.1'	6-Nov-86	6-Aug-91	11
12	WKR4 ^a	Work Ranch	35° 52.0'	120° 23.8'	6-Jun-84	5-Aug-91	17
13	HSW4 ^{ab}	Hearst Southwest	35° 51.8'	120° 25.3'	20-Nov-86	19-Nov-91	14
14	KEN5	Kennedy Ranch	35° 50.7'	120° 22.6'	10-Dec-86	22-Jul-91	13
15	HAR4 ^b	Harlan Ranch	35° 50.4'	120° 22.9'	6-Nov-86	19-Nov-91	14
16	CRR4 ^a	Carr Ranch	35° 50.1'	120° 21.8'	5-Jan-84	17-Mar-88	6
17	GHG4 ^a	Gold Hill Gilman	35° 49.2'	120° 21.0'	23-Aug-83	7-Jul-88	8
18	PHG4 ^a	Gold Hill	35° 49.2'	120° 21.0'	8-Nov-83	23-Jul-91	9
19	XWT4	Water Tank	35° 45.4'	120° 18.4'	11-May-84	18-Jun-91	8
20	H464	Highway 46	35° 44.1'	120° 17.2'	24-Aug-83	18-Jun-91	11
21	X464 ^a	Highway 46 South	35° 43.3'	120° 16.7'	12-Jun-86	19-Jun-91	13
22	PPP4	Palo Prieto Pass	35° 39.2'	120° 12.5'	22-Jul-75	20-Jun-91	6
Total # of surveys							270

^a. Also a creepmeter site.

^b. Located on the Southwest Fracture Zone.

On a broader scale, geodetic measurements of line lengths, (using lines on the order of 30 km in length) have been carried out since 1959 (Langbein, et al., 1990; King, et al., 1987). These lines cross the SAF at oblique angles. Changes in their lengths were interpreted to reflect either block motion or strain accumulation. Burford and Harsh's (1980) alinement array study of near-field deformation across the fault zone determined that block motion is the primary manner of displacement along the Parkfield segment of the fault.

The purpose of this paper is to present results from new alinement array sites, to summarize the surveying techniques used in surveys conducted along the Parkfield seg-

ment of the SAF. This paper presents a summary of the geology of the area, a detailed description of alinement arrays and how they are employed, along with an interpretation of the data. Creep rates documented by Lienkaemper and Prescott, (1989), and measured by creepmeters are provided as a comparison to slip rates determined by alinement array surveys. Also, an improved method of measuring deformation is presented. This method increases the amount of data gathered with each survey, provides information that assists in the determination of monument stability, and allows the surveys to be completed by one person rather than a crew of two. The appendix contains details that should allow other workers to recover and resurvey these arrays.

General Geology

The Parkfield-Cholame segment of the SAF lies west of southern Diablo Range and the northern Temblor Range in central California. It is approximately 25 miles southwest of the town of Coalinga. Movement along the SAF has juxtaposed dissimilar rock units separated by a belt of melange (Fig. 2). The 40-km-long segment of the SAF is the transition zone between the creeping segment, to the northwest, and the locked segment, to the southeast. It is bounded by a 5° bend in the fault trace on Middle Mountain (on the north) and a 1-km right stepover in Cholame Valley (on the south).

Northeast of the SAF lie complexly folded and faulted rocks of the Franciscan assemblage, Coast Range ophiolite, sedimentary rocks of the Great Valley sequence, and upper Cenozoic marine and nonmarine sedimentary rocks (Dickinson, 1966). Deformation of these rocks varies with age and proximity to the fault. Deformation decreases with a corresponding decrease in the age of the rocks. Southwest of the SAF, the Salinian Block is composed of granitic basement rocks overlain by Miocene and Pliocene marine sedimentary rocks capped by Pliocene and Pleistocene nonmarine gravel and sand. The rocks west of the fault are less deformed than the rocks to the east of the fault. Seismic activity is also lower west of the fault.

To the northeast of the SAF, a belt of highly deformed rocks separates the Salinian

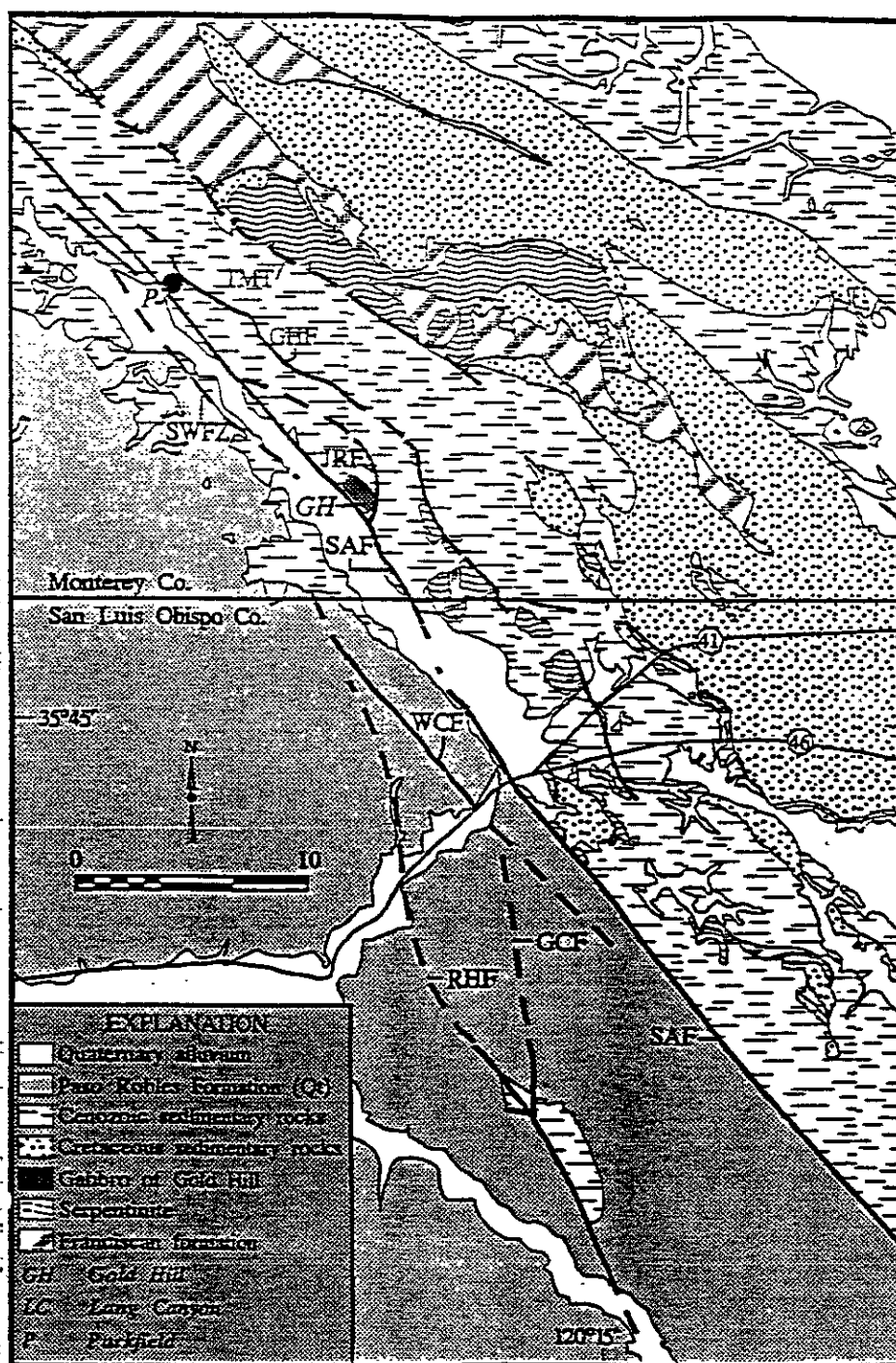


Figure 2. Geologic Map of the Parkfield-Cholame Valley Area. The faults are labeled as follows: Gillis Canyon Fault (GCF); Gold Hill Fault (GHF); Jack Ranch Fault (JRF); Red Hills Fault (RHF); San Andreas Fault (SAF); Southwest Fracture Zone (SWFZ); Table Mountain Thrust (TMT); White Canyon Fault (WCF). From Sims and Hamilton, (1991).

block from the folded and faulted rocks to the northeast. The belt consists of sheared and deformed Franciscan assemblage, upper Cenozoic units and exotic blocks of granite, gabbro, and marble. They were derived from Jurassic and Cretaceous crystalline basement rocks and upper Miocene volcanic units to the northwest and southeast of the Parkfield area (Sims and Hamilton, 1991; Sims, 1989).

Exotic blocks of crystalline basement and associated Tertiary volcanic and sedimentary rocks are found at Gold Hill, and Lang Canyon. They have been sliced away from their counterparts to the south and north, and have been fragmented. The Gold Hill block includes a hornblende quartz gabbro that is similar, petrographically, to a body of the same age about 150 km to the southeast (called Eagle Rest Peak), and to rocks about 165 km to the northwest near Logan. The Lang Canyon block, northwest of the Gold Hill block, is a northwest-trending belt of Miocene volcanic rocks that correlate with similar rocks of the Neenach Volcanics, 220 km to the southeast, and with the Pinnacles Volcanics, 95 km to the northwest (Sims and Hamilton, 1991).

The original position of the Gold Hill block (and its correlative bodies to the northwest and southeast) is at the margin of the Mojave Desert and about 55 km northwest of the restored position of the Lang Canyon group (Ross, 1989). Three stages of deformation account for the reversed positions of the Gold Hill and Lang Canyon blocks. In the first stage, the Pinnacles and Logan blocks were sliced away from their parent bodies and displaced about 95 km to the northwest. This places the Pinnacles about 40 km northwest of the Eagle Rest Peak gabbro. In the second stage, the SAF stepped eastward and separated the Lang Canyon block from the Neenach Volcanics. The Pinnacles and Lang Canyon blocks were both on the west side of the fault and remained 95 km apart. The volcanic blocks and one gabbro moved to the northwest. The third stage began when the Logan gabbro reached the latitude of Gold Hill, at which point the Gold Hill block split off along the east side of the SAF. The Logan gabbro and the Pinnacles Volcanics continued northwestward another 160 km. A total of 310 to 315 km of displacement (Sims and Hamilton, 1991) is recorded by the offset of all of these blocks.

The most notable feature documented by Hanna et al., (1972), was a two-lobed

Bouguer gravity high on the north side of the SAF in Cholame Valley. They report the steep southwest side of the high is caused by shallow Franciscan rocks northeast of the fault in contact with deeper granitic rocks (of similar density) southwest of the fault.

Description of Alinement Arrays

An alinement array is a linear series of buried survey monuments located so as to cross a fault at a high angle ($60-90^\circ$) to the local strike (Fig. 3). Array lengths range from 50 to 300 meters, with an average of about 100 meters. Alinement arrays consist of two to four wing stations and an instrument station (IS). The IS is so named because a surveying instrument called a theodolite is positioned on a tripod over the IS monument. Wing stations consist of at least one orientation station (OS) end station (ES) and as many as two of each. Angles between the various wing stations are measured from the IS. Deflection stations (DS's) are spaced between the IS and ES's. The IS and OS's are located on the same side of the fault and are assumed to remain stationary relative to one another. The most common array geometry is an "L" shape with the ES on the opposite side of the fault from the IS and the OS. To determine the displacement of the deflection stations, their position relative to the line of sight from the IS to the ES is compared from survey to survey. Repeated measurements of array geometries yield information on local slip rates, width of fault zones, and patterns of near-field deformation. Results from repeated surveys of the arrays can sometimes help explain unusual behavior (e.g., little movement or left-lateral displacement) of nearby creepmeters.

Geologic evidence of fault offset (such as offset drainages, sag ponds, linear valleys, shutter ridges, mapped en echelon fault cracks, and offset cultural features) are used in locating alinement array sites. Because alinement arrays require a clear line-of-sight, heavily vegetated areas and high relief areas are avoided, if possible. Once a site is found, that meets the above criteria, the local fault strike is measured and a line (as near to perpendicular to the fault as the local terrane allows) is picked for the azimuth of the array. Station locations are laid out along this line in both directions away from the fault. The interval

Typical Alinement Array Layout

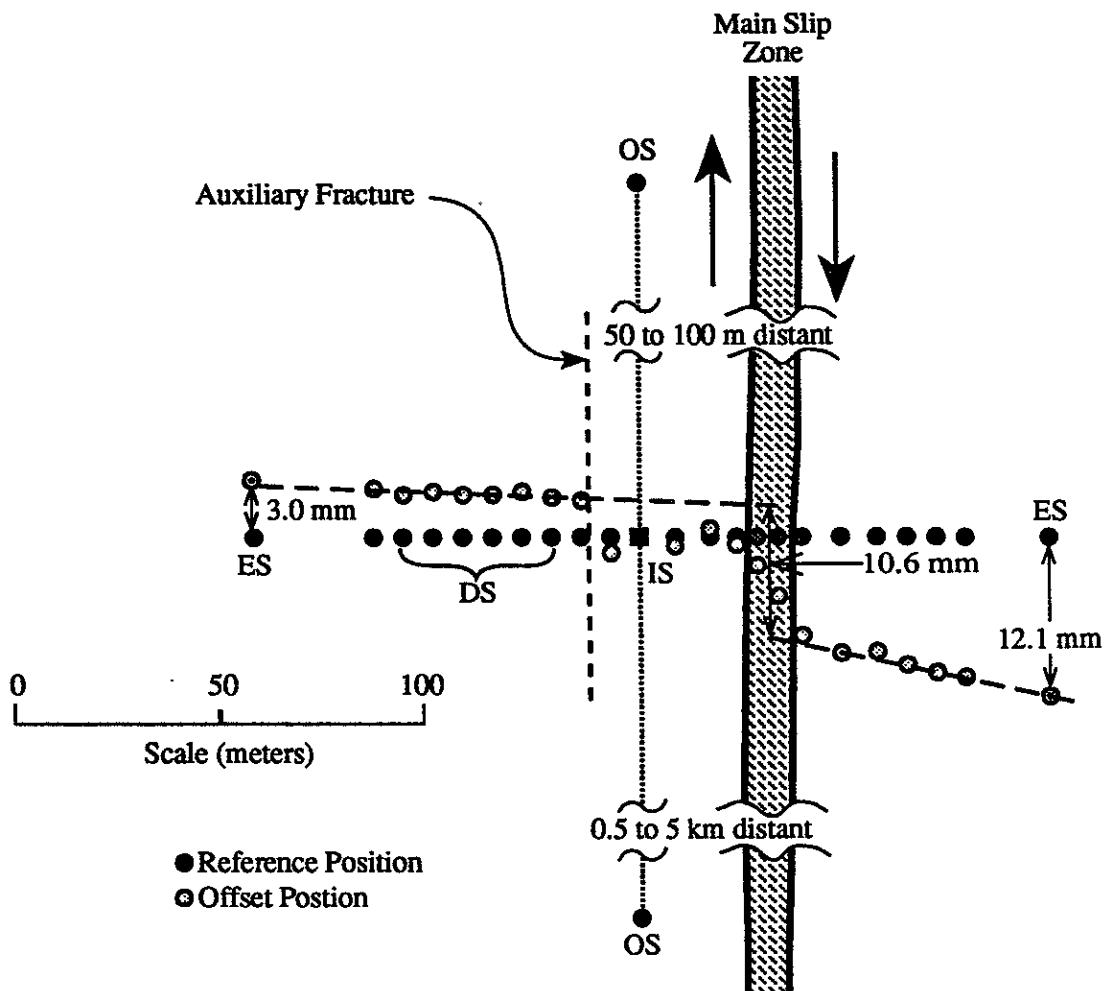


Figure 3. Map View of an Alinement Array Layout. View shows the initial position of the array monuments (dark circles), and positions of monuments (light circles) at a later date after they have been displaced by fault creep (modified from Burford and Harsh, 1980). The theodolite is set up over the instrument station (IS, filled square) in the center of the array. Tripods and targets are set up over the end and orientation stations (ES and OS). The net amount of movement can be calculated three ways: by measuring the fault parallel displacement of the end station (ES), by measuring the distance between two best-fit-lines through the deflection stations (DS) on opposite sides of the fault, and by measuring the distance parallel to the fault between the maximum offset points in the array. The OS's are assumed to be on the same rigid block as the IS.

between stations usually increases with distance from the fault. OS's are located approximately 100 meters from the IS along a line parallel to the local fault strike.

In the past, monuments were made of concrete poured into unlined 6" deep holes with a bar driven into the hole and mounted with a brass cap survey marker. This practice was abandoned after heaving of the clay-rich soils actually caused some of the monuments protrude as much as 6 inches above the ground surface. The expansion and contraction of soils prompted changes in the design of newer monuments so that they would be decoupled from the upper two to three feet of soil. The present monument installation procedure requires inserting a 6" inside-diameter PVC pipe into a 3-4' deep post-hole (Fig. 4) and pounding a 5' long 1" inside-diameter galvanized steel pipe into the post-hole until the top of the pipe is 4-13" below the ground surface. In plowed fields where heavy equipment is used, the monuments are set lower to avoid being disturbed. In areas where arrays cross pavement, subsurface monuments cannot be used, so special surveying nails (P & K nails) are set into the pavement.

Measurement Procedure

The present procedure requires a two man crew, consisting of an instrument operator and a target operator. The instrument operator centers the tripod and theodolite over the IS monument. The target operator centers the horizontal traverse targets and tripods over the ES and OS. Both the theodolite and targets are equipped with optical plummets, which eliminate the need for plumb-bobs. The survey begins with the instrument operator taking readings to the various targets and the target operator recording the data.

The surveys are completed using precise first-order horizontal surveying theodolites, traverse targets, tribrachs (attaches the theodolite and targets to the tripods) with optical plummets, and tripods. A custom designed tent is used to protect the theodolite and its tripod from the sun and wind. When the sun's light hits the wooden tripod legs, they expand, making the theodolite difficult to keep leveled. Large windows are cut in the four walls of the tent to enable viewing of the targets. The target tripods have telescopic legs

Typical U.S.G.S. Alinement Array Monument

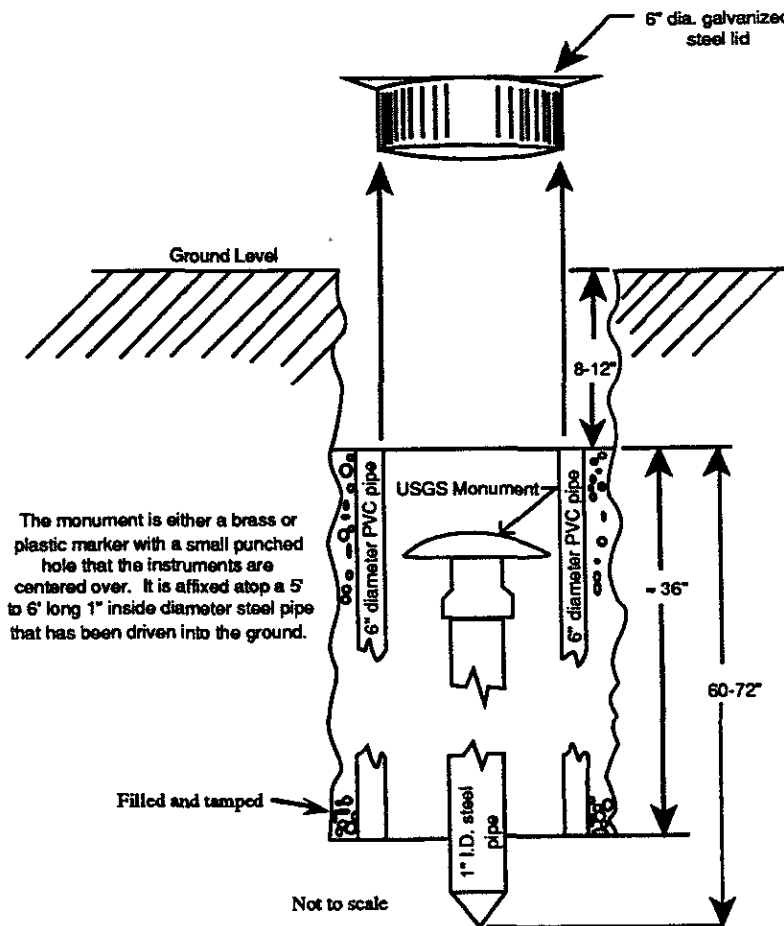


Figure 4. Cross Section of Typical Monument. The monument is set atop a 5 to 6 ft. steel pipe driven into a posthole. A 6 inch (inside diameter) pvc pipe is then placed into the hole around the monument and the area around it is tamped and filled (Modified from Wilmesher, unpublished).

that are easier to set up than the fixed leg instrument tripod. The fixed-leg tripod is better able to handle the extra weight of the theodolite.

Tripods with telescopic legs are positioned over the ES's and OS's with one leg pointing towards the IS, and a fixed-leg tripod is set up over the IS monument with a leg set in the direction of the ES across the main fault. The positioning of the tripod legs in such a manner enables the tribrachs to be set on the tripod head so the optical plummet eye-pieces on the targets may be pointed toward the instrument. Thus, rotation of the tribrachs

on their tripods are consistent from one survey to the next, and any systematic errors can be more easily detected during data analysis. Next, the tribrachs are centered and leveled over their respective monuments and the theodolite and targets are attached to the tribrachs and are centered and leveled. The theodolite is placed on the IS tripod and centered and leveled over the IS monument. Horizontal surveying targets are centered and leveled over their respective monuments at the ES's and OS's. The theodolite scope is then aimed at ES #1 and an angle of $\approx 0^{\circ} 0' 30.0''$ is set on the horizontal micrometer scale and recorded. The scope is then turned clockwise to OS #1 and the micrometer value is recorded. The acute angle subtended by the stations is found by subtracting the two recorded values. This is repeated for the remaining ES's and OS's. The scope is then pointed toward ES #1 again and the angle to OS #1 is repeated. The second reading toward ES #1 and OS #1 must close within 3 seconds of the first reading. If there is a disagreement of more than three seconds the angles are remeasured until the closure error is less than or equal to 3 seconds. When all of the angle measurements close, the deflection stations are measured to complete round one. The targets and the theodolite are then rotated clockwise 120° and the procedure is repeated twice more. Rounds two and three follow the same procedure except the initial horizontal angle readings set at ES #1 are $\approx 240^{\circ} 00' 30.0''$ and $\approx 120^{\circ} 00' 30.0''$ respectively. Setting the micrometer readings at approximately 0° , 120° and 240° eliminates collimation errors and reduces micrometer graduation errors.

To begin the deflection station measurements, the target operator centers the deflection target (Fig. 6) over the first monument toward the ES. The target point, at the end of the vertical rod attached to the scale, is set in the mark on top of the monument. Once the bulls-eye bubble on the target is leveled, the lock nuts are tightened, clamping the level adjustment plate and bar in place. Centering of a carpenter's level behind the scale is accomplished by rotating the level adjustment bar. Once the target is leveled over the monument, the target operator aligns it by pointing the gun sights at the theodolite. This ensures that the scale is perpendicular to the line of sight. At this time the instrument operator locks the horizontal motion of the telescope while pointed at the ES. This defines a vertical plane of sight. The measurement is made by swinging the telescope vertically in this plane and fo-

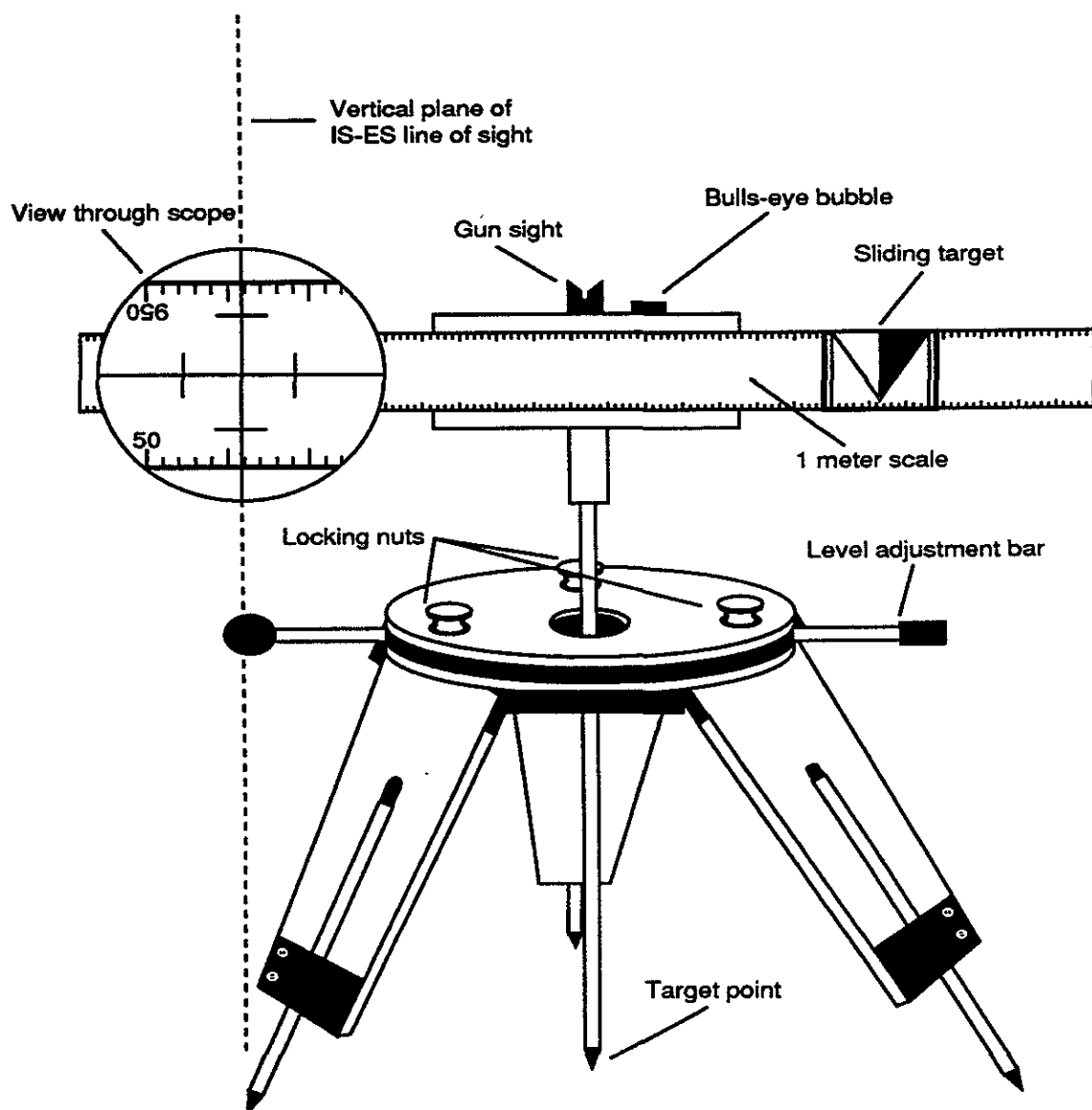


Figure 5. Sketch of the Deflection Target. The circle represents the view through the theodolite telescope showing the vertical and horizontal cross hairs on the target scale. The vertical dashed line through the circle represents the vertical plane passing through the IS and the ES. The bull's-eye bubble on top of the scale is used for rough leveling. Behind the center of the scale is a 4" long carpenter's level (not shown) used in the final leveling of the target.

cusing the vertical cross hair of the telescope on the deflection target scale. The scale is then read to the nearest tenth of a millimeter under the cross hair. The instrument operator records the value and signals the target operator who picks up the deflection target and moves on to the next station. All of the monuments are read after each set of angles for a total of three readings per deflection monument.

Methods of Calculating Displacement

Three different measures have been used to calculate the total amount of displacement recorded between repeated measurements of alinement arrays. Unless otherwise noted, the measure used in this study is the ES displacement along a line parallel to the fault strike from its original position (12.1 mm in Fig. 3). At a few sites, a lack of agreement between rates measured using ES displacement and the rates from nearby creepmeters indicate that a second method is needed to better show the rate of movement at the fault zone. The distance between the maximum displaced monuments on opposite sides of the fault can be used in conjunction with the first calculation to show the difference in rates at the fault and the rate 30-60 meters distant from the fault. The maximum displacement method is used when offset is greatest next to the fault and decreases with distance away from the fault. The third measure is the distance (at the fault) between two least-squares fit lines through monuments on opposite sides of the fault zone (10.6 mm in Fig. 3). This method was used by Burford and Harsh, (1980), as a check, or as an alternative to end point displacement in the absence of reliable angle data. In cases where the deformation is homogenous and simple shear is distributed across the fault zone, this third method consistently underestimates fault slip.

Precision of Measurements

The surveying procedure used in this study is nearly identical to that reported by Burford and Harsh, (1980). They determined that the precision of the measurements de-

depends upon 1) accurate positioning the surveying instruments over the monument centers, 2) how well the instrument operator points the theodolite at each target and reads the micrometer value, and 3) monument stability. To determine the repeatability of survey measurements they occupied an array (Melendy Ranch) twice in four days. Their results

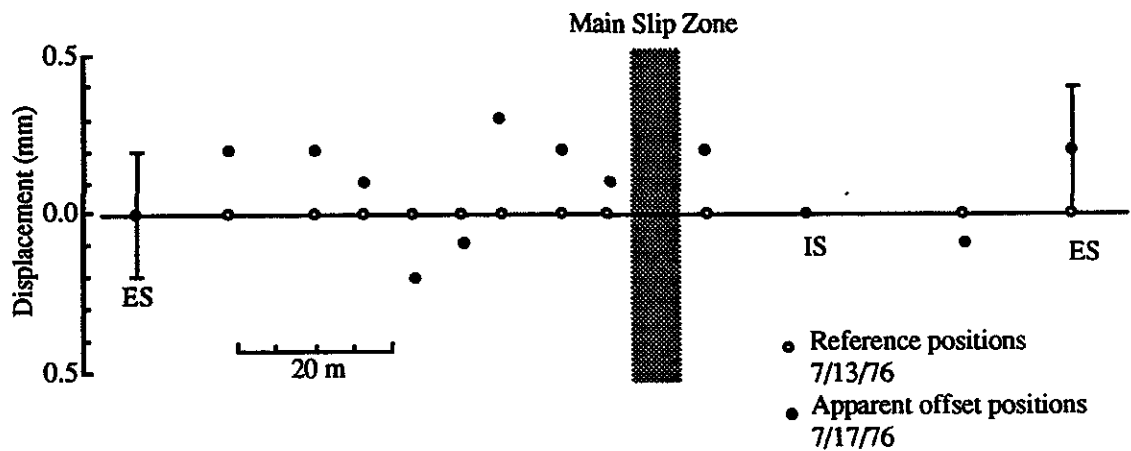


Figure 6. Test of Survey Repeatability. Comparison of two surveys conducted four days apart at Melendy Ranch alignment array to test the measurement repeatability (from Burford and Harsh, 1980). Deflection monuments are resolved to ± 0.17 mm, while the error bars on the ES's designate a resolution of ± 0.2 mm from the accumulation of error in the two sets of angle measurements.

indicate a standard deviation of the ES (approximately 85 m from the IS) of ± 0.2 mm and an average deviation in determination of DS displacements of ± 0.17 mm. These measurements may include tectonic movement in the slip zone if a creep event occurred in the four day period between surveys.

Systematic errors in measured angles and deflection station measurements resulting from the effects of randomly oriented eccentric biases in optical plummets (Fig. 7) or misadjustments of level vials are corrected by rotating the targets and instrument tribrachs 120°

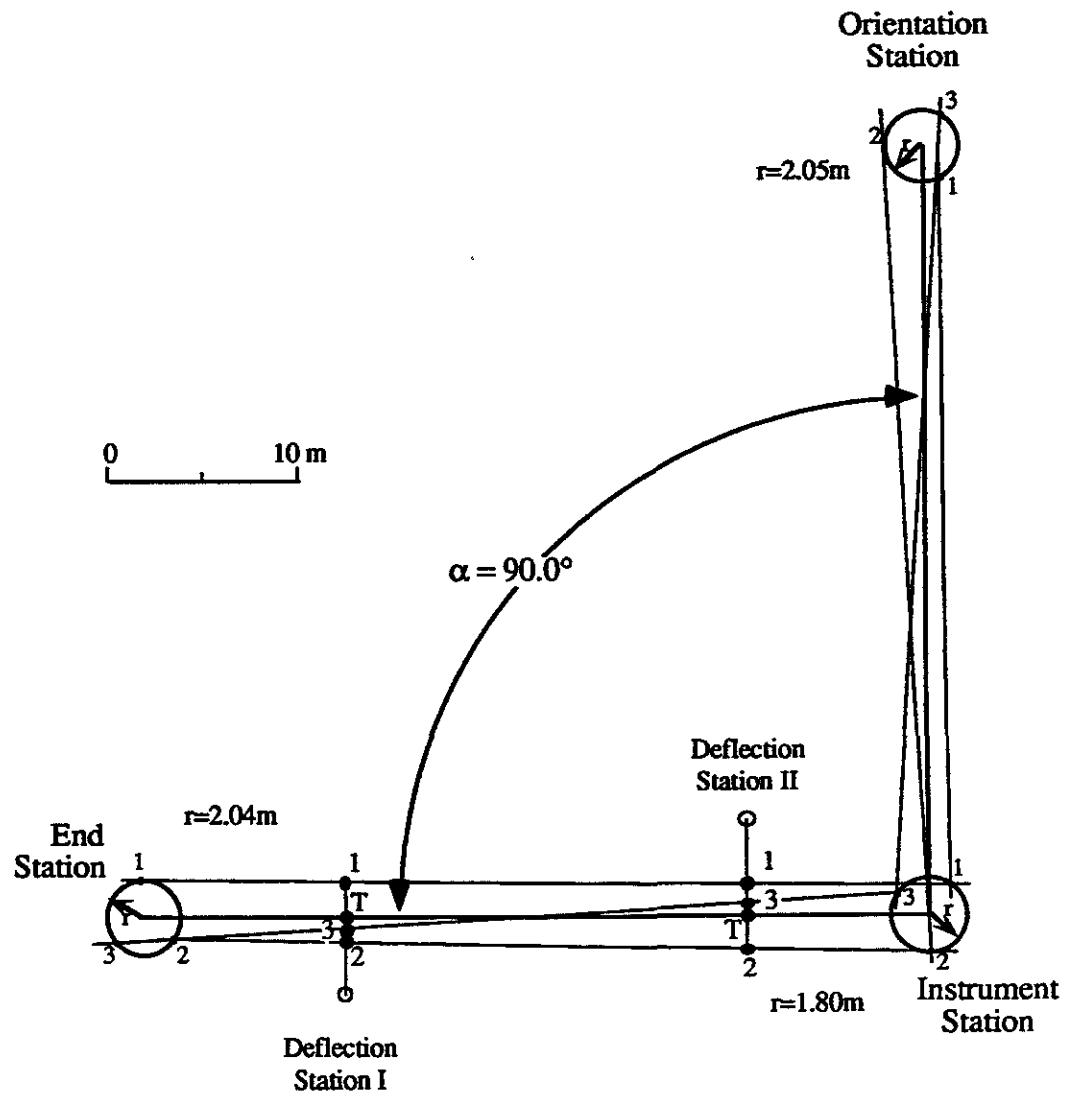


Figure 7. Biased Angle Measurements. The IS, ES, and OS are positioned randomly and rotated clockwise on large eccentric circles about their true monument position (Modified from Burford and Harsh, 1980).

between each set of readings. Errors in the angle measurements caused by the optical plummet being out of true or a level vial out of adjustment are generally noticeable in the readings, but are almost perfectly cancelled when the mean of the three sets of angles and deflection readings is determined. Figure 7 is a hypothetical example of a survey in which

the eccentric errors of the optical plummets are exaggerated to a radius of ≈ 2 meters (normally ≤ 0.2 mm). The results of a comparison of the true angle and deflection values to those from the three eccentric circles is shown in Table 2.

Table 2. Comparison of True Angle and Deflection Values with Mean Values Obtained from Three Sets of Eccentric Centers. See Figure 7 for further explanation (Burford and Harsh, 1980).

Parameter (units)	True Value (T)	Mean Value ^a	Value for 1 st Position	Value for 2 nd Position	Value for 3 rd Position
α (deg)	90.0	90.2	87.3	84.5	98.8
Defl. I (m)	-4.33	-4.38	-6.04	-3.15	-3.96
Defl. II (m)	+4.02	+3.99	+2.53	+5.90	+3.55

^a. An average of three centers.

In these surveys the only changes made to the technique of Burford and Harsh, (1980) are an additional pointing to ES #1 and the use of a newer electronic theodolite of similar precision to the old instrument. The additional pointing to ES#1 means that each wing station is sighted twice and the two readings must fall within a three second range. The digital display of the electronic theodolite eliminates operator errors from the interpretation of the micrometer scale. With the inclusion of the second pointing to ES #1, all of the targets are read twice with a maximum allowable variance of three seconds of arc between each pair of measurements. Before 1983 the surveys were begun by reading OS #1 first, whereas, now they begin at ES #1. The average of the standard deviations of the 12 angles from each survey (270 surveys) is ± 1.57 seconds. The average standard deviation of ES displacement is ± 0.91 mm. The standard deviations determined in this study are probably a better indicator of the average repeatability of the various array lengths and different surveying conditions. The standard deviation is proportional to the length of the array. The average distance from the IS to the ES is 113 meters. The first-order horizontal control standard of accuracy in the United States is one part in 100,000. The average accuracy of alinement array surveys is one part in 124,000.

Site Characteristics

The following section is a brief discussion of characteristics of each site preceded by a short explanation of how they may affect survey measurements. The various characteristics listed in Table 3 include the number of stations, type of monuments, the local fault and array azimuths, and the length of the arrays. The monument types described earlier (Description of Alinement Arrays section) include the subsurface type, nails set in asphalt, and markers embedded in concrete plugs. At PKF4 (Parkfield Bridge), crosses etched into the concrete are used on the bridge as monuments and survey nails are used outside the bridge structure. Several of the older sites installed by Cal Tech have brass cap survey markers crimped on 1.6 cm diameter copper clad rods pounded into the ground.

Table 3. Site Characteristics.

#	Site Code	# of DS	Monument Type ^a	<u>Azimuths</u>		Array Length (m)
				Fault	Array	
1	XMM4 ^b	5	SS	335.5°	227°	94.84
2	MDR4 ^a	8	SS	322°	237°	121.64
3	VAR4 ^a	9	SS	320°	60°	69.40
4	PKW4 ^{ac}	4	SS/N	356°	244.5°	92.35
5	XPN4 ^a	0	SS/N	314°	25.5°	187.04
6	PKN4 ^a	10	SS	314°	47°	92.14
7	PKF4	5	N/E	319.5°	90°	108.80
8	TAY4 ^a	8	SS	320.5°	233°	103.20
9	RCW6 ^b	9	SS	318.5°	92.3°	275.99
10	XDR5	9	C	319°	235°	62.52
11	HST4	5	SS	320°	225°	74.84
12	HSW4 ^{ab}	7	SS	320°	50°	112.11
13	WKR4 ^a	0	SS/CT	316.5°	43.5°	60.71
14	KEN5	7	SS	320°	230°	72.70
15	HAR4 ^b	5	SS	320°	31.5°	106.11
16	CRR4 ^a	6	SS	314°	56.5°	129.28
17	GHG4 ^a	3	SS/CT	320.5°	42°	121.66
18	PHG4 ^a	9	SS	320.5° (309.5)	120°? 53.5	139.41
19	XWT4	9	C	326°	220°	79.23

#	Site Code	# of DS	Monument Type ^a	<u>Azimuths</u>		Array Length (m)
				Fault	Array	
20	H464	4	CT	318°	234°	151.65
21	X464 ^a	6	SS	320°	70°	150.10
22	PPP4	14	SS	320°	50°	200

^a. SS=subsurface monument, N=nail, E=etched cross in concrete bridge slab,
C=monument set in concrete, CT=Cal Tech monument

^b. Also a creepmeter site.

^c. Located on the Southwest Fracture Zone.

The local fault azimuths were measured with a hand-held compass and compared with azimuths from fault maps. The distances from the IS to the various monuments were measured with an electronic distance meter to a precision of ± 1 millimeter.

Patterns of Deformation

Upon initial investigation of the deformation patterns, the patterns grouped naturally into two categories, with the remaining arrays placed into a third category (Fig. 8). The first two categories (I and II), consist of arrays with deformation patterns that can be defined by a general shape, although not restricted by magnitude of displacement or distance from the fault. The third category (III) consists of arrays with deformation patterns that are not easily interpreted with a simple model of deformation. Type I is found at six arrays, Type II is at four arrays, and Type III occurs at seven arrays. Figure 9 shows the spatial distribution of the deformation patterns. PKF4 array is not included because the deflection stations are on concrete slabs on the bridge framework. Arrays XPK4, WKR4, GHG4 either don't have any deflection stations or have too few to determine a pattern.

Deformation Type I is best defined by the displacement pattern at the Middle Mountain array (XMM4, Fig. 10). It is the type section deformation pattern of two rigid blocks ($\approx 100 \text{ m}^2$) separated by a narrow zone of ductile shearing. Monuments away from the fault zone have little or no lateral movement between them, thus, they maintain a rela-

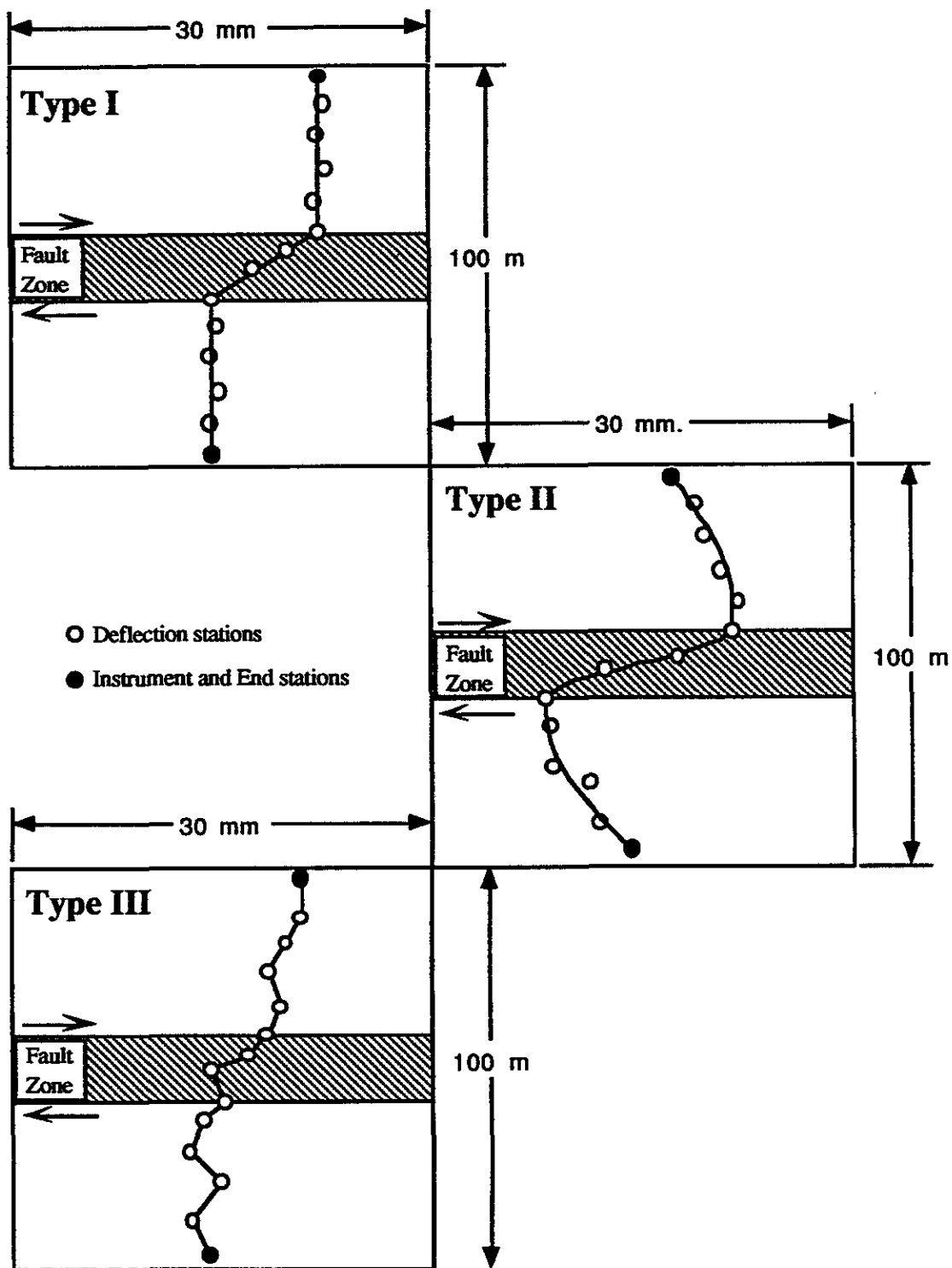


Figure 8. Deformation Patterns I through III. Pattern I shows no deformation outside of the fault zone. Pattern II shows left-lateral displacement of the monuments outside of the fault zone. Pattern III shows random displacement of the monuments across the arrays length.

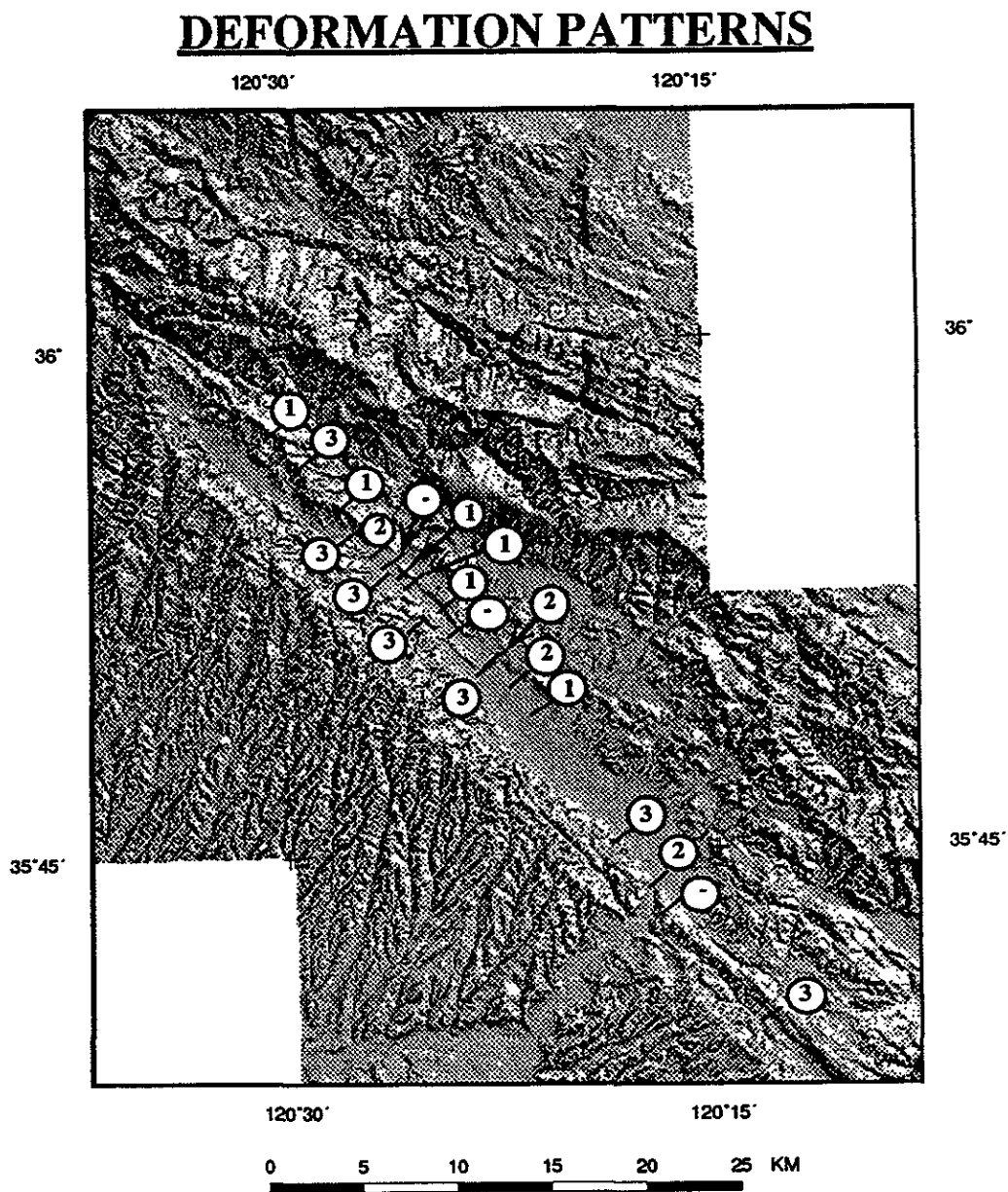


Figure 9. Spatial Distribution of Deformation Patterns. Arrays where the deformation pattern has not been determined are marked with a dash. The arabic numbers 1 to 3 correspond with the roman numbers in the text.

tively straight line. The displacement between the IS and ES closely approximates the total cumulative movement on the fault.

The displacement pattern at PKN4 is the best example of deformation Type II deformation (Fig. 11). The monuments outside of the fault zone remain aligned, although, they are rotated in a counter clockwise manner. The maximum amount of displacement is not at the two most distant stations, the IS and ES, but at the monuments closest to the fault. The creepmeter XPK1 located about 30 meters to the southeast has measured the same amount of displacement over the same time period as is recorded by the displacement of the two monuments nearest the fault zone.

Deformation Type III (Fig. 12) includes the remaining arrays that don't neatly fit into the first two patterns. The arrays may fit into one of the previous categories on one side of the fault but not on both. All of the arrays classified as Type III have less total displacement than any of the arrays of Type I, except MDR4, which is considered unreliable due to unstable monuments. These arrays may represent a complex pattern of diffuse strain across a wide fault zone, or a complex pattern caused by multiple fault traces, or they have not moved enough to present a clear pattern.

Deformation Pattern I

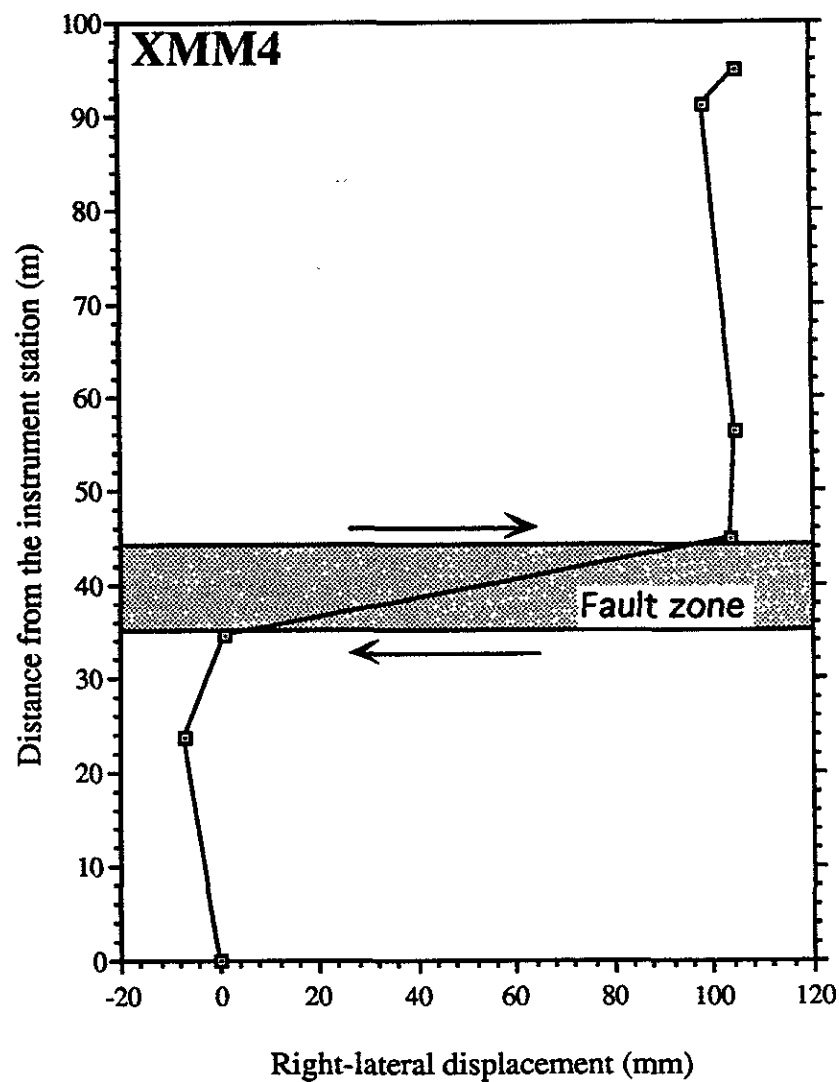


Figure 10. Example of Deformation Pattern I. Plot shows the cumulative movement at Middle Mountain alignment array. Shaded area represents the maximum possible width of the active fault zone. Monuments outside of the fault zone are displaced very little with respect to one another.

Deformation Pattern II

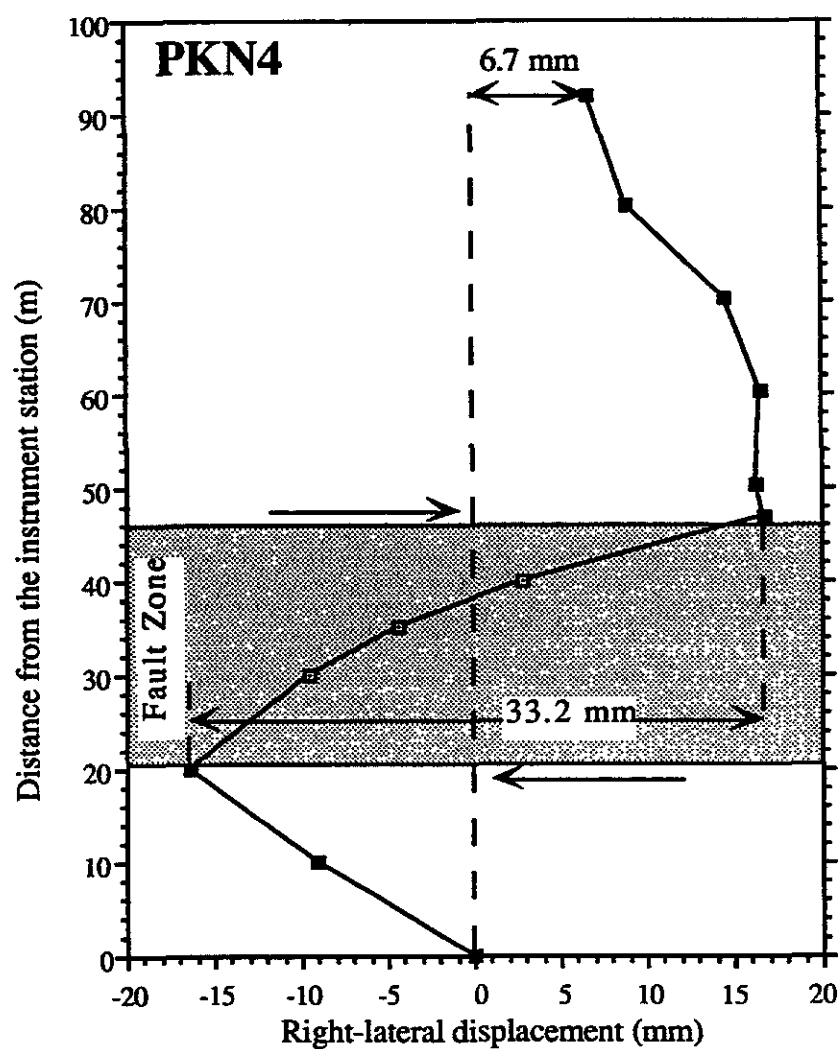


Figure 11. Example of Deformation Pattern II. At the PKN4, array the end points have been offset only 6.7 mm while the points closest to the fault zone have been offset 33.2 mm over the same time period. XPK1 creepmeter (≈ 25 meters SE) agrees with the larger displacement during the same time period.

Deformation Pattern III

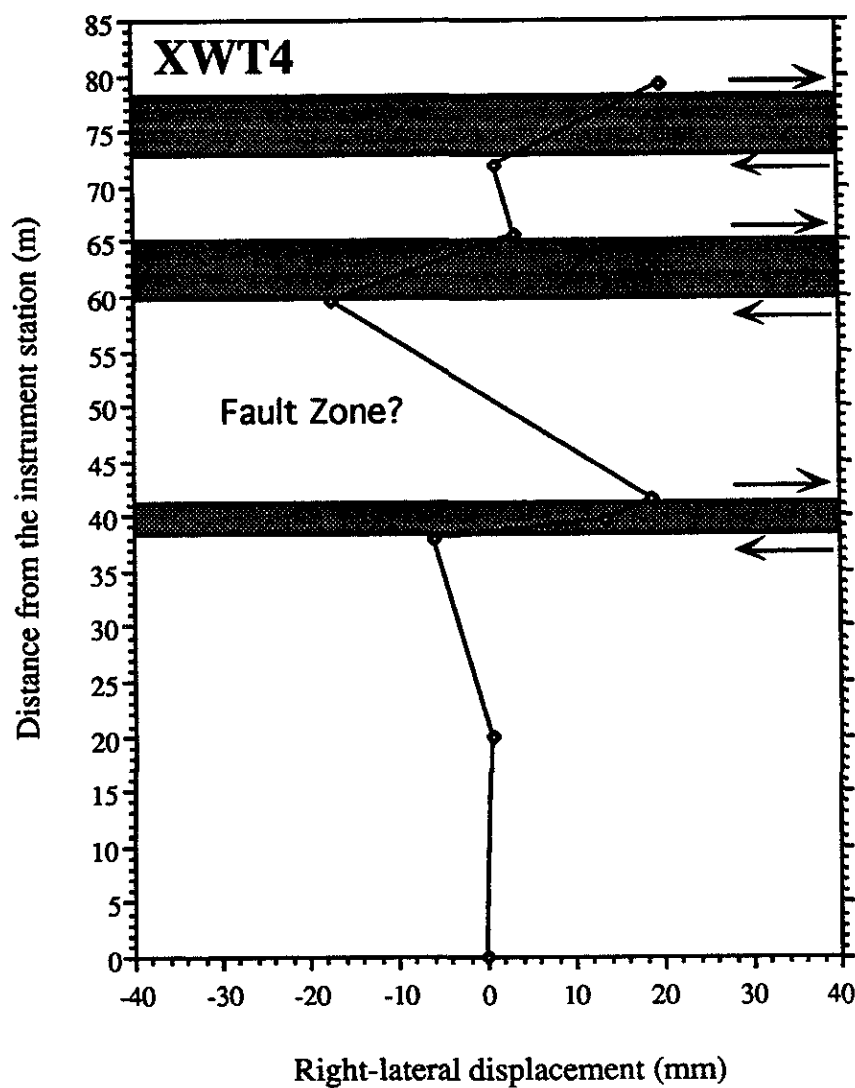


Figure 12. Example of Deformation Pattern III. The determination of the fault zone width, fault location, and total displacement is difficult because of the random pattern of displacement of the monuments.

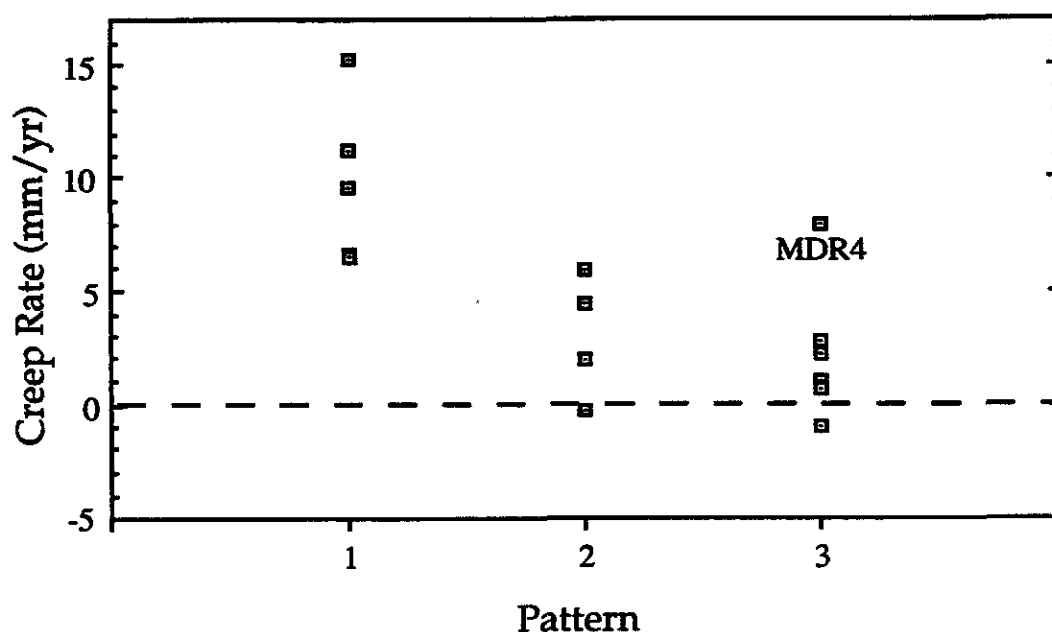


Figure 13. Plot of Creep Rate vs. Deformation Pattern Type. This plot suggests a progression from deformation patterns III and II to I with increasing cumulative movement. The data point MDR4 is considered unreliable due to monument instability.

Figure 13 suggests a correlation between pattern type and amount of creep at each site. An unequal-variance Student's t-test and F-test were conducted (Table 4) to determine

Table 4. *F* and t-Tests on Creep Rate Distributions between Deformation Patterns I, II, and III in Figure 13.

pattern	1 st avg	2 nd avg	t	$t_{\alpha=0.05}^a$	<i>F</i>	$F_{\alpha=0.05}^b$
I vs. II	9.26	2.98	3.18	1.90	1.64	9.12
I vs. III	9.26	1.11	5.33	1.83	7.07	5.19
II vs. III	2.98	1.11	1.26	1.86	4.31	5.41

^a Taken from Table 4, Press, et al., 1986.

^b Taken from Table 6(a), Press, et al., 1986.

if the patterns have significantly different means and variances (Press, et al., 1986) of creep rates. The null hypothesis (that the means of two samples are equal) is rejected when $t >$

$t_{\alpha=0.05}$. This hypothesis can be rejected for the first two cases, but not for the third. The null hypothesis (that the variances of two samples are equal) is rejected when $F > F_{\alpha=0.05}$. This hypothesis can be rejected only for the second case, but not for the first and third. Thus, the statistics show that the creep rates at sites with deformation patterns II and III are not significantly different from one another.

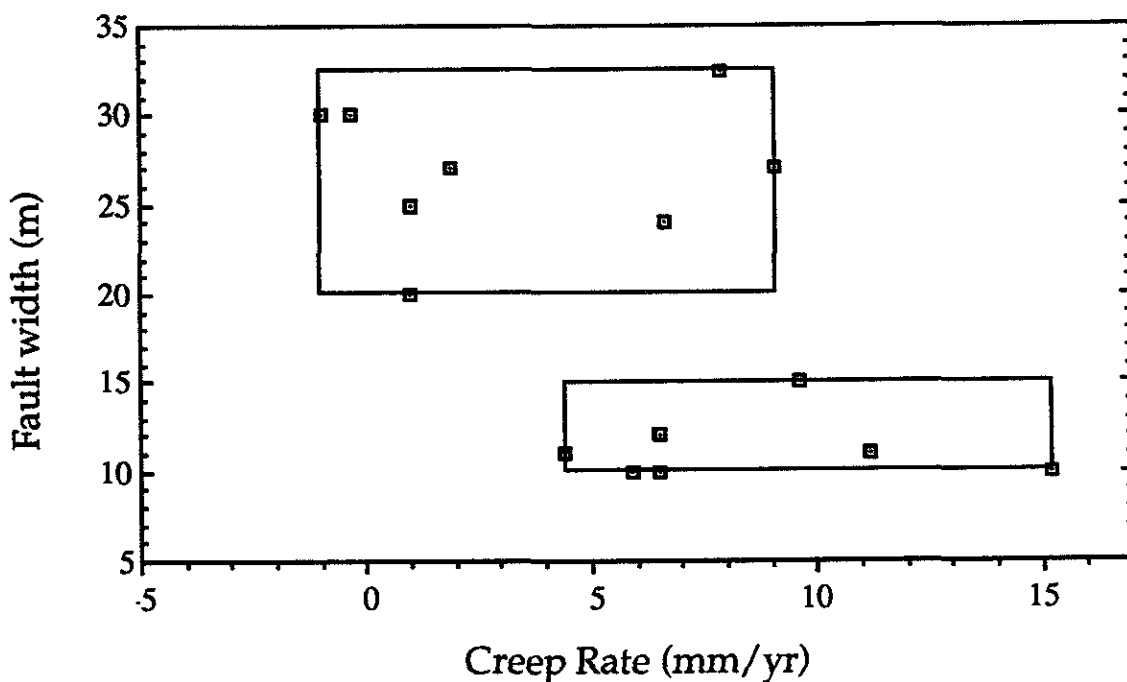


Figure 14. Comparison of Fault Width and Creep Rates. Box #1 includes 7 arrays with fault widths from 20 to 30 meters and creep rates of -1.0 to 9.1 mm/yr (avg. 2.6 mm/yr). Box #2 includes 7 arrays with fault widths from 10 to 15 meters and creep rates of 4.4 to 15.2 mm/yr (avg. 8.5 mm/yr). The data from MDR4 is considered unreliable due to monument instability and is not included.

Two possible explanations for the increase in total slip from patterns II and III to I are: 1) that all sites pass from the more chaotic patterns to the simple pattern I when they exceed a certain amount (~30 mm) of total movement; 2) that sites with Type II deformation are expected to have less displacement at the ES because they are responding to an as-

perity on the fault that inhibits slip at the surface. These explanations are more fully discussed later in the section on Deformation Mechanisms.

A comparison of fault widths and creep rates measured at each site is shown in Figure 14. The average value for arrays in Box 1 (26.1 m wide fault zone and 2.6 mm/yr creep rate) and Box 2 (11.3 m wide fault zone and 8.5 mm/yr creep rate) indicate that areas of the fault with narrow fault zones tend to have higher rates of creep than areas with a wide fault zone (7 of the 10 sites with the highest rate). The high rate of creep recorded across a narrow zone by the creepmeter suggests MDR4 might also fall into box #2 if it had stable monuments. The fault widths are maximum values that are determined from the distance between the two monuments just outside of the fault zone.

The Student's t-test and F-test results are shown in Table 5. The null hypothesis

Table 5. F and t-Tests on Creep Rate and Fault Width Distributions in Boxes 1 and 2 of Figure 14.

	box 1 avg	box 2 avg	t	$t_{\alpha=0.05}^a$	F	$F_{\alpha=0.05}^b$
Creep rates	(mm/yr)					
I vs. II	2.61	8.47	2.91	1.78	1.01	3.79
Fault widths	(m)					
I vs. II	26.1	11.3	18.7	1.78	3.85	3.79

^a Taken from Table 4, Press, et al., 1986.

^b Taken from Table 6(a), Press, et al., 1986.

(that the means of two samples are equal) is rejected for the comparisons of creep rates and fault widths in boxes 1 and 2, as $t > t_{\alpha=0.05}$. The null hypothesis (that the variances of two samples are equal) cannot be rejected for the creep rate comparison, but is rejected in the comparison of fault widths as $F > F_{\alpha=0.05}$. Thus, the statistics show that the means of creep rates and fault widths in the two boxes are significantly different. The variances of the creep rates are not significantly different, but fault widths are different. Table 6 lists creep rates and deformation patterns at each site.

Table 6. Alinement Array Creep Rates and Deformation Patterns.

#	Site Code	Creep rate ^a	Average Sec	St. Dev. mm	Topography ^b	Soil Stability ^c	Deformation Pattern	Fault Width (m)
1	XMM4 ^d	15.2	1.21	0.6	high relief	good	I	10
2	MDR4 ^d	7.9	1.39	0.8	high relief	poor	III	30-35
3	VAR4 ^d	6.6	1.45	0.5	high relief	moderate	I	24
4	PKW4 ^{de}	1.0	1.38	0.7	moderate	good	III	20
5	XPN4 ^d	9.1	1.24	1.2	flat	good	N / A	27
6	PKN4 ^d	1.9	1.63	1.6	slight	good	II	27
7	PKF4	8.6	1.07	1.1	flat	paved	N / A ^f	?
8	TAY4 ^d	11.2	1.82	1.4	high relief	good	I	11
9	RCW6 ^e	2.2	1.43	1.8	flat	good	III	?
10	XDR5	9.6	1.44	1.4	slight	good	I	15
11	HST4	6.5	1.63	1.6	moderate	moderate	I	12
12	WKR4 ^d	7.1	2.45	2.4	moderate	good	N / A	?
13	HSW4 ^{de}	-1.0	1.31	1.3	flat	good	III	20-40
14	KEN5	5.9	1.55	1.6	moderate	good	II	10
15	HAR4 ^e	1.0	1.90	1.9	slight	good	III	25
16	CRR4 ^d	4.4	1.30	1.3	flat	moderate ^g	II	11
17	GHG4 ^d	4.1	1.51	1.5	slight	good	N / A	?
18	PHG4 ^d	6.5	1.19	1.2	slight	good	I	10
19	XWT4	2.8	2.58	2.6	flat	poor	III	?
20	H464	-0.3	2.05	2.0	flat	moderate	II	30
21	X464 ^d	17.6	1.75	1.8	high relief	poor	N / A	?
22	PPP4	0.7	1.17	1.2	high relief	moderate	III	?

^a. From ES displacement (mm/yr).

^b. High relief ≥ 5 meters, moderate 5-3 meters, slight 3-2 meters, flat ≤ 2 meters.

^c. Not quantitatively determined. Good=little expansion or contraction, poor=highly expansive clay rich soils.

^d. Also a creepmeter site.

^e. Located on the Southwest Fracture Zone.

^f. Deformation pattern is controlled by the structure of the bridge.

^g. CRR4 is in an irrigated field.

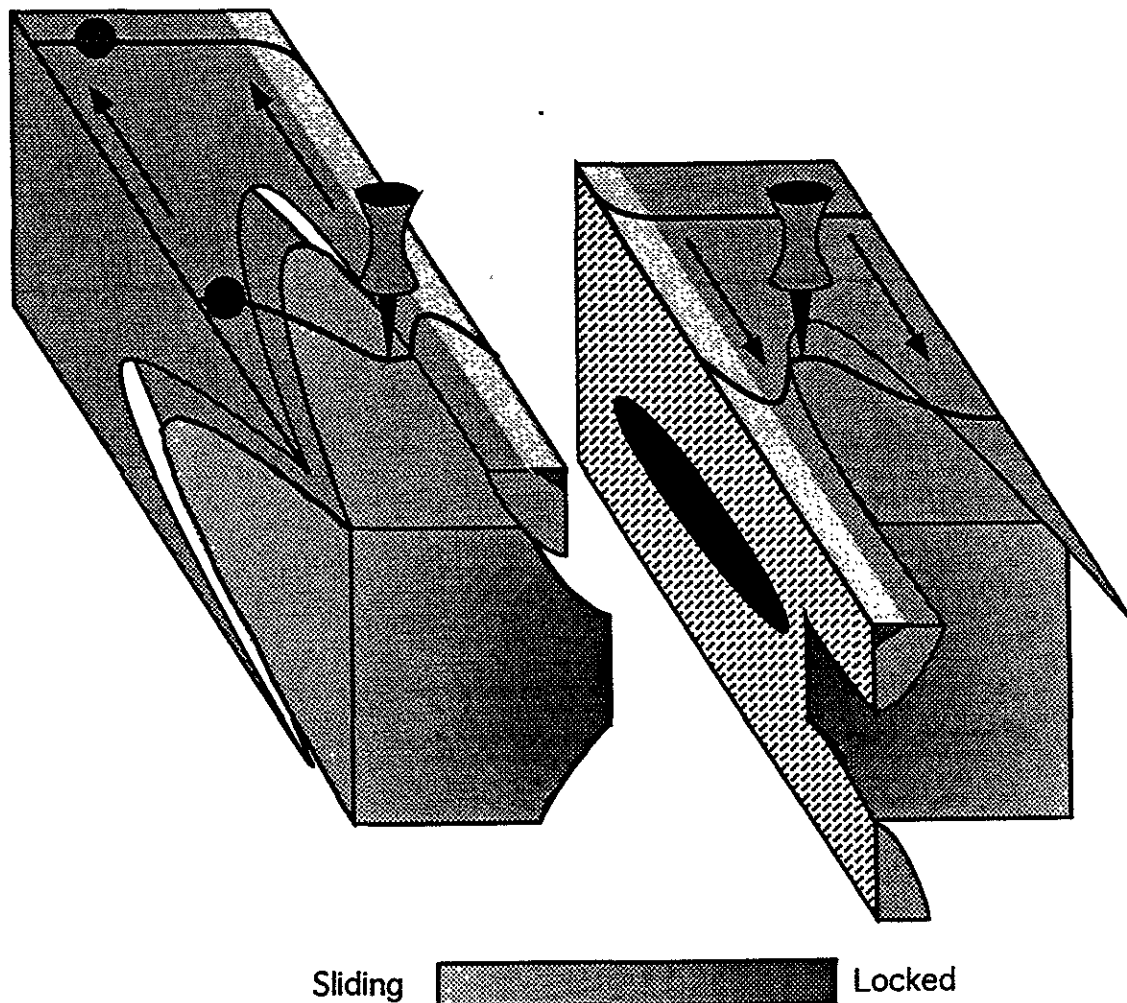
Deformation Mechanisms

Weldon and Springer (1988) suggested that shallow (2.1 km) maximum horizontal stress orientations near the SAF are variable and can differ from those driving the fault at depth. The varying deformation patterns suggests this is also the case at the near surface at Parkfield. The regional stress regime is nearly perpendicular to the trend of the SAF near Parkfield (Zoback and Zoback, 1980). In this section five mechanisms will be presented that can produce the observed deformation patterns. There can be as few as one or as many as five mechanisms causing the displacements, and the mechanism can change over time at a site.

Type I deformation is easily explained by two rigid blocks separated by a weak zone where simple shear is the dominant strain mechanism. The monuments in the rigid block maintain their relative positions while those in the fault zone are progressively displaced (Fig. 15, line I). The two blocks freely slide past each other.

The four mechanisms suggested below for developing Type II deformation are presented for discussion and for possible further investigation. The first possibility involves a shallow asperity below a slipping section of the fault. The second explains the observations on the basis of the timing of the initial survey and relative to a strain event and the subsequent relaxation of that event. The third possibility is that the main fault trace is flanked by auxiliary faults such that the blocks between the faults rotate. The fourth scenario being that the observed displacements are explained by nontectonic movements.

A shallow asperity below a creeping section of the fault could cause the monuments to be displaced in a manner that produces Type II deformation. Line II in Figure 15 shows a possible alignment array response to rocks at depth unable to freely slide because of a shallow asperity in the black area. The shaded area indicates the strain shadow as it spreads away from the asperity and intersects the surface. Even if the rocks at the surface are not strong enough to deform elastically at the scale of the alignment arrays, they could be responding by brittle fracture to strained materials at depth (Burford and Harsh, 1980). As the array passes through such a strain shadow the expected right-lateral displacement is inhibited because the fault is pinned at depth. The affect of the asperity on surrounding rocks



Type I and Type II deformation of alignment arrays.

Figure 15. Deformation Mechanisms. Type I deformation pattern is shown in the upper line (encircled I). The line remains unstrained in the rigid blocks outside of the weaker zone of rocks (stippled pattern). A high percentage of the total fault slip occurs within a narrow zone of simple shearing. The rocks in the shaded area have responded elastically to the asperity on the fault (strain shadow). Type II deformation pattern (encircled II) at the surface responds to elastically deformed rocks at depth across the shaded area and the weak rocks of the shear zone. See text for further explanation. The two blocks are separated to show the subsurface location of a shallow asperity (black filled area).

decreases with distance from the fault. The unaffected rocks (white areas) are displaced right-laterally (as expected).

The second possibility requires that the initial survey at a site occurs when the fault is locked and the rocks surrounding the array are strained. When the fault releases via a creep event or seismic slip the rocks closest to the fault are displaced further than those at a distance. Later surveys would then record the strain release along the fault. Thus, the displacement calculations show the greatest amount of change near the fault and in a left-lateral direction. Figure 16 shows the initial strain state during the first survey in the upper left and the corresponding initial plot of the monuments with zero displacement in the lower left. The upper right diagram shows the position of the rocks after the release of strain. The lower right diagram is the displacement determined by comparing the monument positions determined during the two surveys. This mechanism can also produce Type I deformation. Thus, there does not have to be more than one mechanism acting on the fault to produce two different deformation patterns.

A third possibility is that the main trace is flanked on both sides by auxiliary faults. These scenario gains credibility from the fact that a splay of the fault was mapped approximately 100 meters to the south of PKN4. Right-lateral movement on these faults could cause rotation of the block between the faults. These faults would have to die out or merge at depth with the main fault, otherwise they would add to the total amount of slip measured across the fault by far field geodetic techniques and a large discrepancy would arise between those and near field measurements of fault slip. Arguments against this possibility are that other splays of the fault have not been noted at the other three sites, and that rotation between fault splays would cause a space problem at the fault junction.

The fourth possibility is that Type II deformation is caused by nontectonic movement. Gravity sliding of the near surface material would be a likely form of nontectonic movement. But this can be ruled out as a possibility at three of the four sites because they are on flat ground.

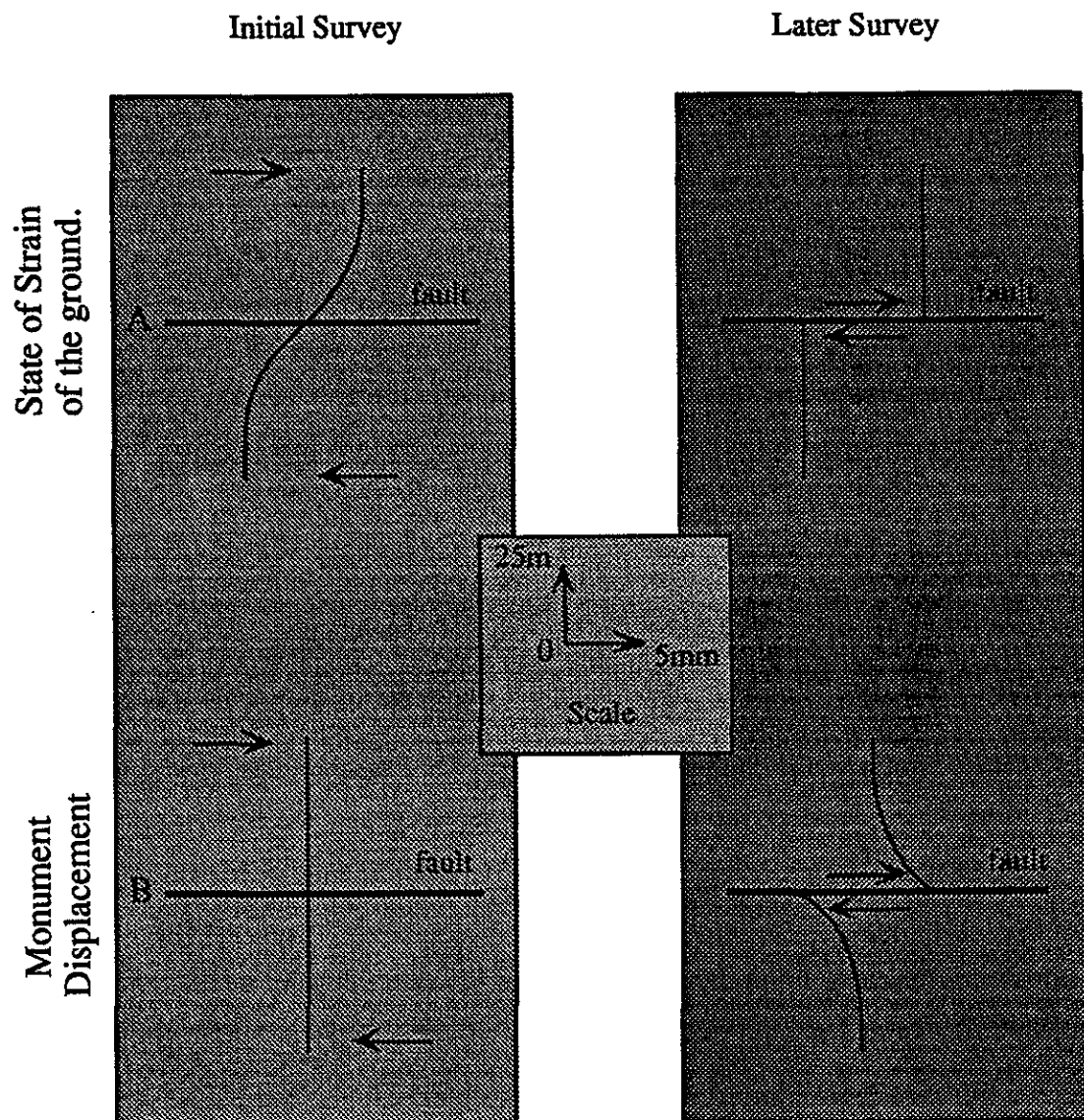


Figure 16. Possible Explanation for Type II Deformation. Top diagrams (A) show the state of strain of the ground around the array. The lower diagrams (B) show the deformation due to a release of strain that existed before the first survey.

Seismicity

Seismic activity along the Parkfield segment of the SAF varies directly with fault creep. The rates of fault creep and seismic activity decrease from the northwest to the southeast. This decrease in creep rates is expected as the Parkfield segment is the transition zone between the creeping section to the north and the locked section to the south (Fig. 17).

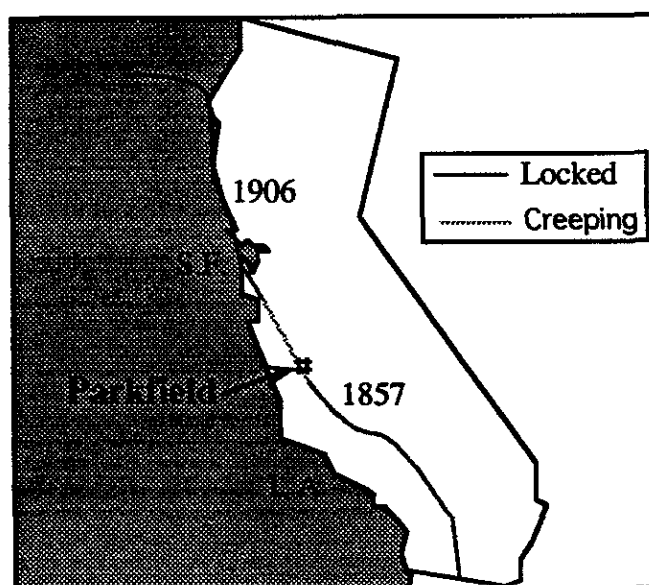


Figure 17. Location of Creeping and Locked Areas of the San Andreas Fault. During the great San Francisco and Ft. Tejon earthquakes in 1906 and 1857, respectively, were the last time these segments slipped.

The relationship of seismicity and aseismic fault movement is shown in Figure 18. Seismic activity and creep rates are both high to the northwest of Middle Mountain (at km 24 in Fig. 18). In the central section of the SAF creep is the dominant process for shallow slip (Hill, et al., 1990). Little if any shear strain is accumulating in the blocks on either side of the fault, and most seismologists believe that this section of the fault is unlikely to rupture in a

great earthquake. Decreases in both the seismic activity and the creep rates define the transition zone between the creeping section and the locked section to the southeast. The transition begins at the location of the 1966 earthquake hypocenter (star in Fig. 18) and the 5° bend in the surface trace of the fault. It terminates to the southeast at the 1 km right step-over.

The epicentral locations of post-1969 seismicity in the Cholame Valley region lie along the mapped traces of the SAF. Although, Poley and Lindh, (1987), report several earthquake epicenters located in southeastern Cholame Valley.

Scattered seismicity within the Coast Ranges surrounding the SAF is distinctly more intense in the Franciscan terrane east of the fault than in the granitic Salinian block to the west. The most significant seismicity away from the SAF is a series of earthquakes and aftershocks near Coalinga, northeast of the Parkfield area. The two largest being the Coalinga M 6.7 earthquake on May 2, 1983 and the Kettleman Hills M 5.7 earthquake on August 4, 1985. Both earthquakes involved reverse slip on northwest-striking planes subparallel to the strike of the SAF (Stein and King, 1984; Eaton, 1989) and are clear evidence of crustal convergence perpendicular to the SAF. These fault movements released much of the strain in the area, such that they slowed and/or reversed the direction of surface creep rates at creepmeters and alinement arrays in the Parkfield area. Also, mid-crustal seismicity rates decreased to near zero and remained low for the following 15 months (Schulz, 1989; Burford, 1988; Simpson, et al., 1988; Burford, et al., 1987; Poley, et al., 1987; Wilmesher and Baker, 1987). The creepmeter at Middle Mountain recorded left-lateral slip (rebound) for more than a year following the Coalinga event. Figure 24 (appendix) shows the initial survey of the alinement array at Middle Mountain just about the time the creepmeter returned to its normal rate of slip in mid-1984.

Comparison of Alinement Array and Creepmeter Creep Rates

The following section is a description of significant events in the alinement array and creepmeter data presented in the appendix. At Middle Mountain (XMM4), Figure 24

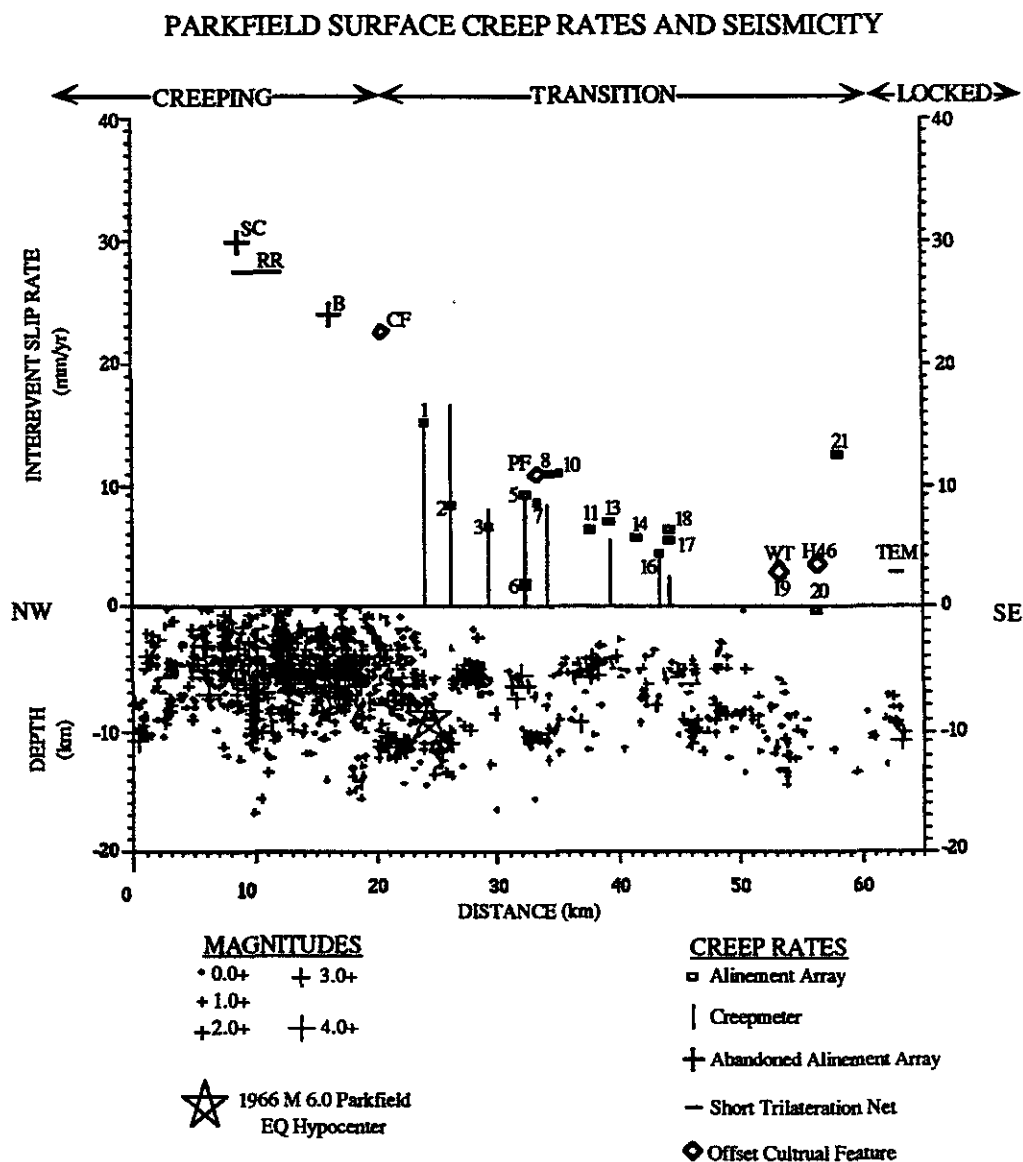


Figure 18. Plot of Seismicity and Surface Creep Rates. Earthquake hypocenters (crosses in lower box) from 1984 to 1992 are plotted on a vertical fault plane with interseismic surface creep rates determined from alinement arrays (boxes), creepmeters (vertical lines), abandoned alinement arrays (crosses), short trilateration networks (horizontal lines), and offset cultural features (diamonds) plotted above. The numbers next to the boxes correspond to the site numbers in Table 1. Both seismicity and creep rates decrease from the northwest to the southeast. The star indicates the approximate position of the 1966 earthquake hypocenter. The earthquakes were recorded at a minimum of ten stations with an rms of <0.008 .

shows a comparison of the creepmeter and ES displacement during the time period spanned by the first and last surveys (April 29, 1984-August 8, 1991). The beginning and ending alinement array data points very nearly overlie the creepmeter record. Although, data gathered from June 1985 to May 1988 and the single 1989 data point indicate a higher rate of fault slip recorded by the alinement array than is seen in the creepmeter data. Both instruments show a long-term creep rate of over 15 mm/yr averaged over the period from April 29, 1984 to August 8, 1991. The May 2, 1983 M_L 6.7 Coalinga earthquake (Simpson, et al., 1988; Poley, et al., 1987; Schulz et al., 1987) caused a period of left-lateral slip lasting more than a year after the earthquake. The fault creep returned to right-lateral slip in June, 1984.

At MDR4, the creepmeter record (XMD1) and displacement of the end points of the array do not agree (Figure 27). The creepmeter shows a slip rate of about 18 mm/yr from 1987 to 1990, then a decrease in rate to a little over 11 mm/yr from April 1990 to November 1991. The alinement array data shows a fairly constant rate of 8 mm/yr ± 0.3 from 1979 to November of 1991. The last two surveys indicate a similar decrease in creep rate as the creepmeter. The data from the alinement array is suspect because monuments may have been affected by gravitational movement on slopes. The OS is located on a fairly steep slope as are some of the DS's.

In Figure 30, the addition of insulation in VAR1 creepmeter vault in 1990 caused a decrease in the amplitude of the seasonal signal. The prominent rainfall-activated event recorded in the spring of 1991 does not affect the alinement array measurements. At the site of co-located alinement arrays PKN4, XPK4 and nearby creepmeter XPK1 an interesting relationship is seen in the displacement of monuments (Fig. 38). The amount of slip and strain measured were expected to increase with distance from the fault. But, at this site, the separation of DS's 2 and 6 parallel the measurement at the creepmeter and array XPK1 (no DS's). These measurements are markedly greater than the displacement at the ES. Hypotheses explaining this type of movement were presented earlier.

At PKF4, the data from two OS's agree fairly closely (Fig. 41). The shorter distance to OS#2 is the probable cause of the slightly higher measurement fluctuations. The TAY4

array should be extended, as the deflection plot in Figure 44 shows the instrument station on the edge of the fault. The result of adding insulation in the creepmeter vaults can be seen in the creepmeter record in 1990.

At WKR4 (Fig. 59) three lows in the alinement array reading correspond with highs in the creepmeter data. If the data are correct, this suggests that a phase shift of the seasonal signal is possible over a short distance. If two instruments could be installed in a manner that their combined records would cancel the seasonal signal, many alarms resulting from creep events caused by nontectonic forces could be avoided. Although the seasonal signal in the array data set is highly aliased, it would be interesting to see the results of more frequent surveys. In Figure 68, the large amplitude of the seasonal signal in the creepmeter data is due to irrigation. Irrigation in the area caused several surveys to be postponed.

Figure 83 shows divergence of two alinement arrays data sets from each other at alinement array X464. Both angle sets disagree with the flat creepmeter reading. Monument instability was certainly the cause. This is evident because the angle between the OS's changed over time.

The data from the four alinement array sites with Type II deformation, PKN4, KEN5, CRR4 and H464, suggest that a small change in the location of creep measuring instrumentation at these sites would result in a large change in the amount of creep measured.

Nontectonic Displacement of Monuments

Factors that adversely affect interpretation of the data are the position of monuments relative to the fault, non-tectonic movement of monuments, precision of the measurements and the frequency of measurements. If the monuments are too few or are poorly positioned across the active fault zone, the interpretation loses accuracy. Thus, arrays with closely spaced monuments in the area of interest better define displacements than do arrays with few monuments spanning long distances. Because the monuments were installed before the fault zone was well defined it is difficult to know where each monument should be

placed in order to characterize deformation across the fault zone. Non-tectonic movement of one or more stations will introduce error into the survey. Gravity sliding or expansion and contraction of the soils are potential causes of monument displacement. Also, P & K nails set in paved roads can be displaced by expansion and contraction of the asphalt. If the surveys are repeated infrequently, a shift of displacement from one area of the fault to another will be missed, as will seasonal affects.

Interpreting the survey data can also be difficult at sites where the rate of slip is very slow because of a low signal to noise ratio. For example, at site PKW4 the amount of movement of the monuments from the first survey to the second is very small and produces a pattern that is difficult to explain with a simple model (Fig. 33, lower plot). When the second survey was compared to the first survey (11/15/85), the changes in position of the monuments appear to be almost random.

One explanation for an unusual pattern of deformation such as this, is compensating affects of elastic strain and relaxation of the monuments in the ground. When the monuments are installed the steel pipes are pounded into the ground. Sometimes the pipe tilts, bends, and/or stops penetrating the ground when it encounters an obstacle. Random displacement of the monuments might be explained by elastic rebound of the monuments as they gradually recover their original shape after the first survey. Figure 19 A shows how a monument could undergo elastic strain when it is pounded into the ground. Figure 19 B shows how change in the near surface stress pattern could allow the pipe to rebound to its original shape, and cause the top of the pipe to tilt as it moves in the PVC pipe. A one degree bend in the pipe at its midpoint would produce a 13 mm offset of the top of the pipe if it were to return to its original shape while the pipe remains fixed from its midpoint to the bottom. Either tectonic or non-tectonic processes could cause a reduction of stress on the monument, and allow the pipe to return to its original shape. Once the pipe and the monument have stabilized, measurements of displacement should be accurate. In the case of PKW4, results of the second survey (7/17/86) may be used as the reference to which the others are compared (Fig. 33). Later position changes are then much easier to interpret.

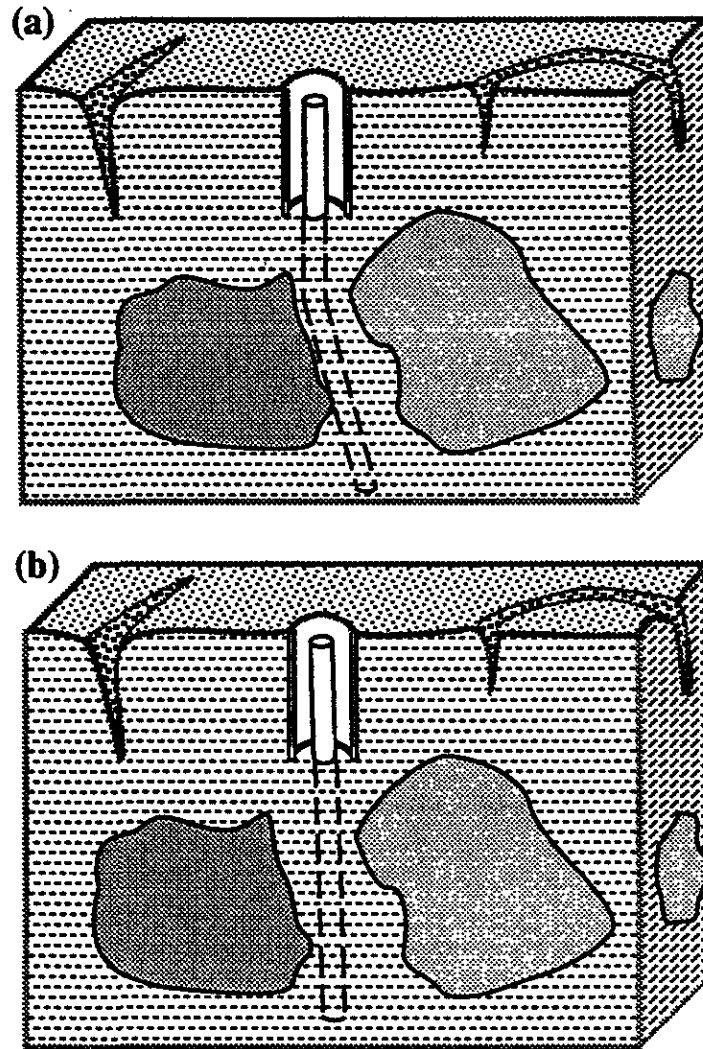


Figure 19. Block Diagrams of a Subsurface Monument. (a) The monument is forced to bend around a rock. (b) Slight movement of the rock allows the pipe to straighten, which causes a tilting of the top of the pipe.

New Survey Techniques

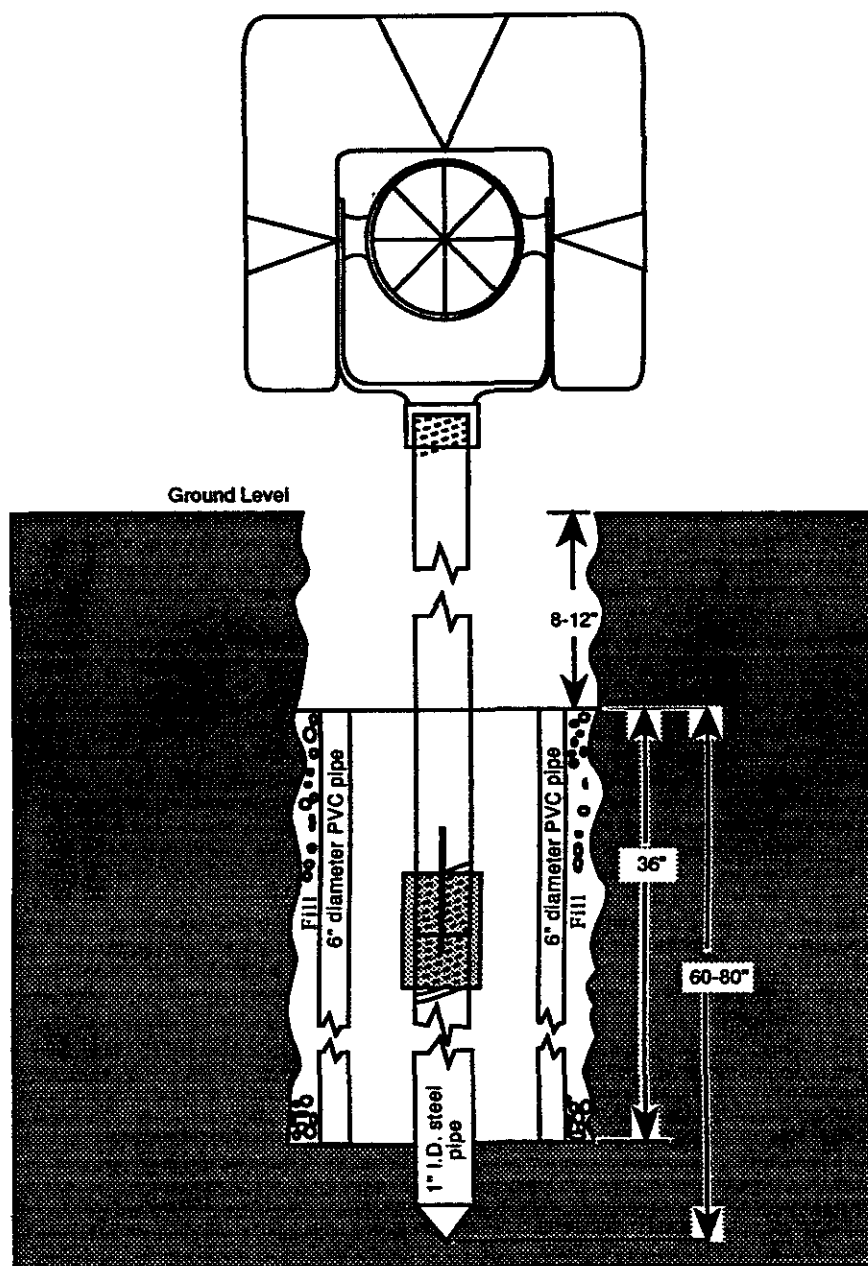
The technique used in this study cannot determine whether movements are due to fault slippage or to non-tectonic forces. Sites where the angle from the IS to two separate OS's (on the same side of the fault) change over time show where the present technique

falls short. But, if vertical angles and distances were measured to the OS's they could be used to determine which, if any of the monuments might not be stable. It might then be possible to ignore the moving reference point and not have to discard the data from the survey. The procedure suggested here has not been field tested to see if it can indeed produce the desired results.

At site X464 end point displacement varies widely depending on which OS is used in the determination. The monument at OS #1 (as shown in Fig. 4) is ≈ 100 meters to the northwest. OS #2 is a power line pole on the horizon approximately 2 miles to the south. The rate of creep measured by nearby creepmeters (Fig. 18) and offset cultural features are much lower than the alinement array rate for the last several years (Fig. 83). The creepmeter indicates little to no fault creep. The rate determined from the ES1/OS1 angle is approximately twice that of the ES1/OS2 angle. Also, the angle subtended by Station X464's two OS's and the IS (all of which are supposed to be on the same rigid block) changes over time. One possible explanation is that the three stations are not on the same rigid block, or perhaps, one or more of the monuments are unstable. At present it is not possible to determine the cause of the error.

With a new method of surveying using an electronic distance meter and measuring vertical angles, the amount of data per survey is tripled. In addition to the presently acquired angle data will be distance and leveling data to each station, including the wing stations. Also, instead of using a horizontal traverse target and the deflection target, a target that attaches directly to the monument via threads and holds a reflector and traverse target could be used (Fig. 20). This will eliminate errors inherent in setting up tripods over the wing stations and leveling the deflection target over each DS. A carpenter's level attached to the target would enable the investigator to take monument tilt measurements. Also, the precision of DS measurements will be equal to that of wing stations. The disadvantage to such targets would be the increased potential for disturbance of the monuments. Any time a monument touched there is some risk of displacing it. It might be possible to make a very precise coupling that would allow the target to be removed and then re-attached for each survey to reduce the risk of incidental contact.

Proposed New Monument



Not to scale

Figure 20. New Monument. A rod holding a traverse target and reflector threads into the subsurface monument, eliminating the need of targets with optical plummets.

The new procedure is shown in Figure 21. Although, it probably won't be faster,

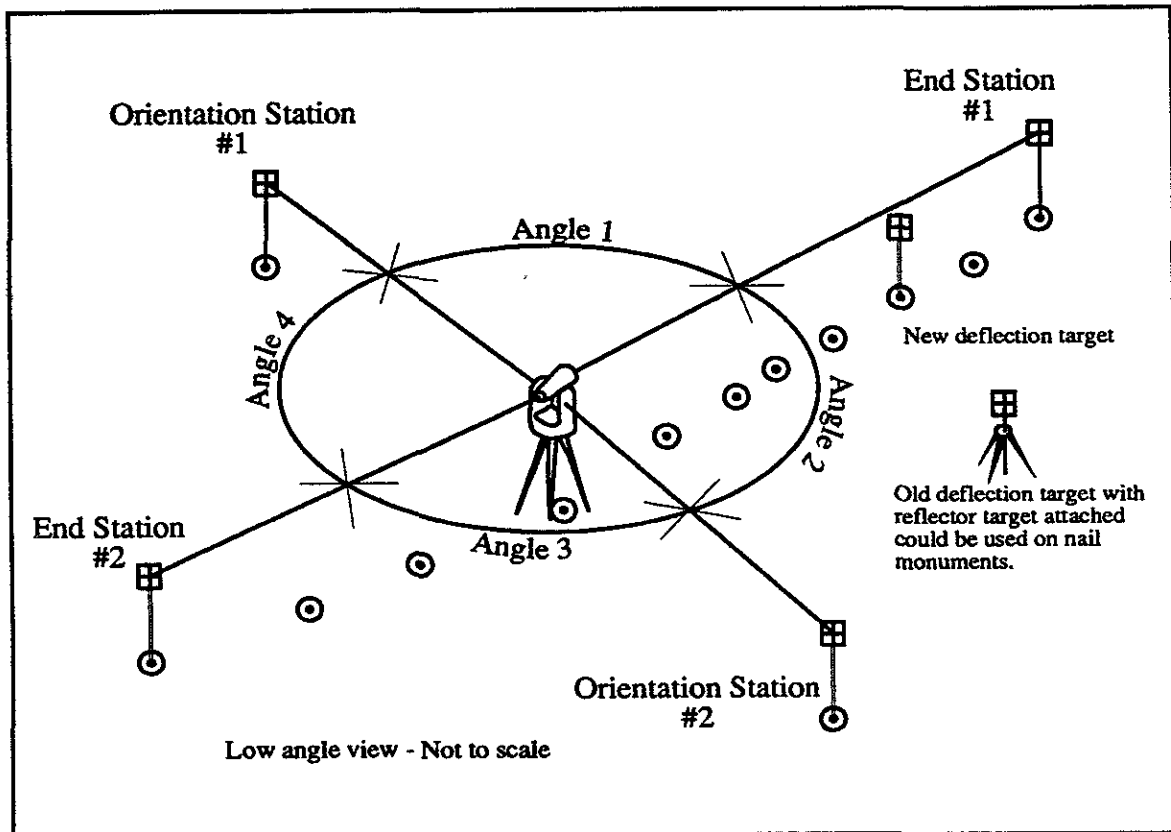


Figure 21. Proposed Field Procedure. A rod holding a target and reflector replaces the tripods, traverse targets and the deflection target.

the procedure could be completed by one person. After the instruments are set up, horizontal and vertical angles could be read for each monument. Three sets of angles would no longer be necessary because there are no longer optical plummets at the wing stations. With the same Wild T2000 theodolite at the instrument station, rotating the tribrach would not be necessary because the optical plummet is attached to the upper part of the theodolite and not in the tribrach. Once the horizontal and vertical angle measurements are completed, distances to each monument would be measured. Down-slope movement of monuments could be determined from the relative elevation changes between the monuments and the tilt measurements.

Conclusions

Results from repeated surveys of alinement arrays show creep rates on the SAF decreasing from a high at Middle Mountain (XMM4) of 15.2 mm/yr to a low of <1 mm/yr just southeast of Cholame Valley (PPP4). These creep rates are in general agreement with those determined from creepmeter records and from offset of some cultural features. The decrease in creep rates corresponds directly to a similar decrease in seismicity.

Fault widths vary from 10 meters (possibly less) at Middle Mountain to 35-40 meters at several other sites. The active fault trace is narrower to the northwest and wider to the southeast.

Data from WKR4 alinement array although sparse, suggests that recording of 180° phase shifts of the seasonal signal may be possible over a short distance. With careful study it may be possible to install an instrument in a creepmeter vault whose record summed with the creepmeter reading would cancel out the seasonal signal.

Deformation patterns determined by surveys of alinement arrays may have been produced by one to four different mechanisms, or a combination of the four, along the active fault trace. Type I deformation shows rigid-block motion on both sides of the fault separated by a narrow zone of homogenous simple shear. Type II deformation shows left-lateral offset in areas flanking the active fault and right-lateral simple shear across the fault. Two plausible explanations for Type II deformation are offered: 1) the array was first surveyed after a strain event and but before strain release; 2) a shallow asperity has pinned the fault at some depth resulting in local redistribution of stress and strain. Thus, an array crossing the pinned section would deform in a manner similar to Type II deformation. By lengthening the array at these sites, this effect could be positively identified.

Loss of usable data from two of the sites indicates that a better technique should be developed for alinement array surveys. Distance measurements, monument tilt measurements, and vertical angle readings gathered along with the data presently being collected should allow for more confident interpretation of the data, especially where one or more of the monuments are unstable.

References Cited

- Allen, C.R. and S.W. Smith, 1966, Pre-earthquake and post-earthquake surficial displacement, in Parkfield earthquakes of June 27-29, 1966, Monterey and San Luis Obispo Counties, California--preliminary report., *Bulletin Seismological Society of America*, v. 56, #4, p. 966-967.
- Argus, D.F., and R.G. Gordon, 1990, Pacific-North American plate motion from very long baseline interferometry compared with motion inferred from magnetic anomalies, transform faults, and earthquake slip vectors, *Journal of Geophysical Research*, v. 95, p. 17315-17324.
- Bakun, W.H. and A. G. Lindh, 1985, The Parkfield California earthquake prediction experiment, *Science*, v. 229, # 4714, p. 619-623.
- Bakun, W.H. and T.V. McEvilly, 1979, Earthquakes near Parkfield, California: Comparing the 1934 and 1966 sequences., *Science*, v. 205, p. 1375-1377.
- Bakun, W.H. and T.V. McEvilly, 1984, Recurrence models and the Parkfield, California, earthquakes, *Journal of Geophysical Research*, v. 89, #B5, p. 3051-3058.
- Brown, R.D.J., J.G. Vedder, R.E. Wallace, E.F. Roth, R.F. Yerkes, R.O. Castle, A.O. Waananen, R.W. Page and J.P. Eaton, 1967, The Parkfield-Cholame, California, earthquakes of June-August 1966--Surface geologic effects, water-resources aspects, and preliminary seismic data., *U.S. Geological Survey Professional Paper 579*, 66 pp.
- Burford, R.O., 1988, Retardations in fault creep rates before local moderate earthquakes along the San Andreas fault system, Central California, *PAGEOPH*, v. 126, #2-4, p. 499-529.
- Burford, R.O., S.S. Schulz and R.W. Simpson, 1987, Retardations in fault creep rates before local moderate earthquakes along the San Andreas fault system, central California., *U.S. Geological Survey Open File Report 87-591*, p. 845-867.
- Burford, R.O. and P.W. Harsh, 1980, Slip on the San Andreas fault in central California from alinement array surveys., *Bulletin of the Seismological Society of America*, v. 70, #4, p. 1233-1261.
- DeMets, C., R.G. Gordon, D.F. Argus, S. Stein, 1990, Current plate motions, *Geophysical Journal International*, v. 101, #2, p. 425-478.
- Dickinson, W.R., 1966, Structural relationship of San Andreas fault system, Cholame Valley and Castle Mountain Range, CA., *Geological Society of America Bulletin*, v. 77,

#6, p. 707-726.

Duffield, W.A., and R.O. Burford, 1973, An accurate invar wire extensometer, *Journal of Research U.S. Geological Survey*, v. 1, #5, p. 569-577.

Eaton, J.P., 1989, Dense microearthquake network study of northern California earthquakes, chap. 13 of *Litehiser, J.J., ed., Observatory seismology, a centennial symposium for the Berkeley Seismograph Stations*, Berkeley, University of California Press, p. 199-224.

Goult, N.R., and R. Gilman, 1978, repeated creep events on the San Andreas fault near Parkfield, California, recorded by a strain meter array, *Journal of Geophysical Research*, v. 83, #B11, p. 5415-5419.

Hanna, W.F., S.H. Burch, and T.W. Dibblee, Jr., 1972, Gravity, magnetics, and geology of the San Andreas fault area near Cholame, California, U.S. Geological Survey Professional Paper, 646-C, 29 pp.

Hill, D.P., J. P. Eaton, and L. Jones, 1990, Seismicity, *in The San Andreas fault system, California*, R.E. Wallace ed., U.S. Geological Survey Professional Paper, 1515, 283 pp.

King, N.E., P. Segall, W. Prescott, 1987, Geodetic measurements near Parkfield, California, 1959-1984, *Journal of Geophysical Research*, v. 92, p. 2747-2766.

Lachenbruch, A.H., and A. McGarr, 1990, Stress and Heat Flow, *in The San Andreas fault system, California*, R.E. Wallace ed., U.S. Geological Survey Professional Paper, 1515, 283 pp.

Langbein, J.O., R.O. Burford, and L.E. Slater, 1990, Variations in fault slip and strain accumulation at Parkfield, California: Initial results using two-color geodimeter measurements, 1984-1988, *Journal of Geophysical Research*, v. 95, #B3, p. 2533-2552.

Lienkaemper, J.J. and W.H. Prescott, 1989, Historic surface slip along the San Andreas fault near Parkfield, California., *Journal of Geophysical Research*, v. 94, p. 17647-17670.

Lindh, A.G. and D.M. Boore, 1981, Control of rupture by fault geometry during the 1966 Parkfield earthquake, *Bulletin of the Seismological Society of America*, v. 71, p. 95-116.

Mavko, G.M., S.S. Schulz and B.D. Brown, 1985, Effects of the 1983 Coalinga, California, earthquake on creep along the San Andreas fault, *Bulletin of the Seismological Society of America*, v. 75, p. 475-489.

Nason, R.D., 1973, Fault creep and earthquakes on the San Andreas fault, *In Proceedings of the Conference on Tectonic Problems of the San Andreas fault system*, Stanford University Publications in Geological Science, v. 13, p. 275-285.

- Poley, C.M., A.G. Lindh, W. H. Bakun, and S.S. Schulz, 1987, Temporal changes in microseismicity and creep near Parkfield, California, *Nature*, v. 327, p. 134-137.
- Poley, C.M., and A.G. Lindh, 1987, Parkfield seismicity: An overview-1969 to present, *EOS Transactions American Geophysical Union*, v. 68, p. 1345.
- Prescott, W. H., M. Lisowski, and J. C. Savage, 1981, Geodetic measurement of crustal deformation on the San Andreas, Hayward, and Calaveras Faults near San Francisco, California, *Journal of Geophysical Research*, v. 86, p. 10853-10869.
- Press, W.H., B.P. Flannery, S.A. Teukolsky, and W.T. Vetterling, 1986, *Numerical recipes: The art of scientific computing*, Cambridge University Press, pp. 818.
- Ross, D.C., 1989, Chronology of displacement on the San Andreas fault in central California: evidence from reversed position of exotic rock bodies near Parkfield, California., U.S. Geological Survey Open File Report, 89-571, p. 40.
- Schulz, S.S., G.M. Mavko, R.O. Burford, and W.D. Stuart, 1982, Long-term fault creep observations in central California, *Journal of Geophysical Research*, v. 87, #B8, p. 6977-6982.
- Schulz, S.S., G.M. Mavko, and B.D. Brown, 1987, Response of creepmeters on the San Andreas fault near Parkfield to the May 2, 1983, Coalinga earthquake, U.S. Geological Survey Professional Paper, 1487, p. 409-417.
- Schulz, S.S., and R.O. Burford, 1977, Installation of an invar wire creepmeter, Elkhorn Valley, California, August, 1977, U.S. Geological Survey Open File Report, 78-203.
- Schulz, S.S., 1989, Catalog of creepmeter measurements in California from 1966 to 1988, U.S. Geological Survey Open File Report, 89-650, microfiche.
- Sieh, K. E., R. H. Jahns, 1984, Holocene activity of the San Andreas Fault at Wallace Creek, California, *Geological Society of America Bulletin*, v. 95, p. 836-896.
- Simpson, R.W., S.S. Schulz, L.D. Dietz, R.O. Burford, 1988, The response of creeping parts of the San Andreas fault to earthquakes on nearby faults, *PAGEOPH*, v. 126, #2-4, p. 665-685.
- Sims, J.D., 1990, Geologic map of the San Andreas fault in the Parkfield 7.5 minute quadrangle, Monterey and Fresno counties, California, U.S. Geological Survey MF-2115.
- Sims, J.D., 1989, Field Guide to the Parkfield-Cholame segment of the San Andreas fault, central California., *in* The San Andreas Transform Belt: 28th International Geological Congress Field Trip Guidebook, T309, p. 98-103.
- Sims, J.D., 1988, Geologic map of the San Andreas fault zone in the Cholame Valley and Cholame Hills quadrangle, San Luis Obispo and Monterey counties, California, U.S. Geological Survey MF-1995.

- Sims, J.D., and J. Hamilton, 1991, Geologic map of the Cholame Quadrangle, San Luis Obispo County, California, U.S. Geological Survey MF-2170.
- Stein, R.S., and G.C.P. King, 1984, Seismic potential revealed by surface folding: 1983 Coalinga, California, earthquake, *Science*, v. 224, #4651, p. 869-871.
- Steinbrugge, K.V., E.G. Zacher, D. Tocher, C.A. Whitten, and C.N. Claire, 1960, Creep on the San Andreas fault, *Bulletin of the Seismological Society of America*, v. 50, p. 389-415.
- Tocher, D., 1960, Creep on the San Andreas fault - Creep rate and related measurements at Vineyard, California., *Bulletin of the Seismological Society of America*, v. 50, p. 396-404.
- Tocher, D., A. K. Cooper, and R. D. Nason, 1968, Fault creep measurements along the San Andreas fault (abstract), *Geological Society of America Program*, 62nd Annual Meeting, Reno, Nevada, p. 72.
- Tocher, D., 1969, Fault creep in central California, *in* *Premonitory Phenomena Associated with Several Recent Earthquakes and Related Problems*, L. E. Alsop and J. E. Oliver, Editors, EOS, *Transactions American Geophysical Union*, v. 50, p. 385.
- Zoback, M.L. and M.D. Zoback, 1980, State of stress in the western United States, U.S. Geological Survey Open File Report, 80-801, p. 359-432.
- Weldon, R.J., and J.E. Springer, 1988, Active faulting near the Cajon Pass well, southern California; Implications for the stress orientation near the San Andreas fault, *Geophysical Research Letters*, v. 15, #9, p. 993-996.
- Wesson, R.L., 1988, Dynamics of fault creep., *Journal of Geophysical Research*, v. 93, #8, p. 8929-8951.
- Wilmesher, J.F., and F.B. Baker, 1987, Catalog of alignment array measurements in central and southern California, from 1983 through 1986, microform, U.S. Geological Survey Open File Report, 87-280, pp. 157.

APPENDIX

Site Descriptions, Site Maps and Data Plots

Introduction

This appendix is a site by site catalog providing the reader with a site description, a site map and a plot of the results from repeated surveys. The purpose of the appendix is to provide the data for interpretation and to allow investigators to resurvey the site and compare their measurements to the original survey. The following section is a brief explanation of the data in the appendix.

The site description includes: the site name, the code name, longitude and latitude, the 7 1/2' USGS topographic quad that it can be found on, the original angles between wings stations, how to reach it; and a general description of the site. Below the description, the site is marked on the 2 1/2' square of the topo quad in which the site is located. The original angles along with the date of the first survey (Table 1.) will allow an investigator to resurvey a site and compare their results to previous surveys to determine displacements of monuments.

The site map follows the site description page and shows a map view of the array and surrounding instrumentation. The azimuths from the IS to the ES's and OS's are listed along with distances between all of the monuments, including the deflection stations. Azimuths and distances from local landmarks are given where possible to aid locating the monuments. Locating many of the monuments requires a metal detector because they are buried with no trace at the surface.

The third and last page of data for each site contains two x-y graphs. The first plot is a time series showing fault movement versus time. Time is marked along the x-axis (the beginning of a year is directly above the year text) and right-lateral displacement of the ES

parallel to the fault trace as a positive value and left-lateral as a negative value along the y-axis. The points are plotted with vertical error bars showing the uncertainty in their measurement. Although, the points are connected this is not meant to imply that fault motion was measured between the plotted points. The second plot displays deformation parallel to the local strike across the fault zone. The y-axis is distance, in meters, from the instrument station. The x-axis represents displacement of monuments, in millimeters, from their original positions to a position measured during a later survey. Each survey is offset along the x-axis from the previous survey an appropriate amount to prevent them from overlapping. The plots are not a time series, but a sequential plot of surveys showing displacement of the monuments from their original positions. Although, they do increase in elapsed time from left to right, with the initial survey at the left and the last at the right side of the plot. If a survey was completed without a measurement of the deflection stations then its data point on the top graph will not have a corresponding deformation plot on the bottom graph.

The determination of the rate of fault creep, the width of the fault zone, and the manner of deformation is from interpretations of these graphs. The rate of fault creep can be determined by using either of the two methods mentioned earlier, end station offset or least squares fit offset at the fault. The width of the fault zone is defined as the distance between the closest monuments on opposite sides of the fault that are relatively unaffected by fault zone shearing. The precision of this determination is constrained by the spacing of the monuments. The fault zone widths presented here are the maximum possible widths of the fault that has been active during the period of study.

Site Description

Station Code XMM4 Name Middle Mountain County Monterey
 Quad Stockdale Mountain Latitude 35° 57.5' Longitude 120° 30.1'
 ES1/OS1 100° 57' 52.3"

To Reach: From San Miguel take Vineyard Canyon Road 19 miles to a "T" intersection and turn south.

Proceed 4 miles to the Parkfield turnoff to the left, pass through town and proceed 5 miles to Varian Ranch on the left. Immediately past the entrance turn left on to dirt track, across the field and follow the trail ~2 miles. The creepmeter will be visible to the west in a swale. The alinement array runs east-west near the creepmeter instrument end.

General Description: The monuments are covered by rocks. The array crosses just north of the creepmeter and solar panels. The ES is on top of a ridge in the center of a dirt road. The IS is the 6th station northeast of the ES and is closest to the road. The OS is 9.03 meters northwest from a large tree southeast of the IS. Monuments were installed by the USGS in 1979.

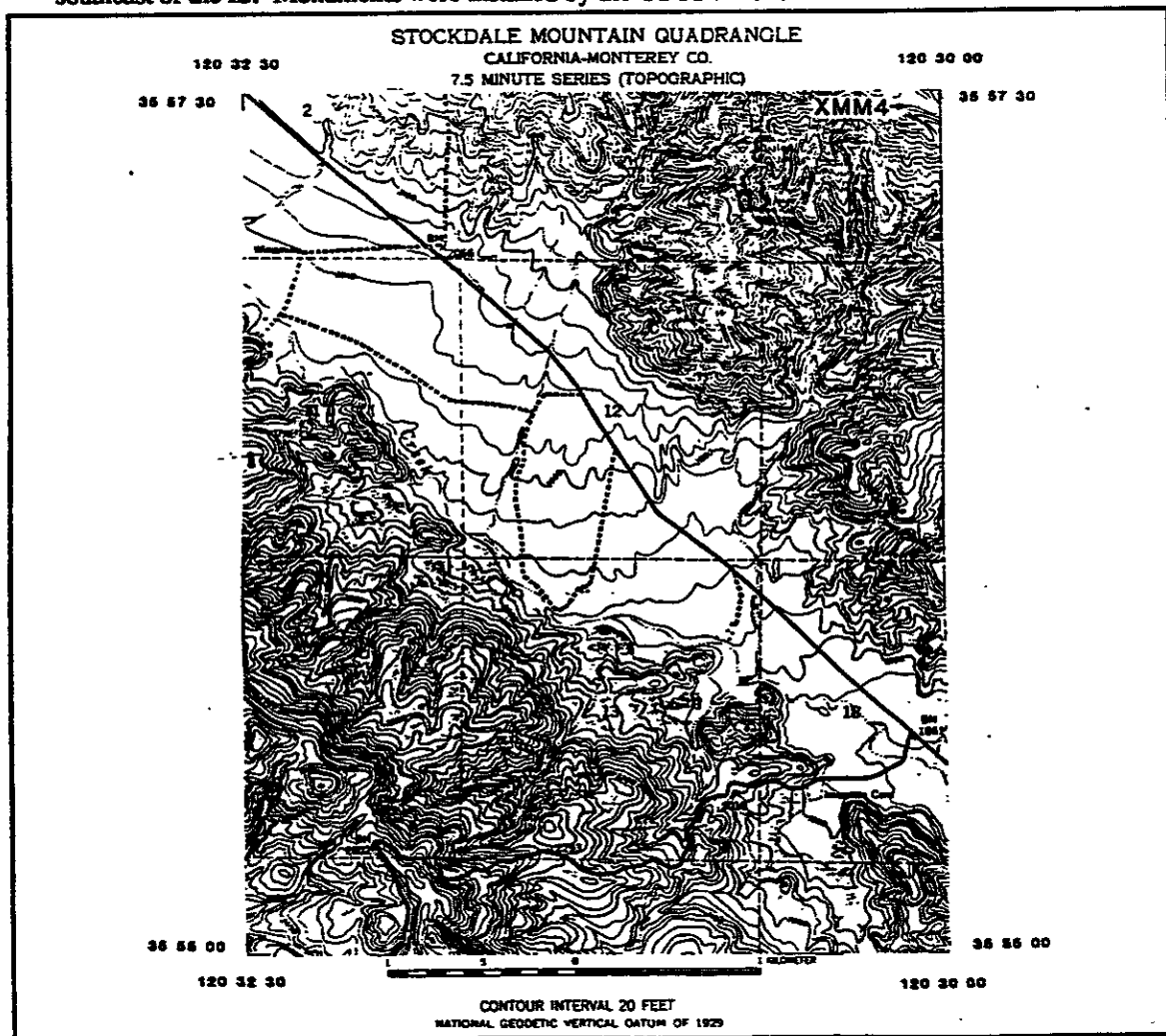


Figure 22. XMM4 Site Description.

Site Map

USGS : MIDDLE MOUNTAIN ALINEMENT ARRAY (XMM4)

4/29/84

(STOP AT RANCH HOUSE PRIOR TO ENTRY)

IS-ES	94.838m
IS-OS	69.71m
IS-1	23.788m
2	34.697m
3	44.717m
4	56.189m
5	91.117m

All survey marks of USGS
subsurface transit type

IS-ES Az 227.0°

IS-OS Az 131.5°

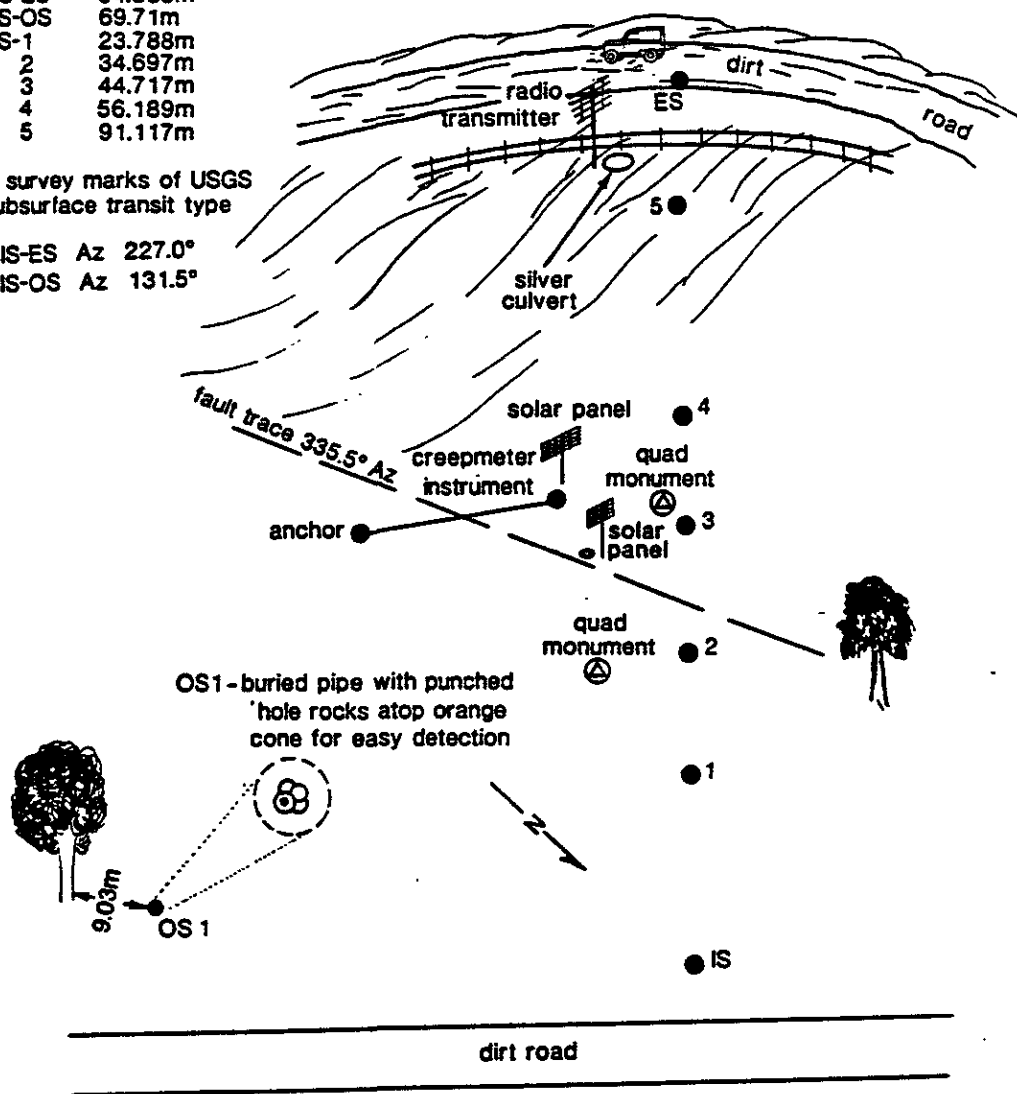


Figure 23. XMM4 Site Map.

Data Plots

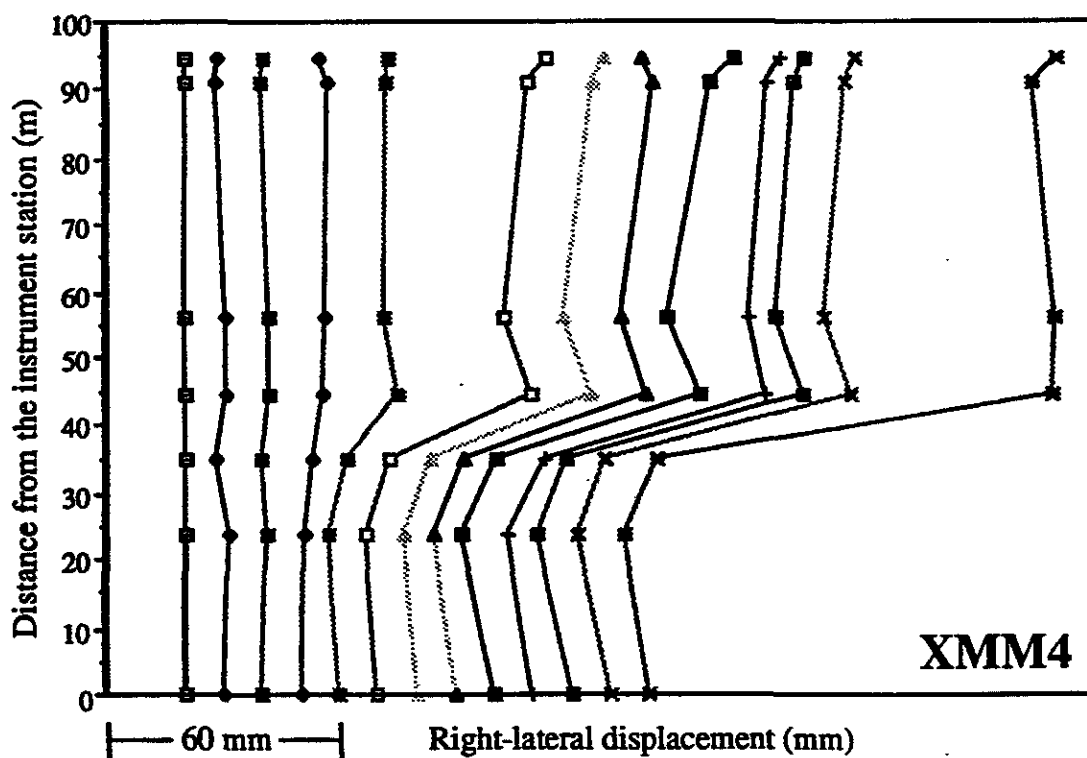
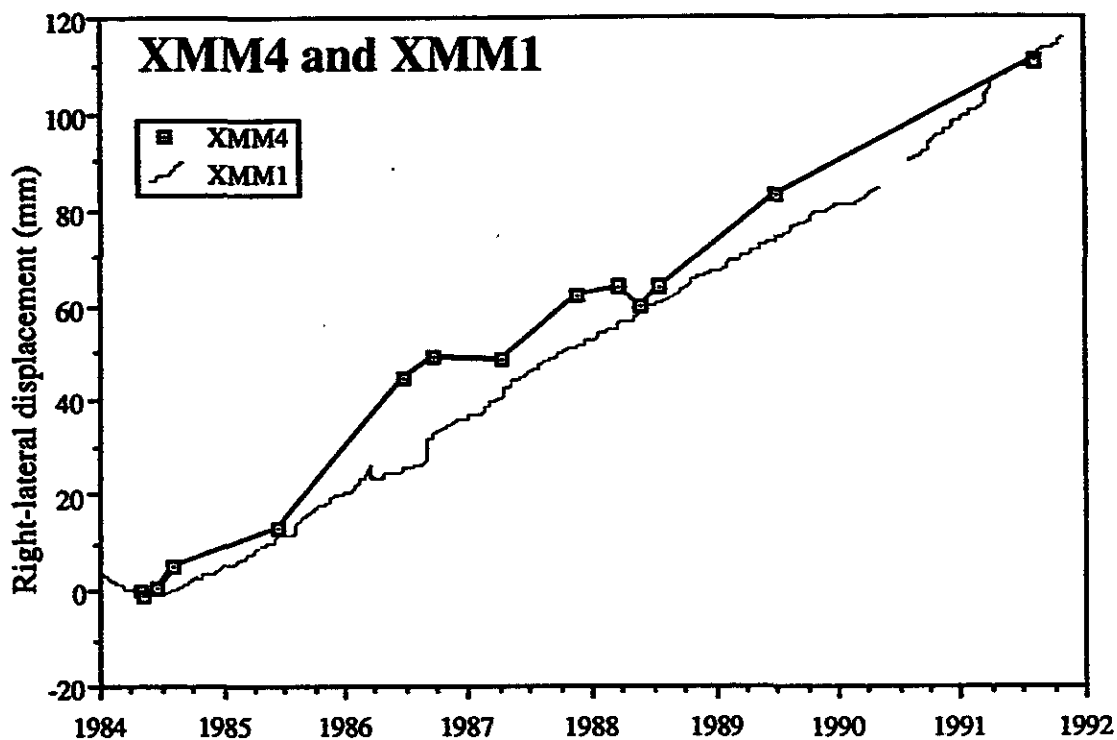


Figure 24. XMM4 Data Plots.

Site Description

Station Code MDR4 Name Middle Ridge County Monterey
 Quad Parkfield Latitude 35° 56.6' Longitude 120° 29.1'
 ES1/OS1 99° 24' 11.3" ES2/OS1 51° 16' 53.1"

To Reach: From San Miguel take Vineyard Canyon Road 19 miles to a "T" intersection, turn south and travel 0.6 miles and pass through a gate on the left near 2 mailboxes. Follow along the fence 0.17 miles and turn left. Proceed 0.6 miles through gate, right at fork, 0.3 miles left at fork. Then go .25 miles through gate, .22 miles left at fork, .036 miles veer left at windmill around corral and up the steep grade to the left. Proceed 0.57 miles, go right at fork through gap in fence. Make left turns at fork at 0.35 miles and again 0.10 miles further. Follow the trail 0.33 miles to the site.

General Description: The array is on top of a small ridge. The IS, both ES's and the OS are brass monuments marked with station numbers. The deflection targets are numbered yellow survey plugs. ES1 is 121.6 meters from the IS at an azimuth of 237°. ES2 is 61 meters from the IS at an azimuth of 91°. The OS is on a knoll 136.7 meters southwest of the IS beside a cow trail.

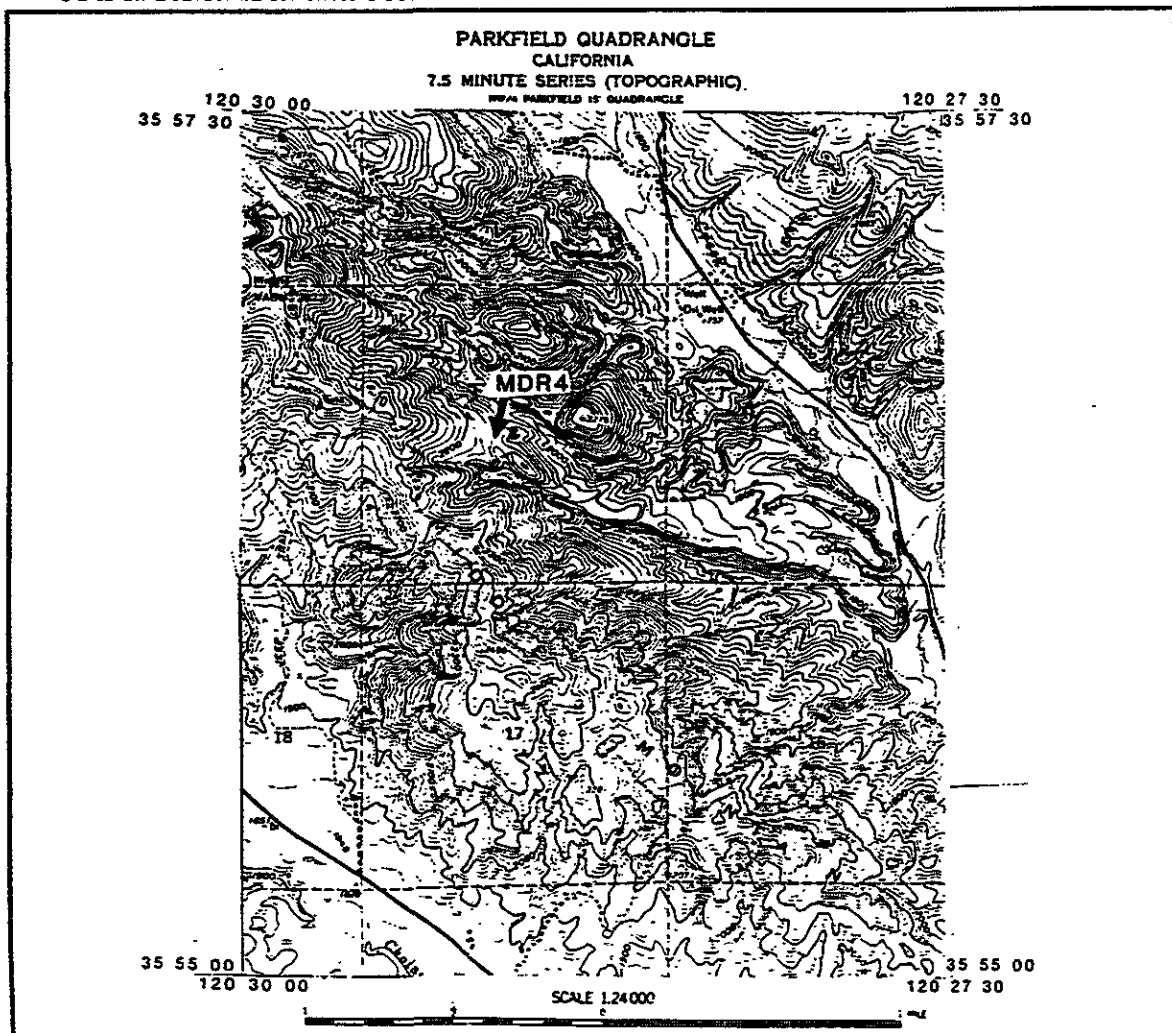


Figure 25. MDR4 Site Description.

Site Map

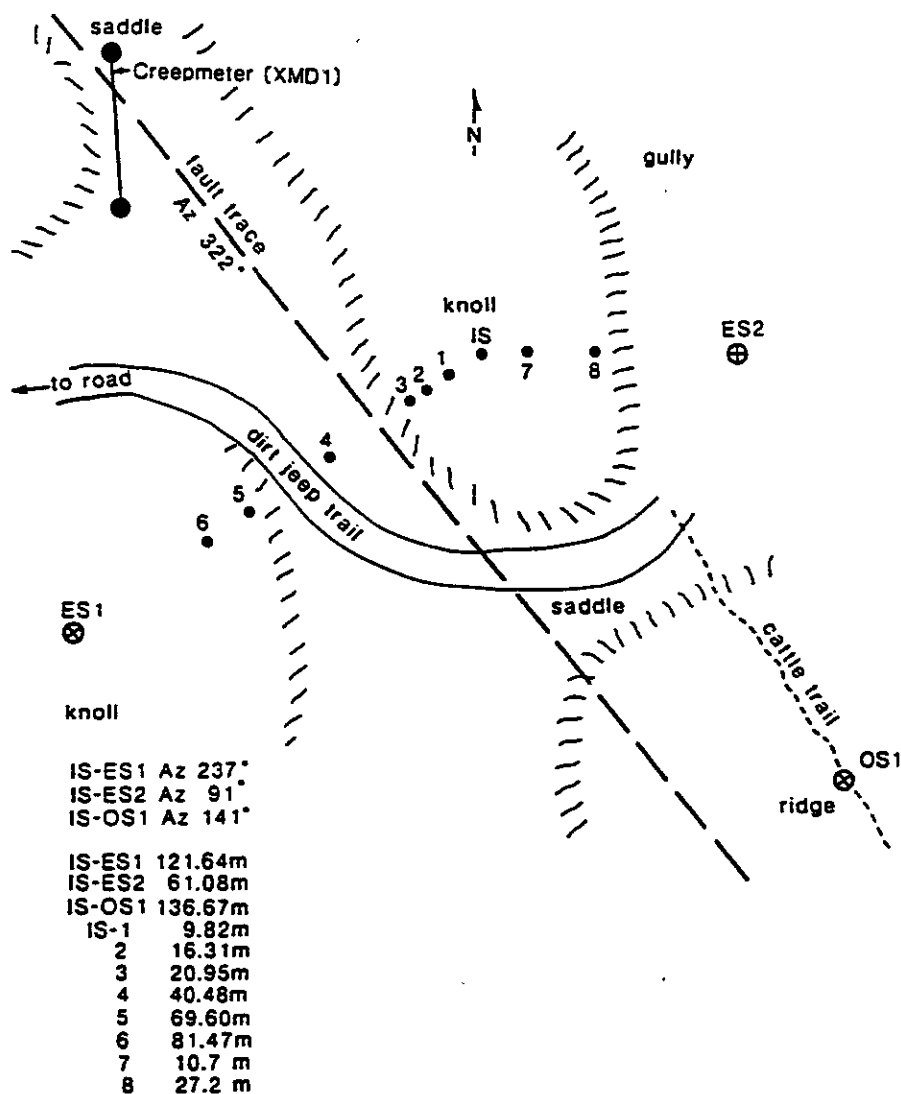
 USGS : MIDDLE RIDGE ALINEMENT ARRAY
 (MDR4) 6/10/86


Figure 26. MDR4 Site Map.

Data Plots

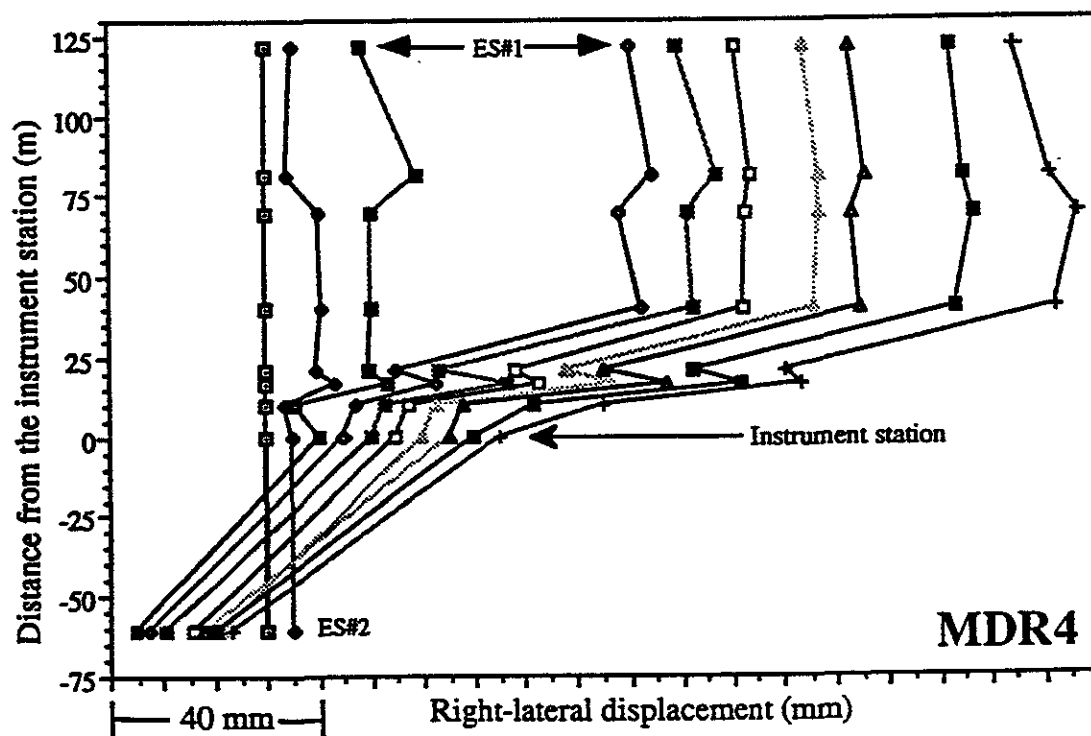
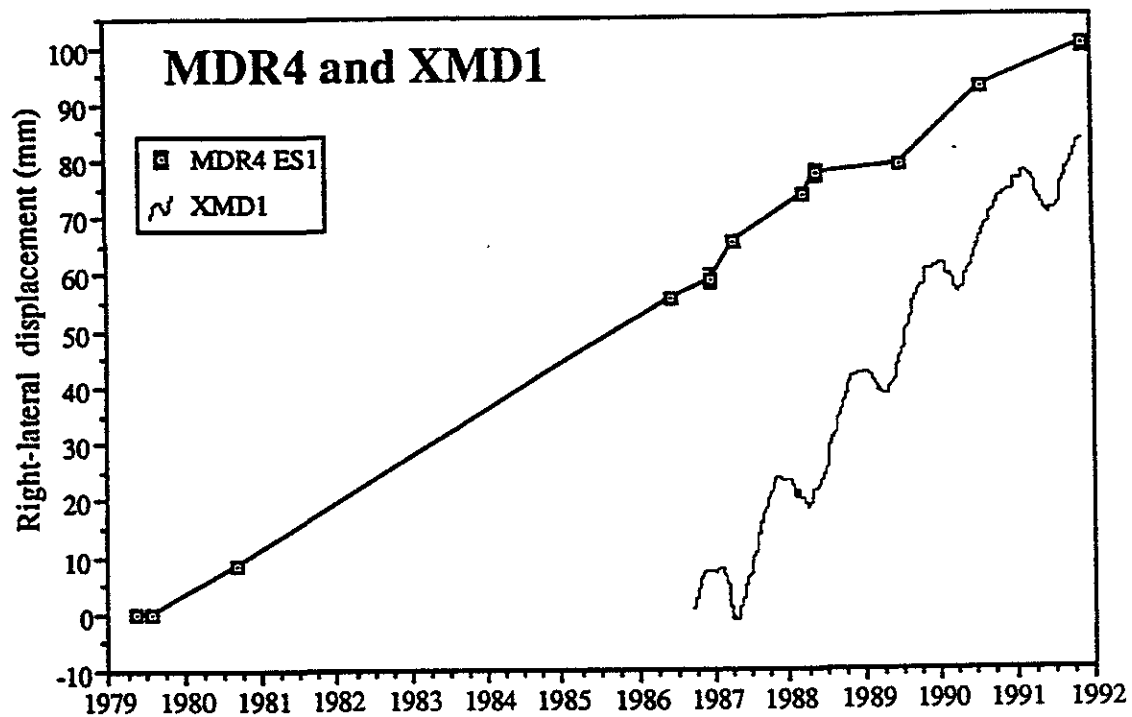


Figure 27. MDR4 Data Plots.

Site Description

59

Station Code VAR4 Name Varian Ranch County Monterey
 Quad Parkfield Latitude 35° 55.3' Longitude 120° 27.7'
 ES1/OS1 97° 58' 01.7" ES2/OS1 76° 46' 37.0"

To Reach: From San Miguel take Vineyard Canyon Road 19 miles to a "T" intersection and turn south.

Proceed 4 miles to the Parkfield turnoff to the left, pass through town and proceed 3.3 miles to the home of Blaine and Katy Santos (sign over the gate). Pass through wire gate at the north side of the house (lock combination is 2364). Cross the field toward the hill. Follow the jeep trail 0.7 miles and turn right at the fork. Continue to two metal fence posts on the left side of the trail protecting DS's 5 and 6 from traffic.

General Description: The IS and wing stations are brass monuments and the DS's are numbered yellow plastic plugs. The IS and ES are on opposite sides of the gully, southwest and northeast respectively.

The ES2 is on a knoll 112 meters away at an azimuth of 251° from the IS. The OS is beside an oak tree 89 meters away at an azimuth of 323° from the IS.

NOTE: BEFORE VISITING, CALL BLAINE SANTOS (805)463-2354 FOR PERMISSION TO ENTER.

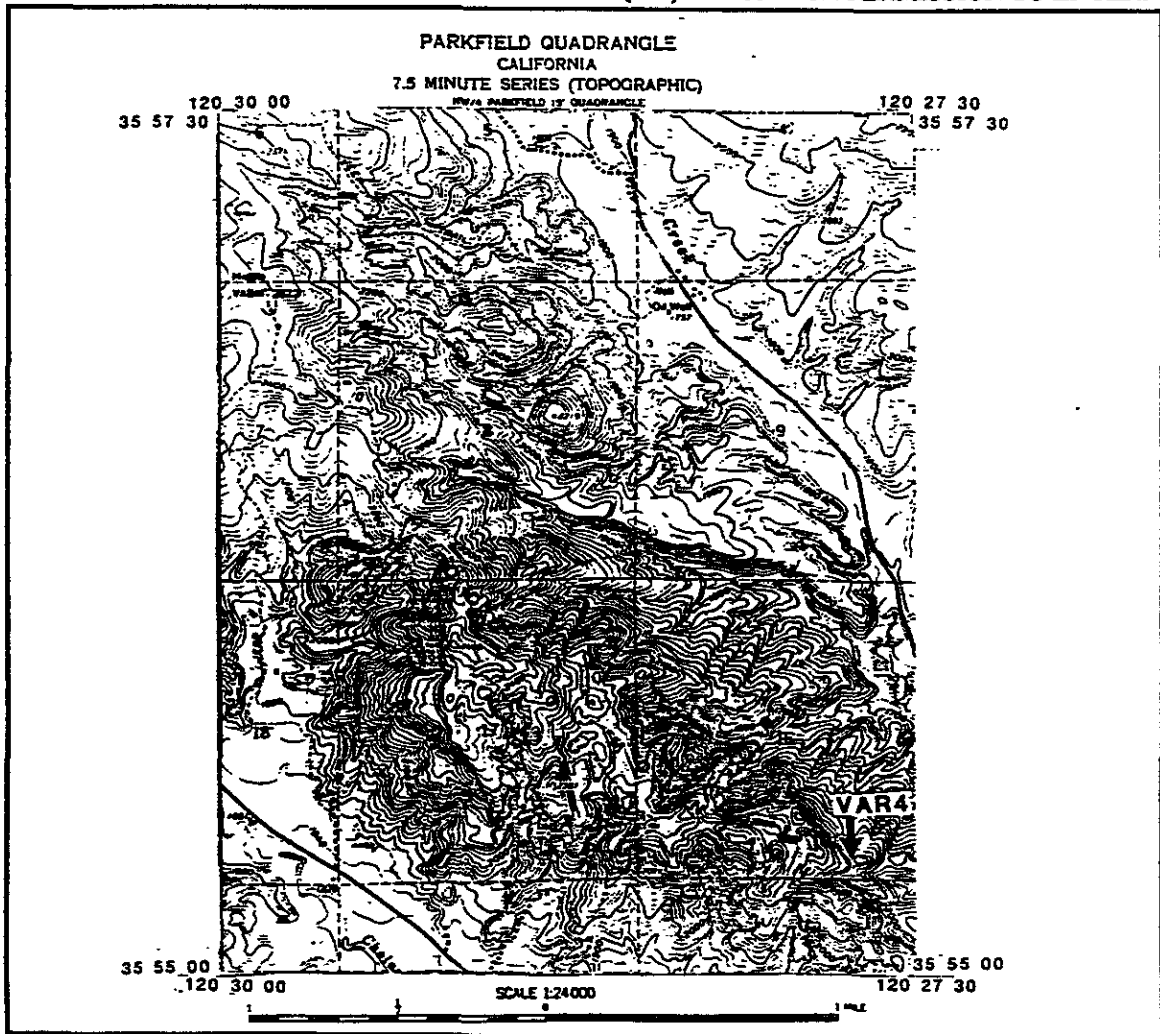


Figure 28. VAR4 Site Description.

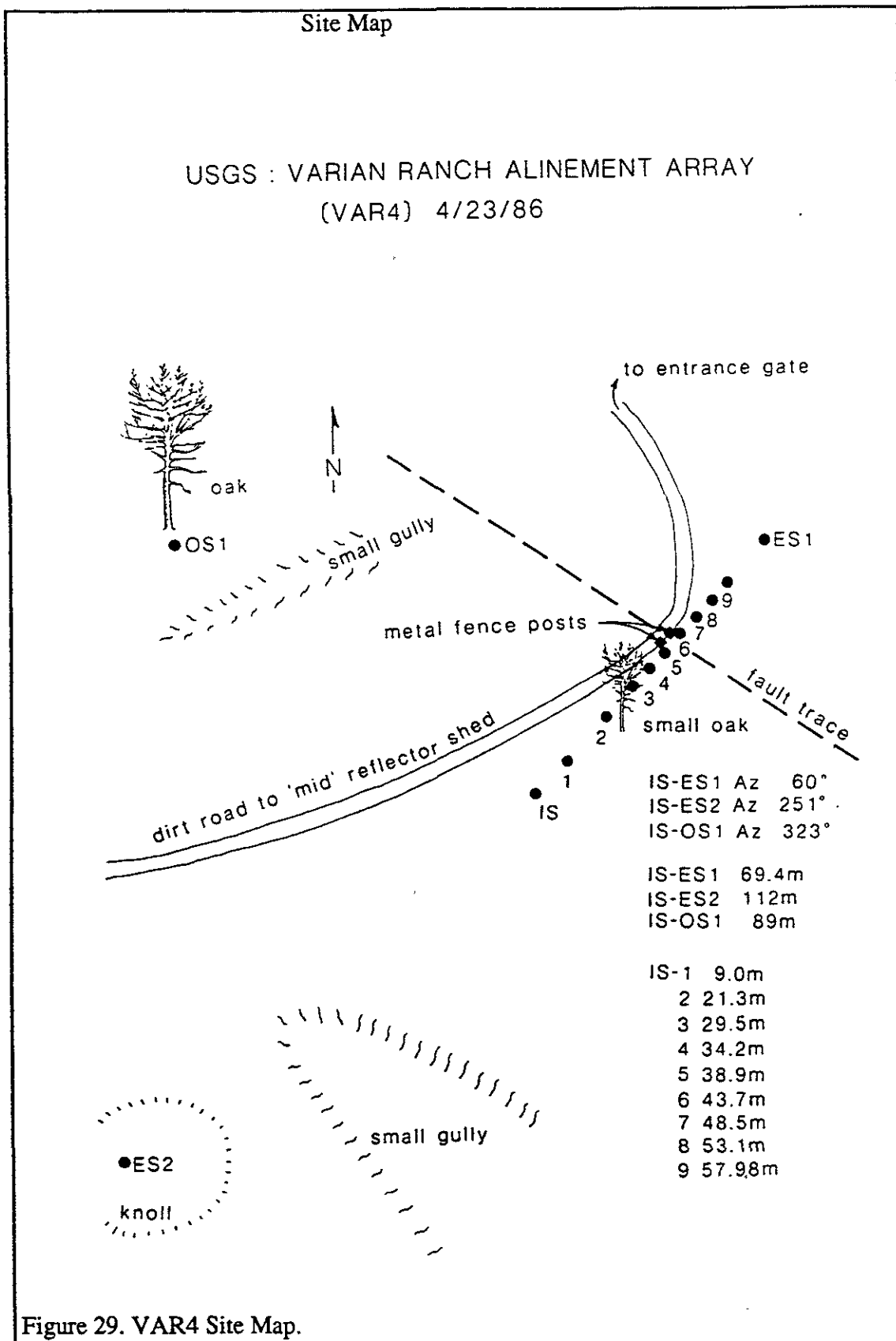


Figure 29. VAR4 Site Map.

Data Plots

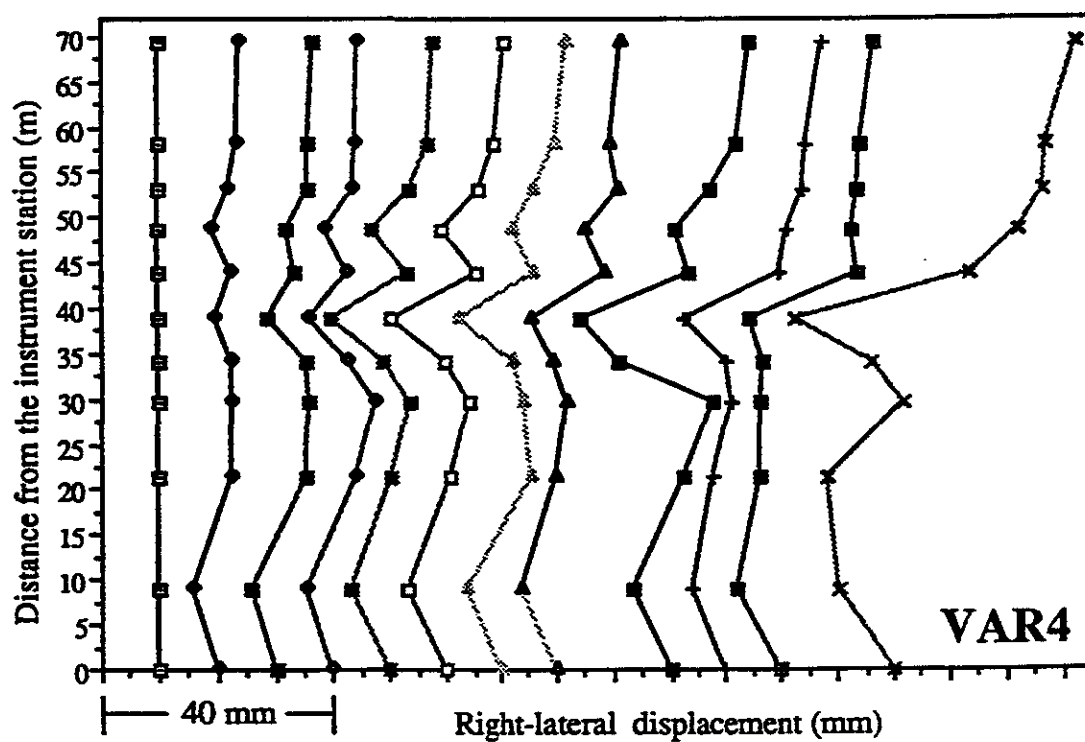
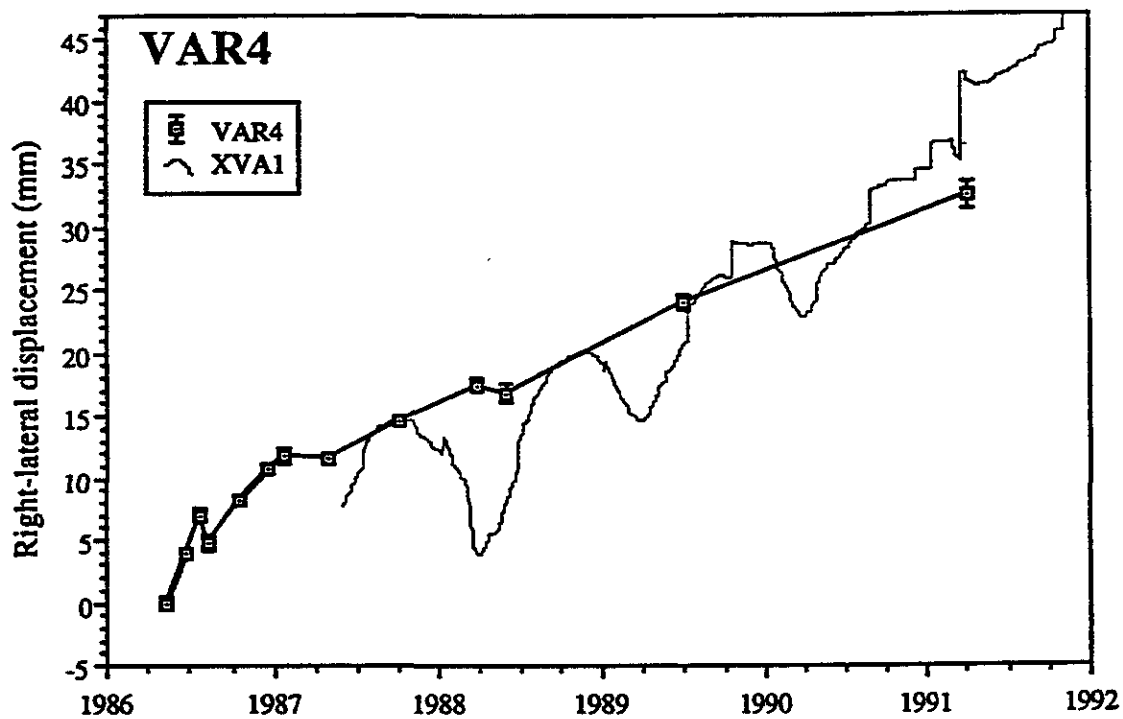


Figure 30. VAR4 Data Plots.

Site Description

Station Code PKW4 Name Parkfield Kester West County Monterey
 Quad Parkfield Latitude 35° 54.4' Longitude 120° 27.6'
 ES1/OS1 130° 55' 53.8"

To Reach: From San Miguel take Vineyard Canyon Road 19 miles to a "T" intersection and turn south. Proceed 2.75 miles to the Kester Ranch. Make a "U" turn in the driveway and park on the east side of the road next to the silos.

General Description: The array crosses the road about 50 meters north of the driveway. The IS is a P&K nail in asphalt 1 meter from the northeast side of the road and 10.4 meters from a tree just south of the 2 grain silos. ES1 is just west of a dirt jeep trail on top of the ridge in the field west of the main road. The OS is a P&K nail just south of the driveway, 3.93 meters from the first tree and 1 meter from the southwest edge of the road.

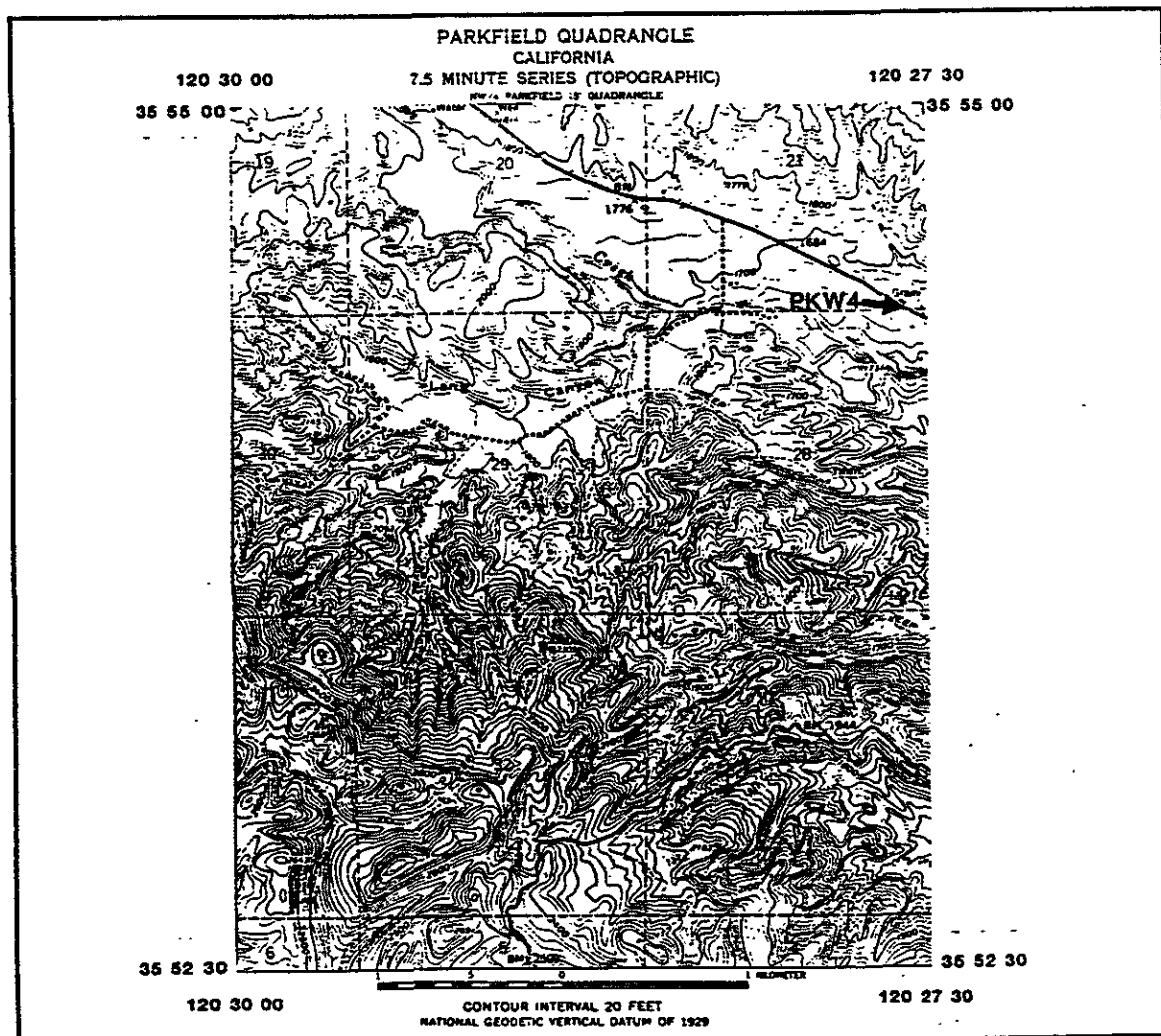


Figure 31. PKW4 Site Description.

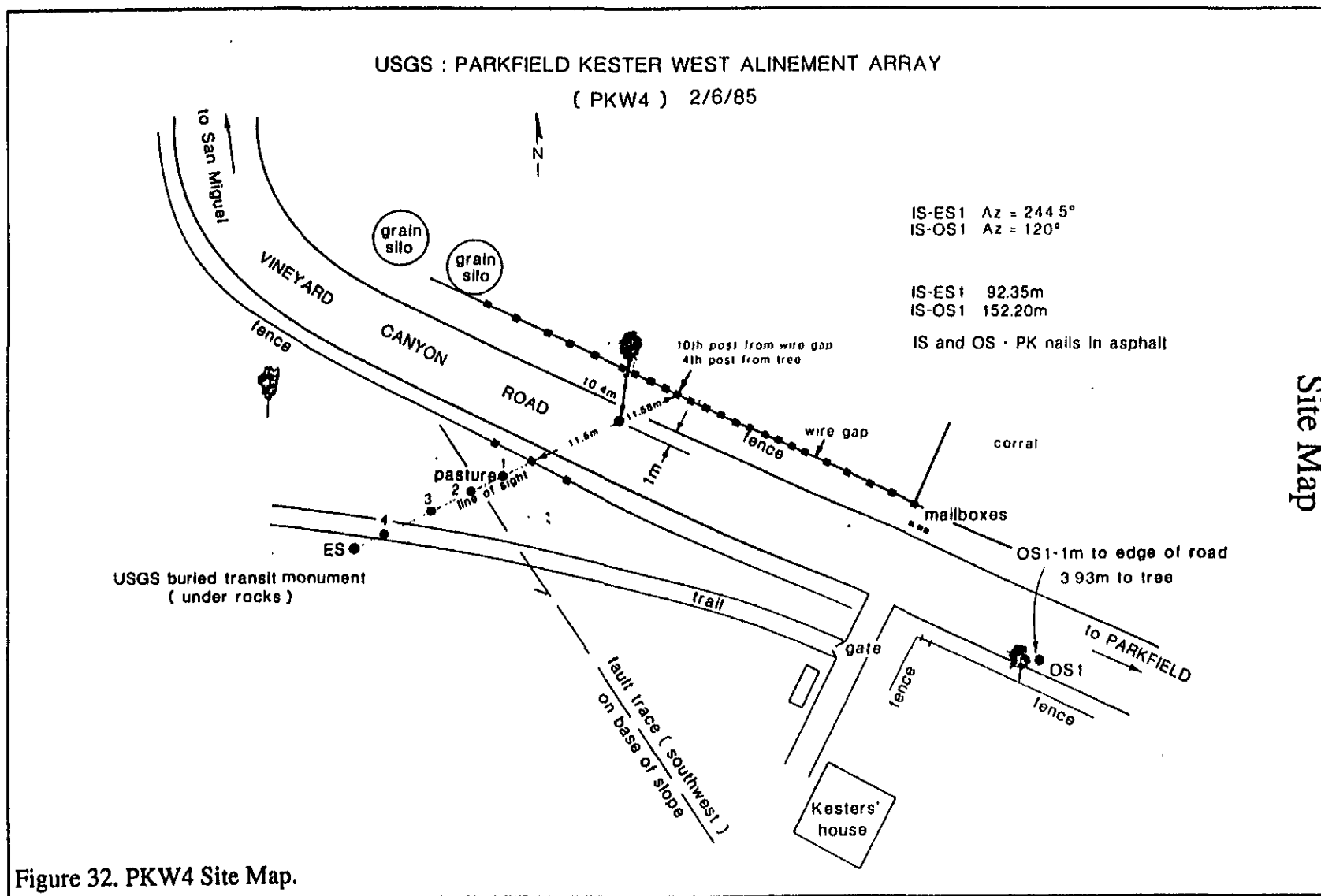


Figure 32. PKW4 Site Map.

Data Plots

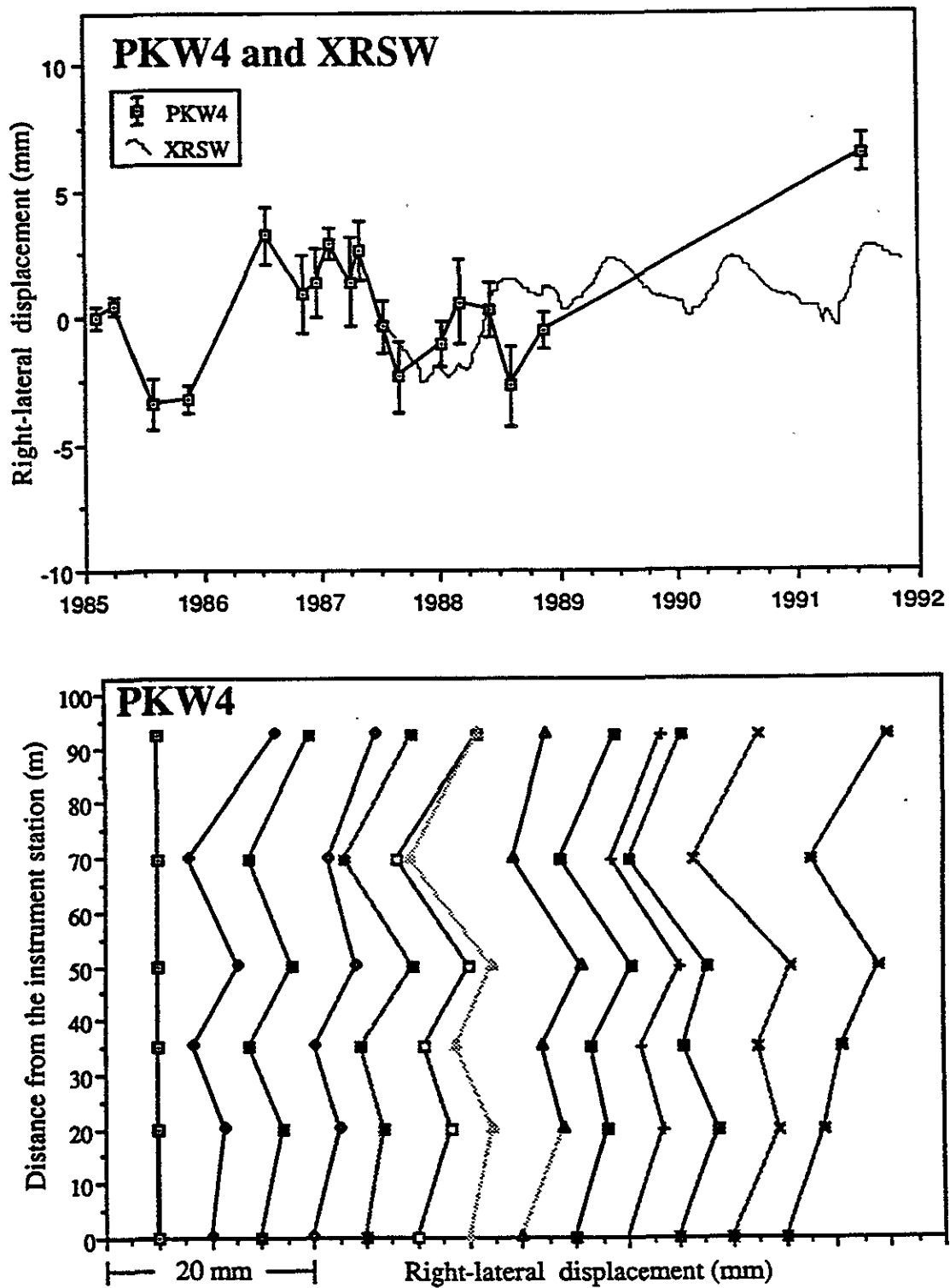


Figure 33. PKW4 Data Plots.

Site Description

65

Station Code XPN4 Name Parkfield North County Monterey
 Quad Parkfield Latitude 35° 54.0' Longitude 120° 18.5'
 ES1/OS1 96° 47' 30.4"

To Reach: From San Miguel take Vineyard Canyon Road 19 miles to a "T" intersection and turn south.

Proceed 3.83 miles to a driveway on the left side of the road. Park alongside the road next to the driveway.

General Description: The IS and OS are P&K nails set in the road. The IS is 0.9 meters from the edge of the asphalt in front of the driveway. The OS is 0.37 meters from the north edge of the road and 5.25 meters from the second telephone pole north of the driveway. The ES is a subsurface monument near the northwest corner of the goat barn at the base of the slope.

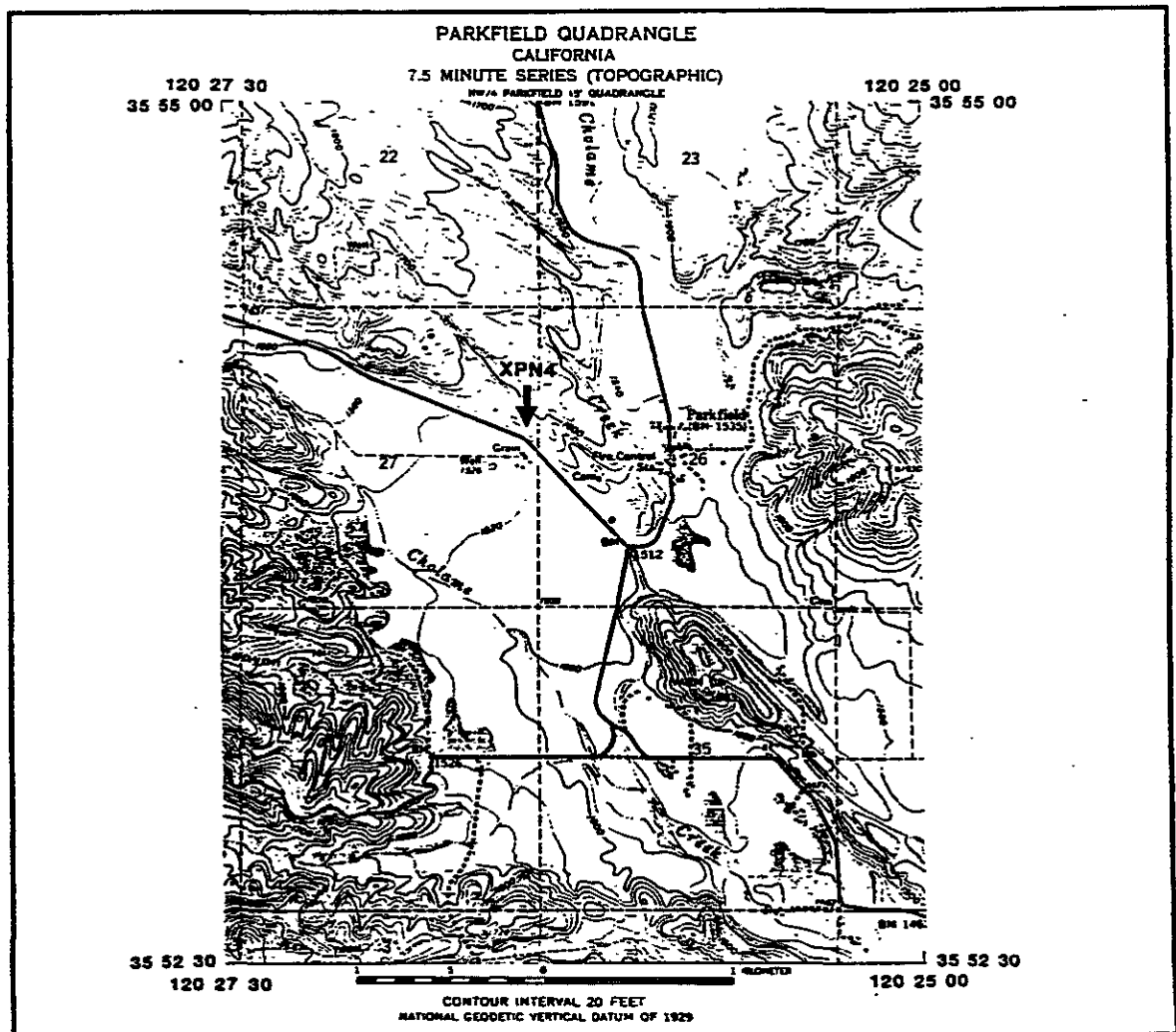


Figure 34. XPN4 Site Description.

Site Description

66

Station Code PKN4 Name Parkfield New County Monterey
Quad Parkfield Latitude 35° 54.0' Longitude 120° 18.5'
ES1/OS1 115° 50' 01.3"

To Reach: From San Miguel take Vineyard Canyon Road 19 miles to a "T" intersection and turn south.

Go 3.83 miles and turn left into a driveway. Park near the entrance to the corral.

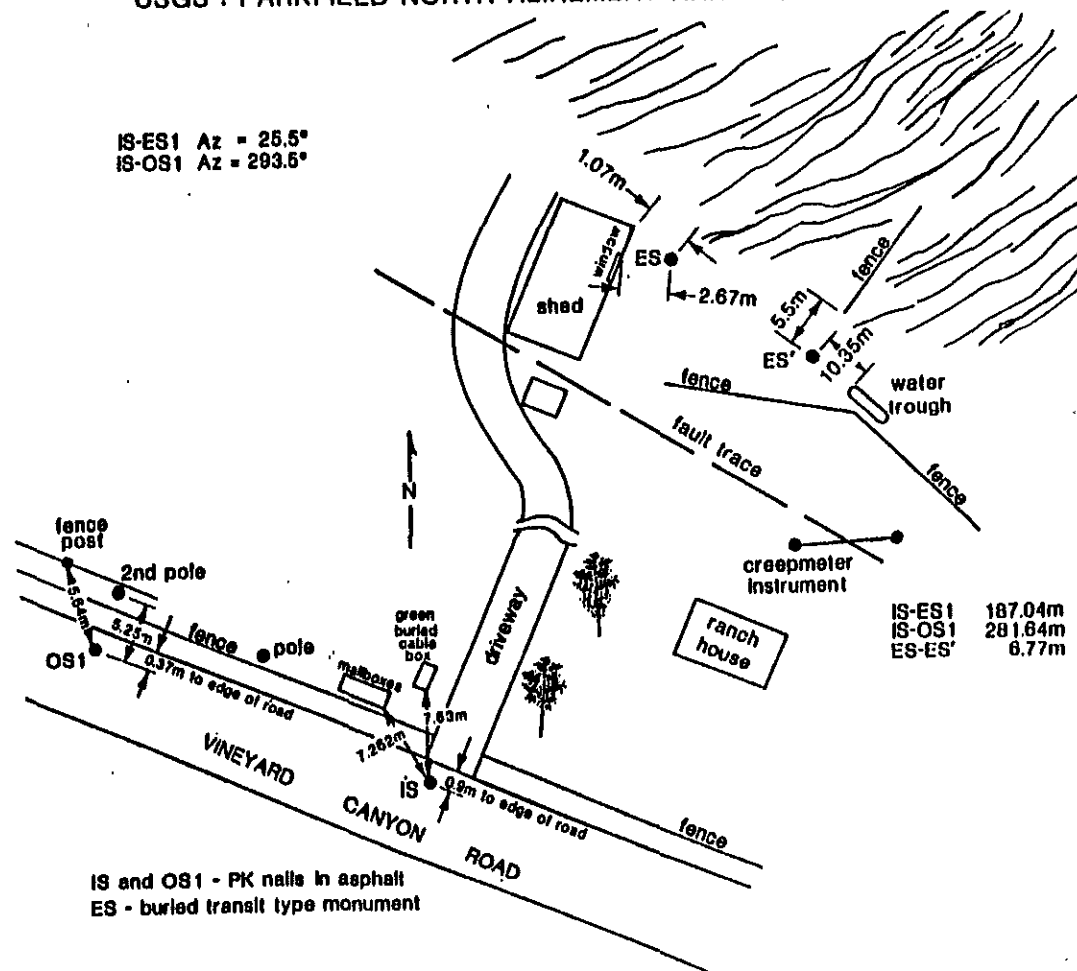
General Description: The monuments are subsurface pipes with yellow plastic plugs except the OS which is a P&K nail set in an oak tree northwest of the IS. The IS is just outside the entry to the corral. The deflection stations and ES are aligned at a bearing of 47° from the IS. The ES is just outside the corral on the hillside.

See XPN4 Map. These sites are colocated.

Figure 35. PKN4 Site Description.

USGS : PARKFIELD NORTH ALINEMENT ARRAY (XPN4) Installed 12/27/84

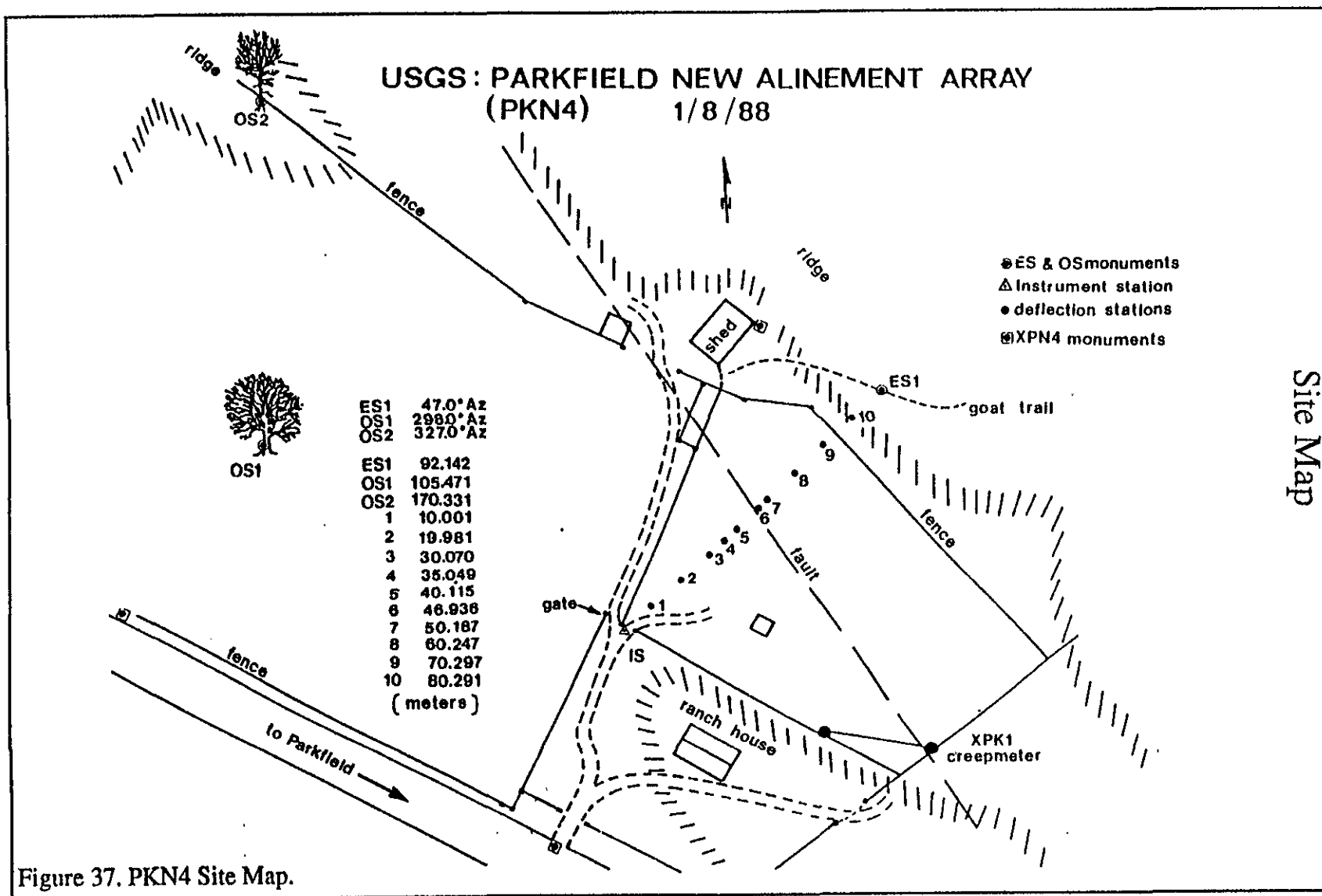
IS-ES1 Az = 25.5°
IS-OS1 Az = 293.5°



IS-ES1 187.04m
IS-OS1 281.84m
ES-ES' 6.77m

Site Map

Figure 36. XPN4 Site Map.



Site Map

Data Plots

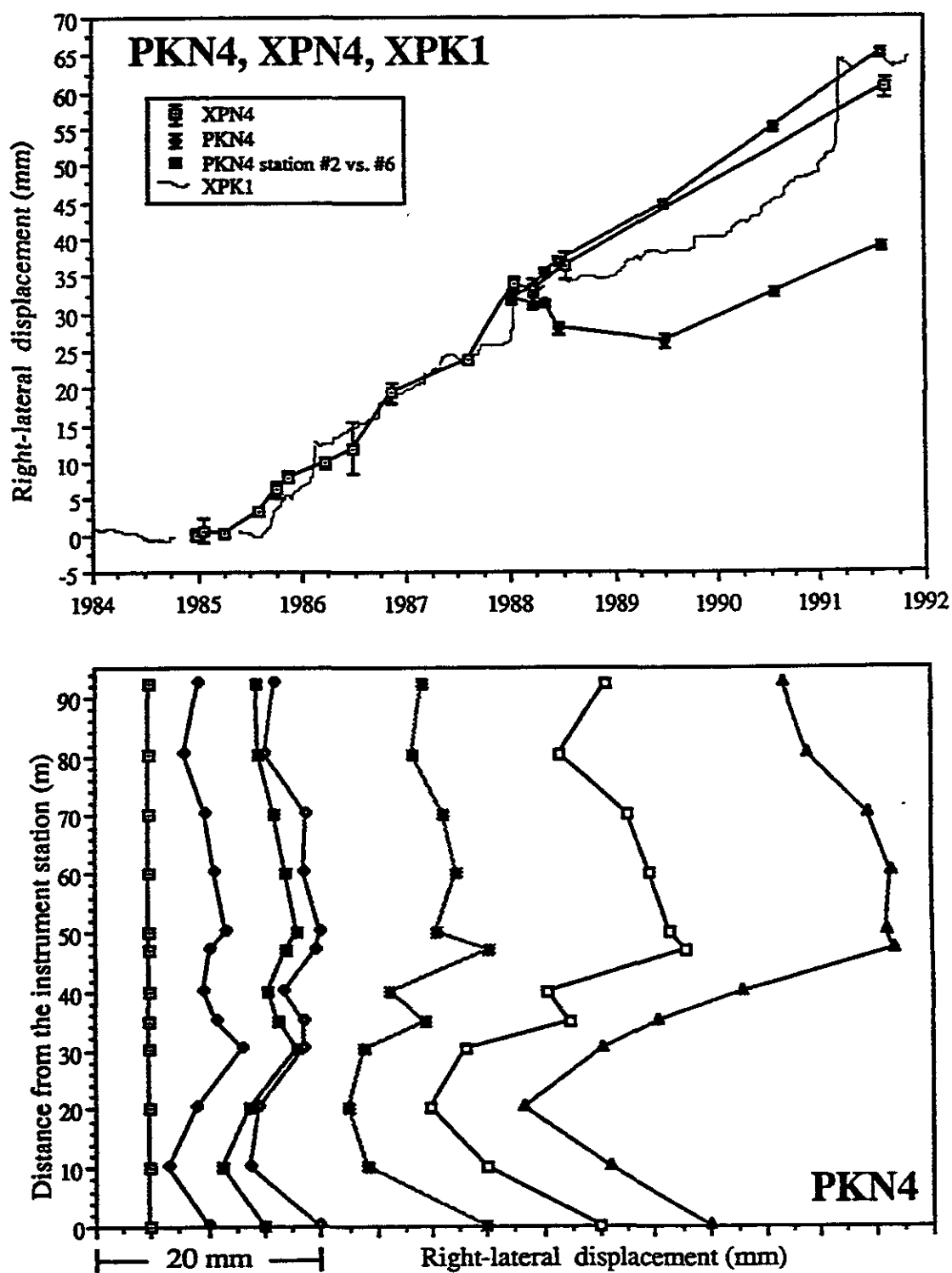


Figure 38. PKN4 and XPN4 Data Plots.

Site Description

70

Station Code PKF4 Name Parkfield Bridge County Monterey
 Quad Parkfield Latitude 35° 53.7' Longitude 120° 26.0'
 ES1/OS1 87° 57' 40.1" ES1/OS2 130° 06' 08.0"

To Reach: From San Miguel take Vineyard Canyon Road 19 miles to a "T" intersection and turn south.

Proceed 4 miles to the Parkfield turnoff to the left. Park in shade on the southeast corner of the intersection. The array crosses the bridge.

General Description: The IS and wing stations are P&K nails set in asphalt. The deflection stations are spikes, nails and crosses chiseled into the concrete roadway of the bridge. There are 2 OS's, one to the north and another to the south.

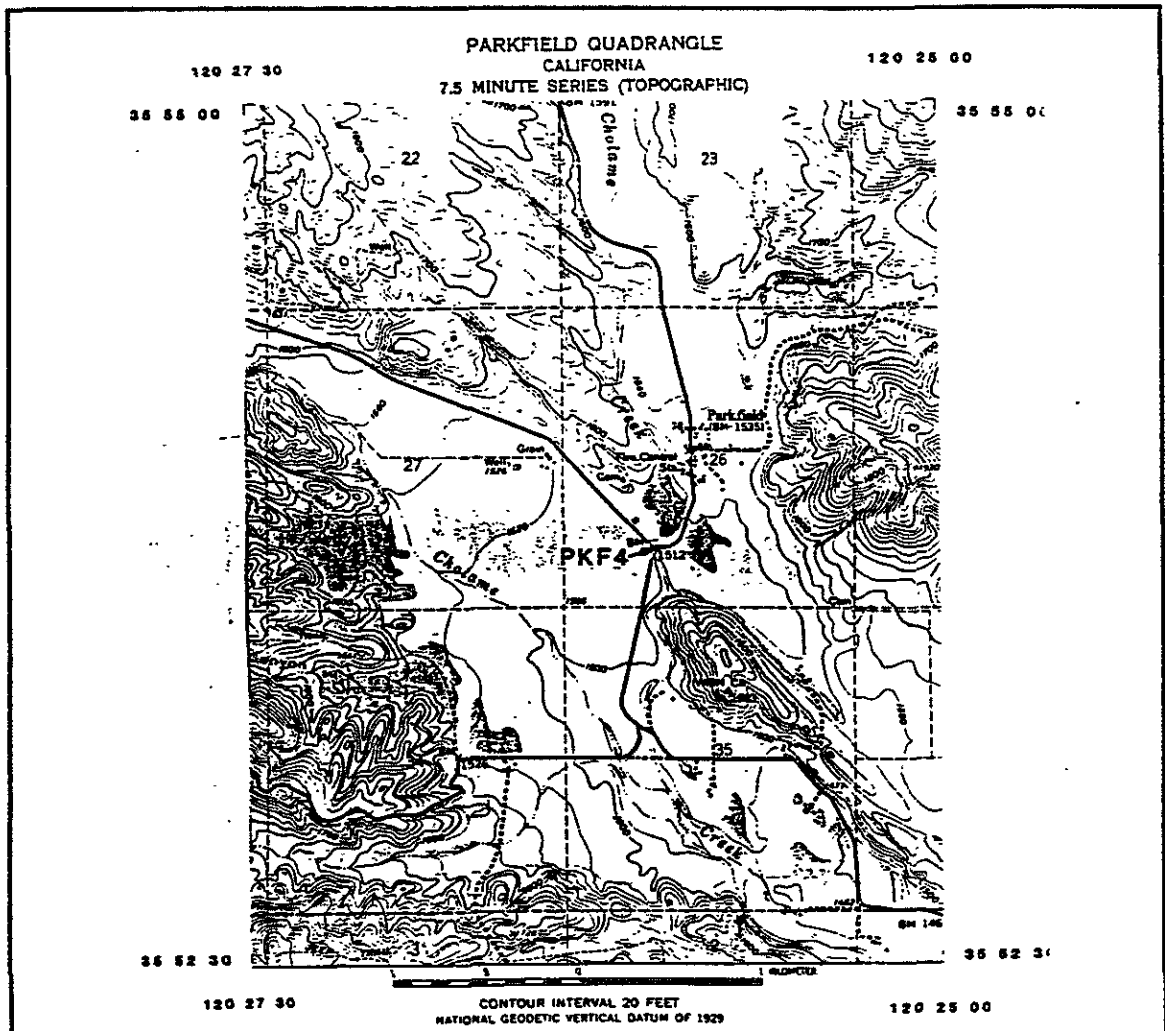


Figure 39. PKF4 Site Description.

Site Map

USGS : PARKFIELD BRIDGE ALINEMENT ARRAY (PKF4)
installed 5/17/83

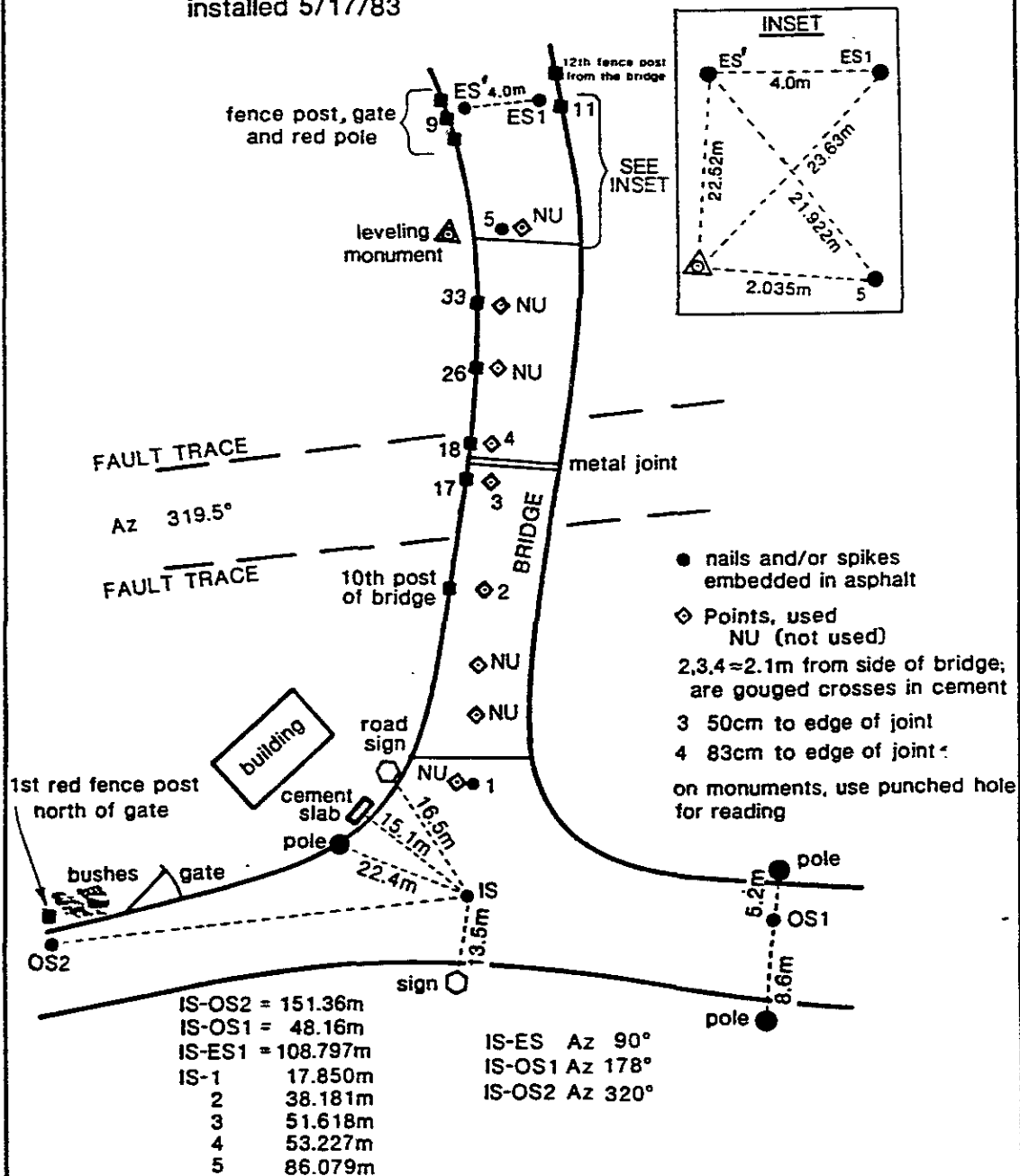


Figure 40. PKF4 Site Map.

Data Plots

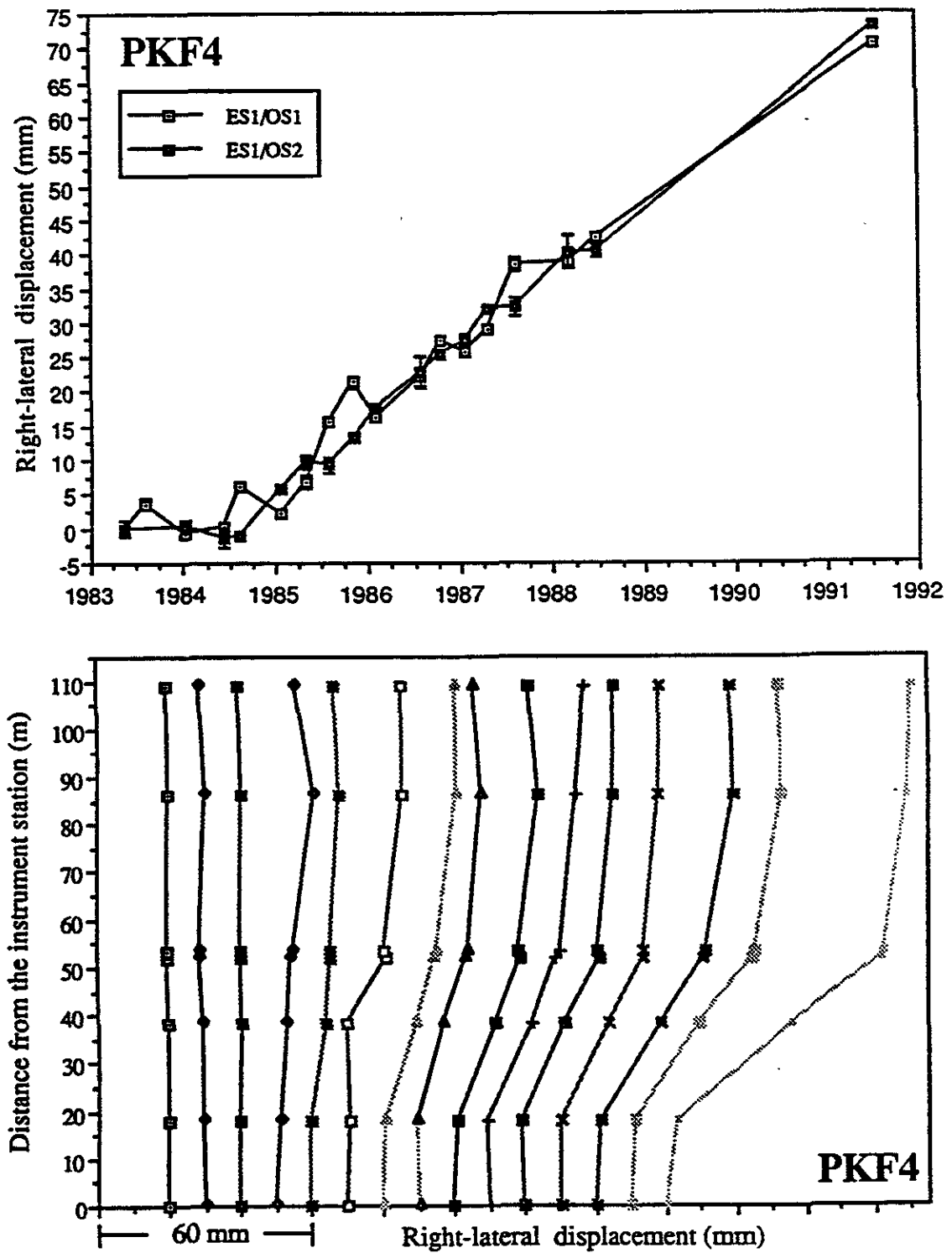


Figure 41. PKF4 Data Plots.

Site Description

73

Station Code TAY4 Name Taylor Ranch County Monterey
 Quad Parkfield Latitude 35° 53.4' Longitude 120° 25.6'
 ES1/OS1 109° 52' 00.1" ES1/OS2 69° 55' 31.0"

To Reach: From San Miguel take Vineyard Canyon Road 19 miles to a "T" intersection and turn south.

Go 4.5 miles passing the turn off to Parkfield and a green trestle bridge to a gate on the left. Contact Tom Burdette of the U.S.G.S. for permission to enter. Travel east on gravel road, right at the fork and left at the ponds. Pass the small shed and continue up the hill to the creepmeter.

General Description: The monuments are all subsurface pipes. The IS is on a knoll near the creepmeter and battery vaults, and between two solar panel poles. The OS is between the fence and the road just before the fork by the ponds. ES1 is across the road to the two color laser shed on top of the hill. ES2 is near the fence north of the ranch house.

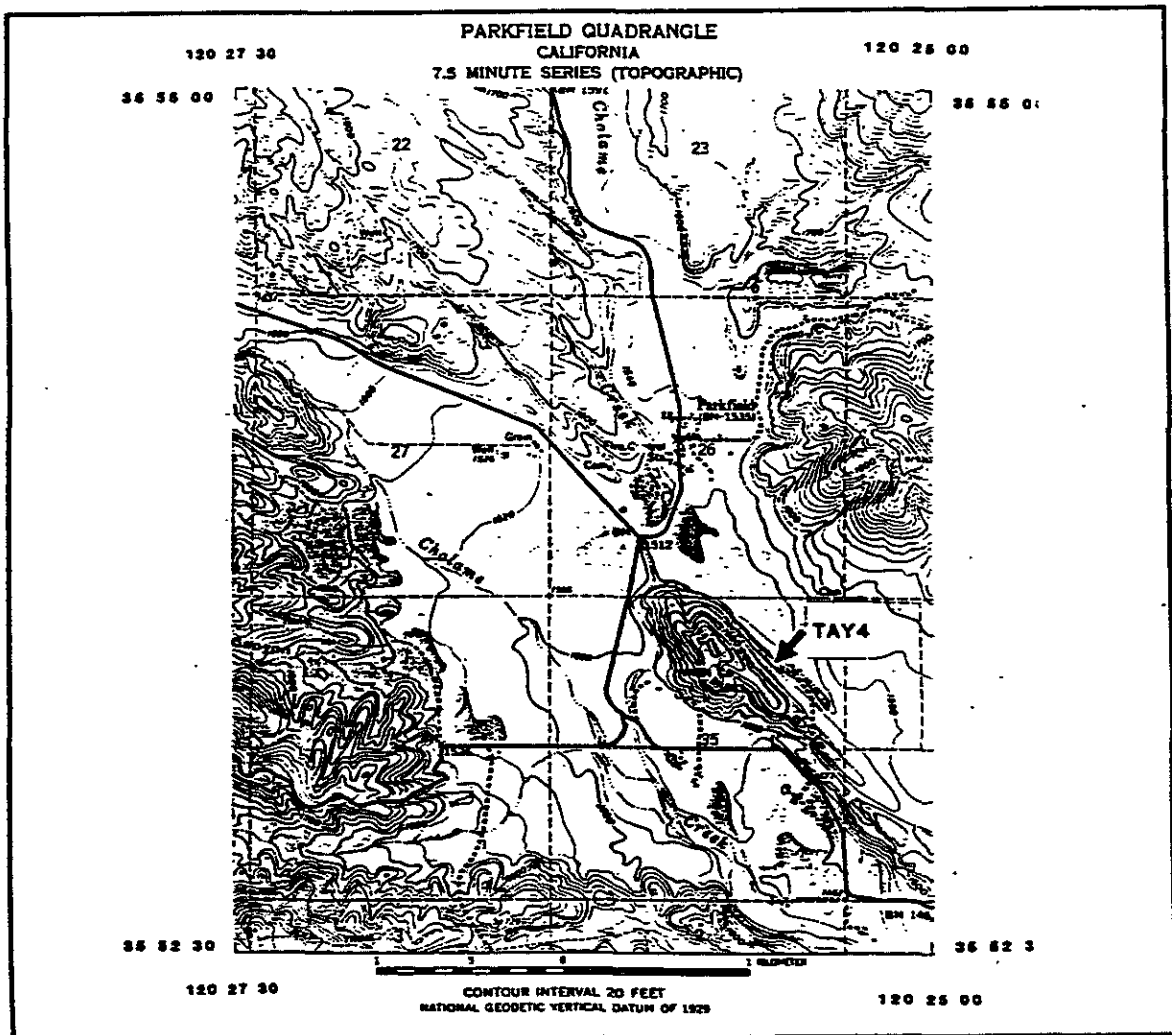


Figure 42. TAY4 Site Description.

Site Map

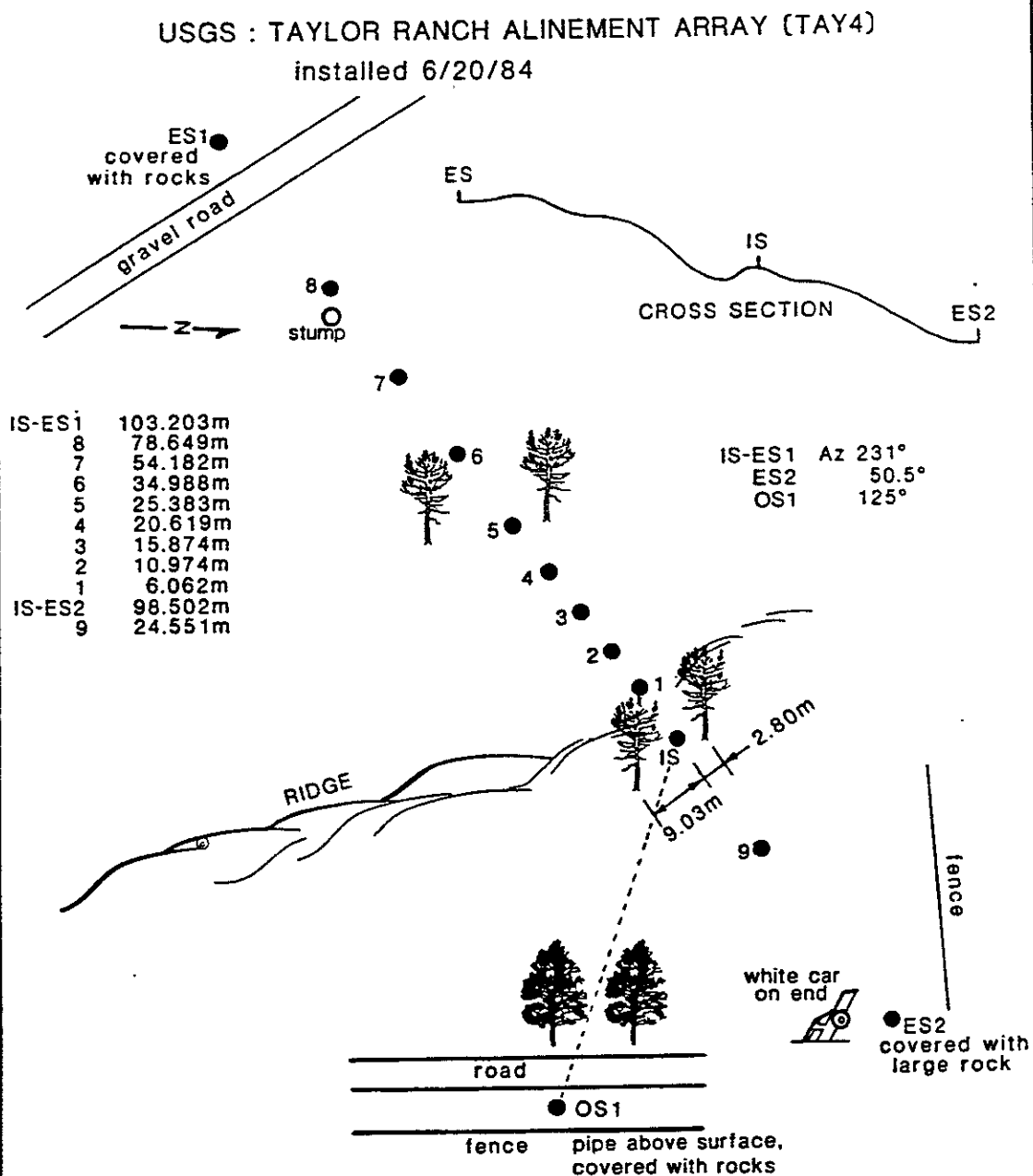


Figure 43. TAY4 Site Map.

Data Plots

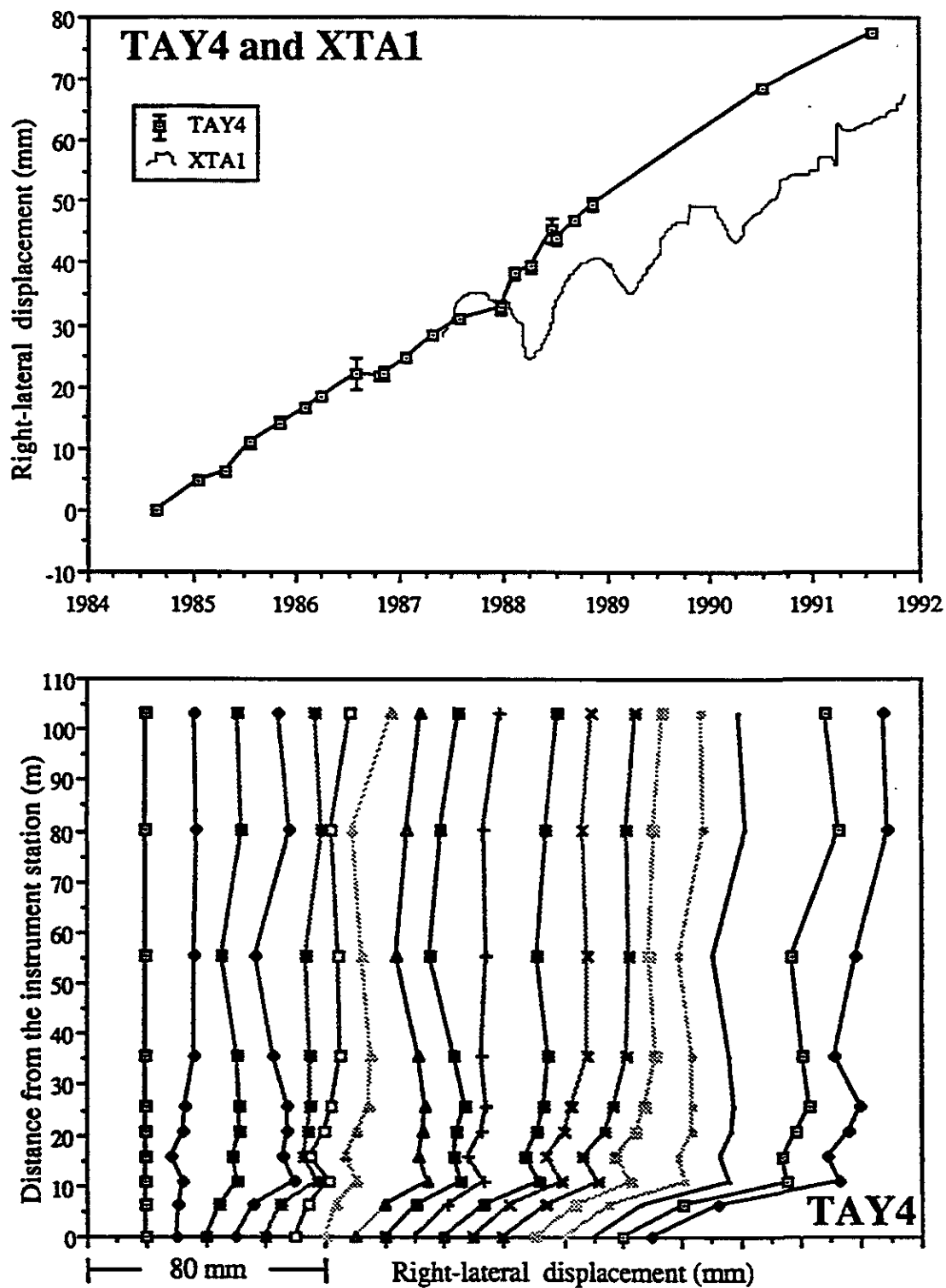


Figure 44. TAY4 Data Plots.

Site Description

76

Station Code RCW6 Name Ranchita Cyn. Rd. County Monterey
 Quad Parkfield Latitude 35° 53.1' Longitude 120° 26.5'
 ESI/OSI 84° 25' 48.6"

To Reach: From San Miguel take Vineyard Canyon Road 19 miles to a "T" intersection and turn south.

Pass the turn off to Parkfield and continue 0.62 miles to Ranchita Canyon Road, just before a green trestle bridge. The array is 0.52 miles to the west on the north side of the road.

General Description: The monuments are all subsurface pipes with yellow plastic plugs. The IS is near a telephone company "Buried Cable" sign and a barbed wire gate. The OS is just south of the field to the south of the road. The ES is across the road (north) of leveling monument PF611 to the east of the IS.

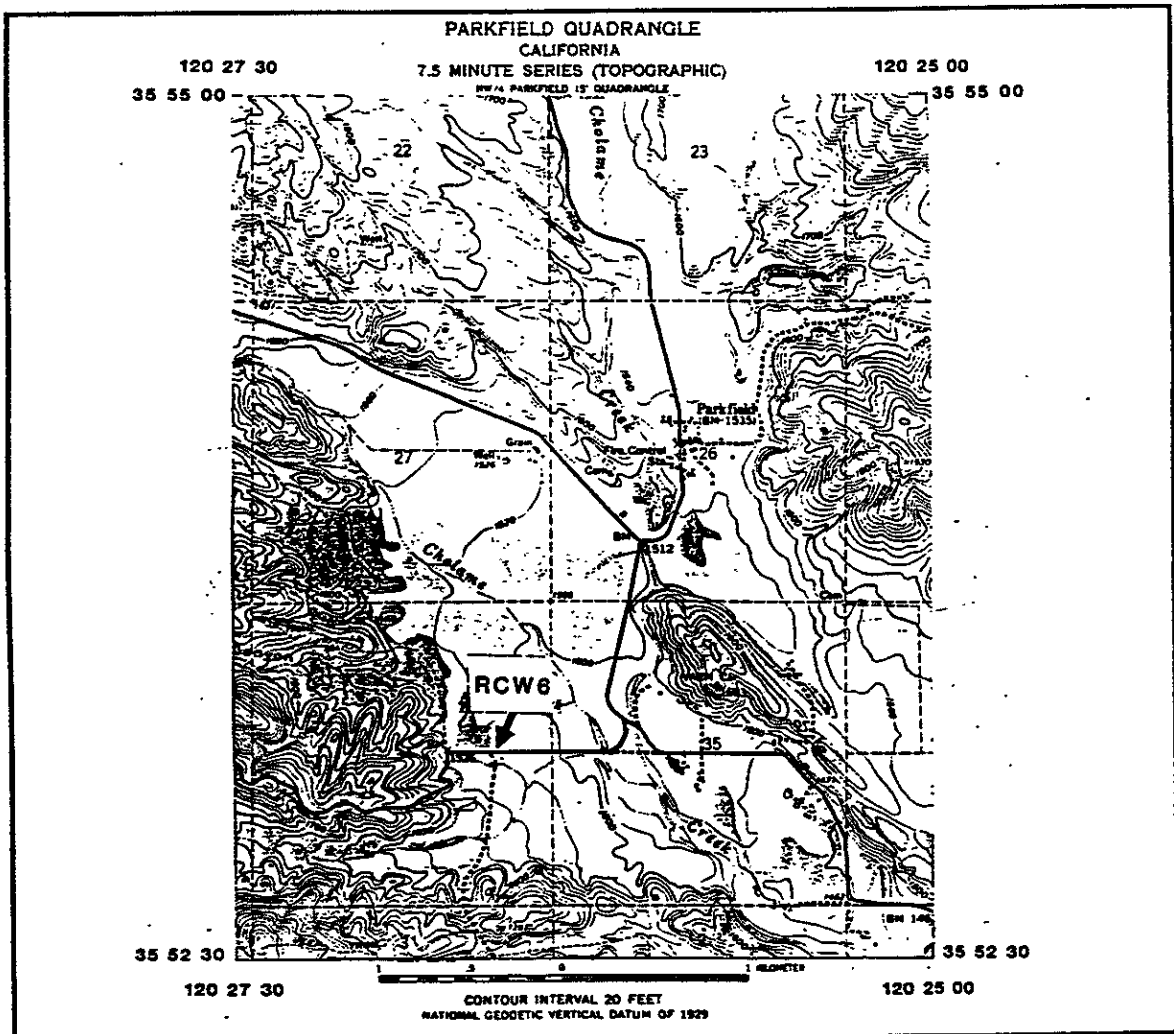
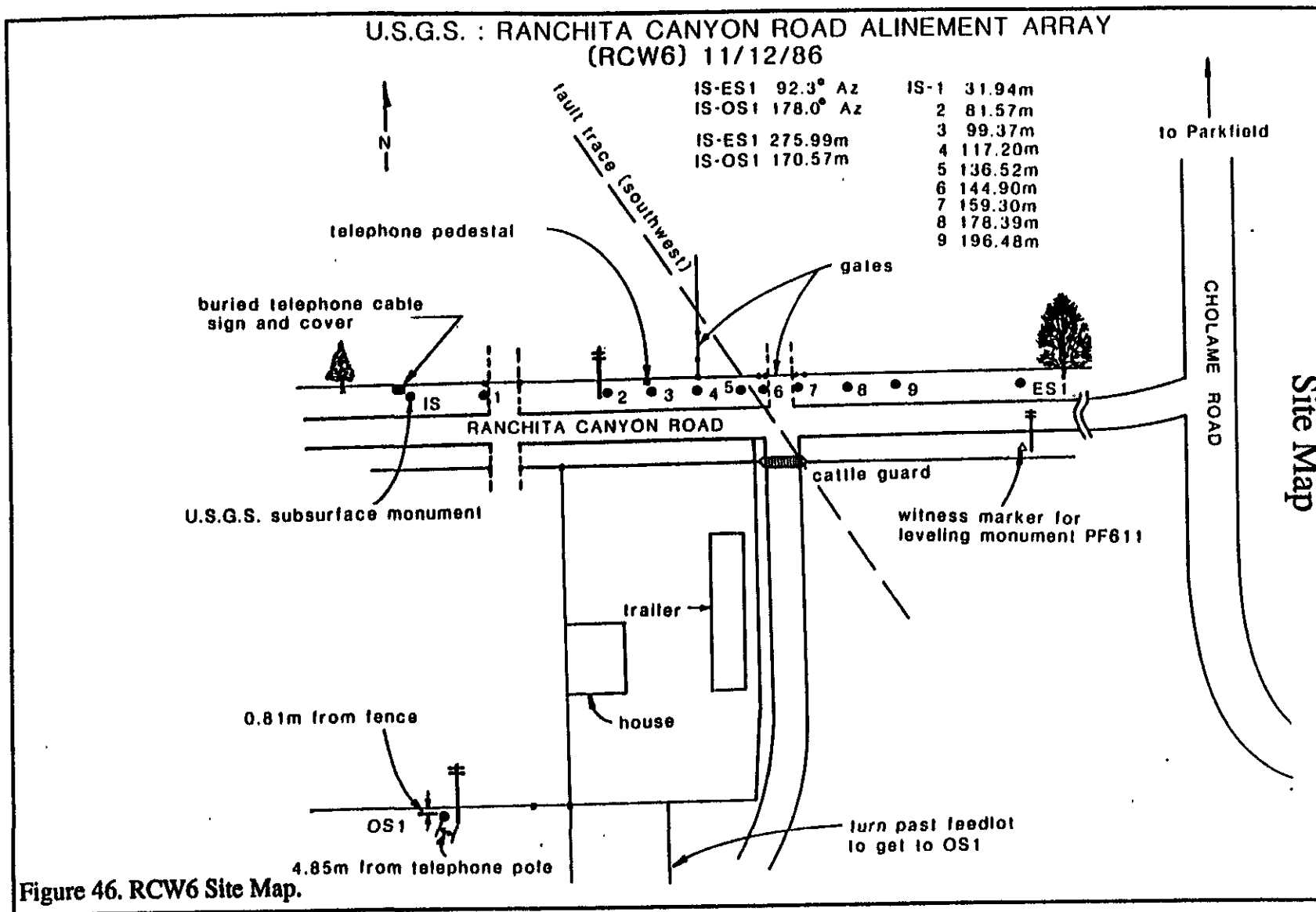


Figure 45. RCW6 Site Description.



Data Plots

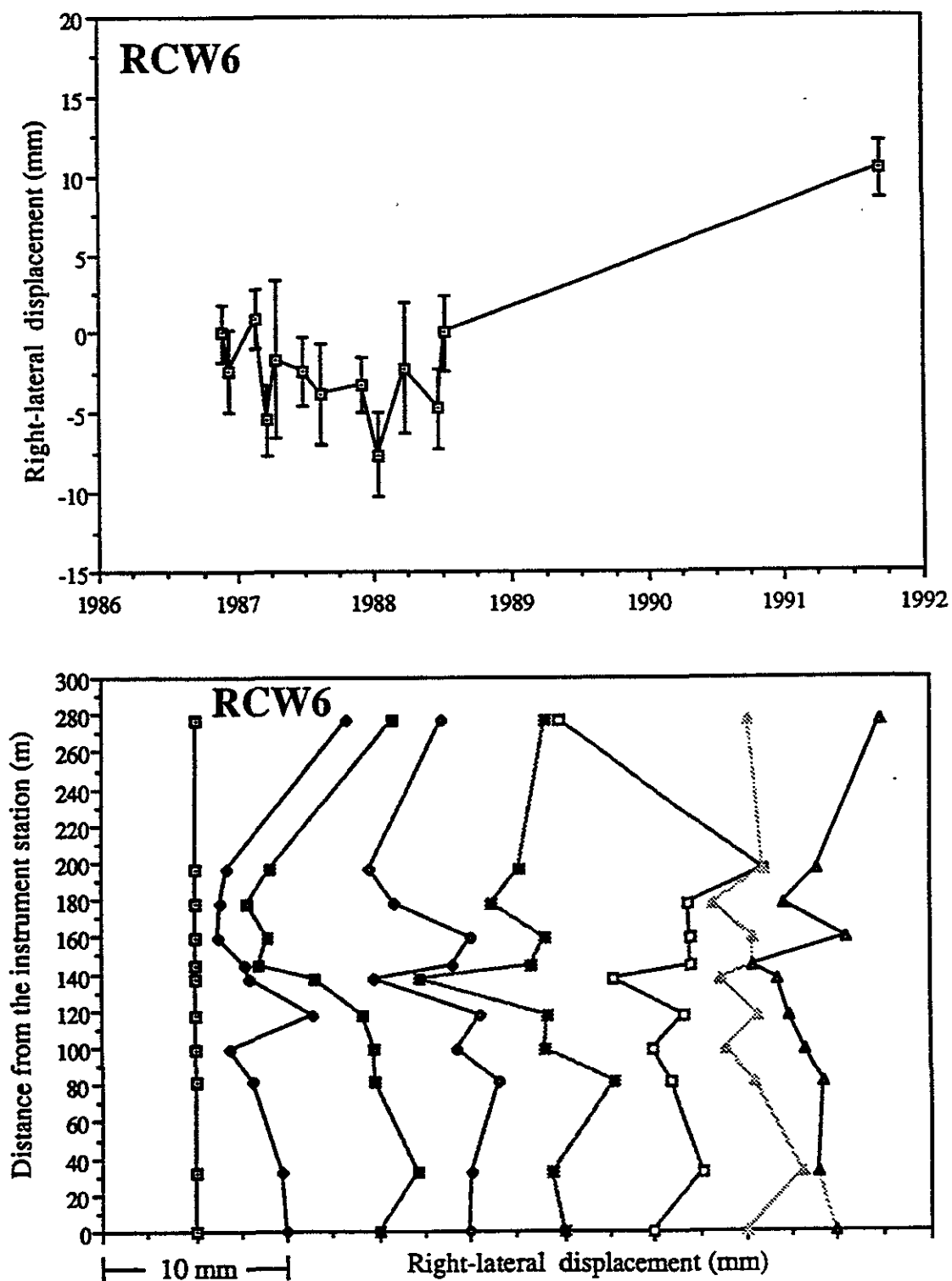


Figure 47. RCW6 Data Plots.

Station Code XDR5 Name Durham Ranch County Monterey
 Quad Parkfield Latitude 35° 53.1' Longitude 120° 25.3'
 ES1/OS1 128° 37' 42.4" ES1/OS2 76° 57' 18.0"

To Reach: From San Miguel take Vineyard Canyon Road 19 miles to a "T" intersection and turn south.

Go ~5 miles to left turn onto Turkey Flat Road. At 1/4 mile head north through first gate on left (Eade Ranch). Follow road past the ranch house across the airfield and pass through barbed wired gate. Make the first left, then right at the water trough, right at feeder, and west past oak to fence. Array is approximately 51 meters south of fence. Creepmeter solar panel and Strong Motion housing are visible just past the array. NOTE: This site has been abandoned due to loss of entry permits.

General Description: The IS is about 2 meters east of the dirt road. ES is atop a ridge near the creepmeter vault. The OS is north of the IS between the road and the fence near the shed. The ES and deflection stations are embedded in cement on the ground surface. The IS and OS are subsurface monuments.

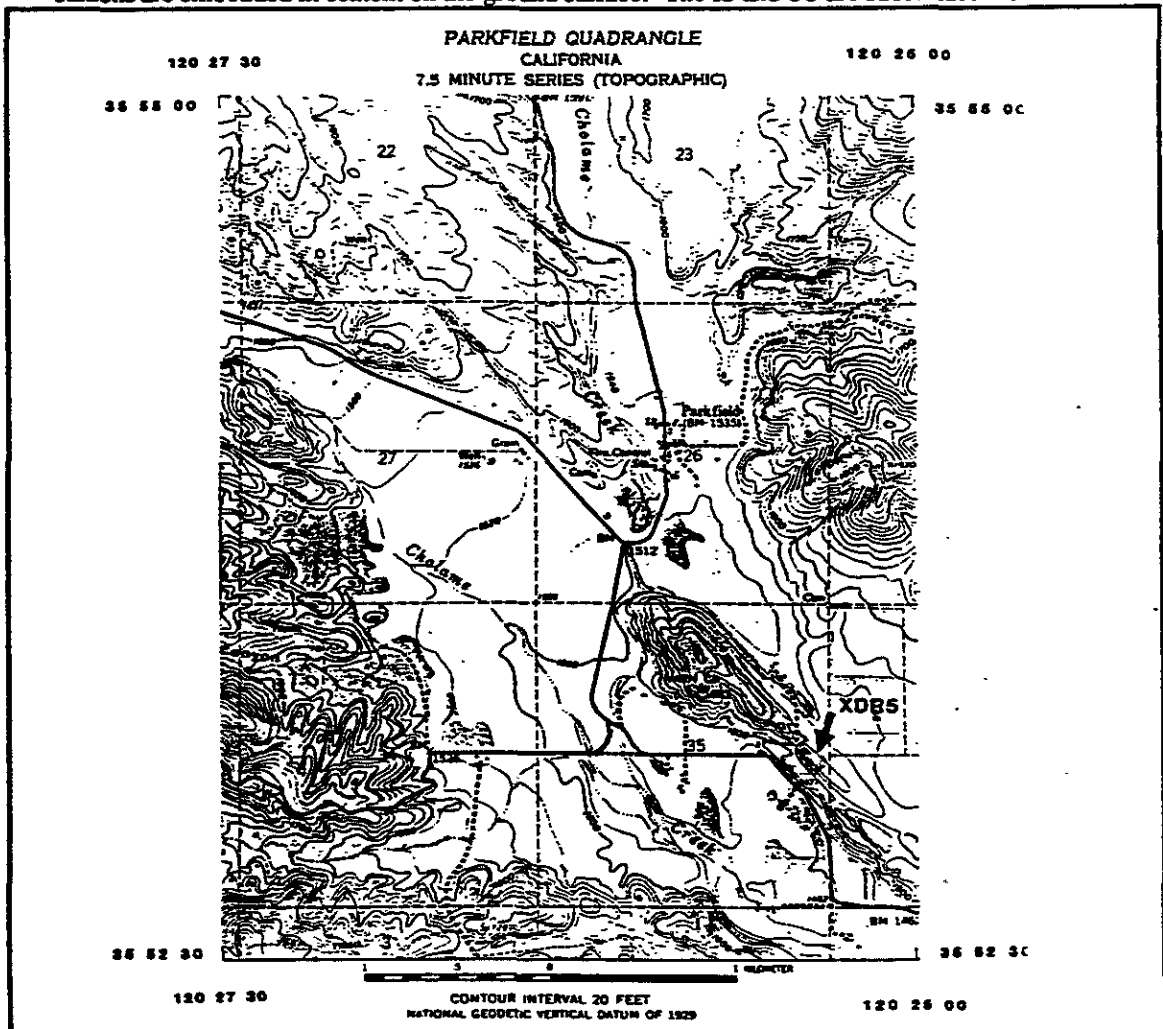


Figure 48. XDR5 Site Description.

USGS : DURHAM RANCH ALINEMENT ARRAY XDR5 11/7/83

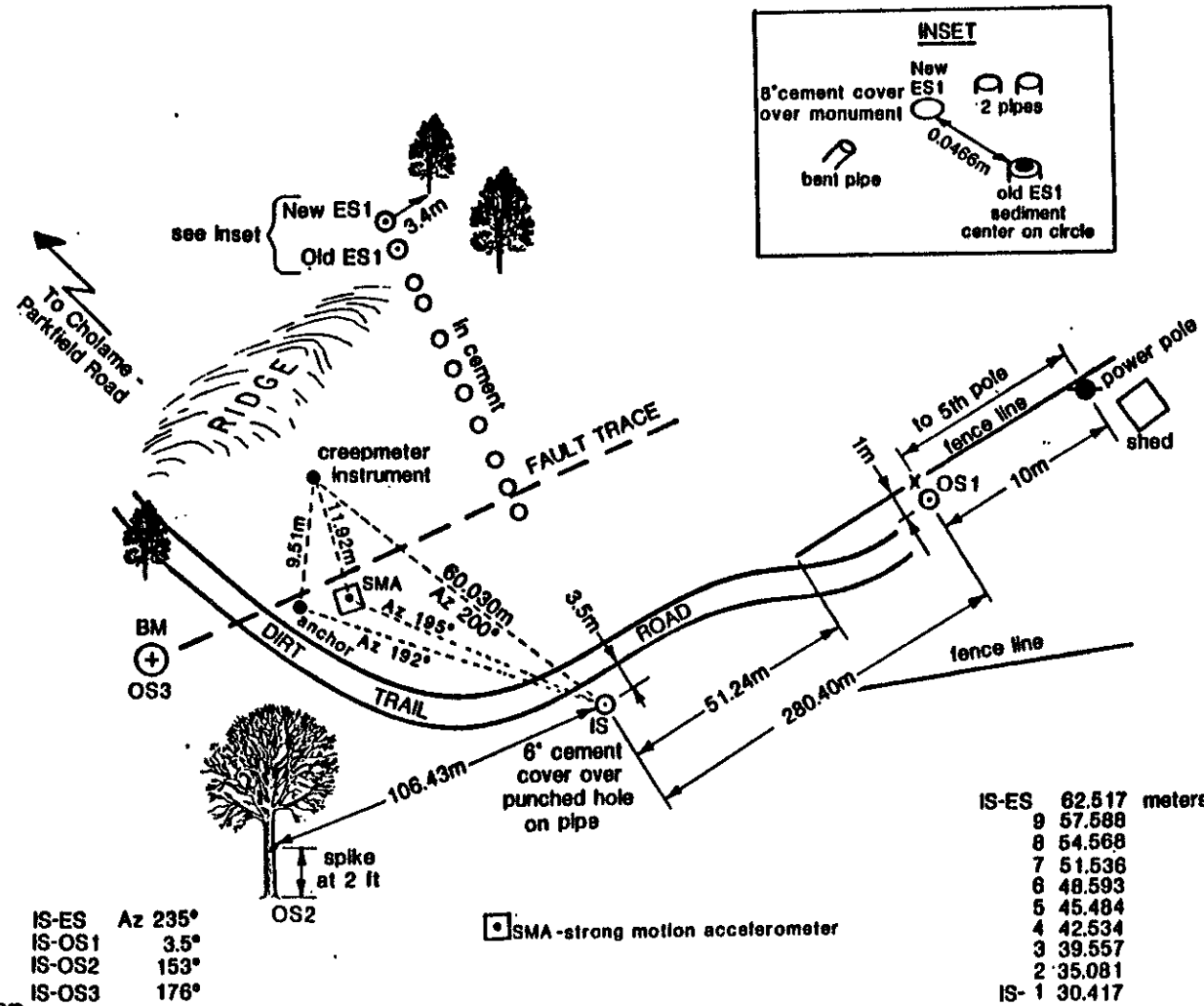


Figure 49. XDR5 Site Map.

Data Plots

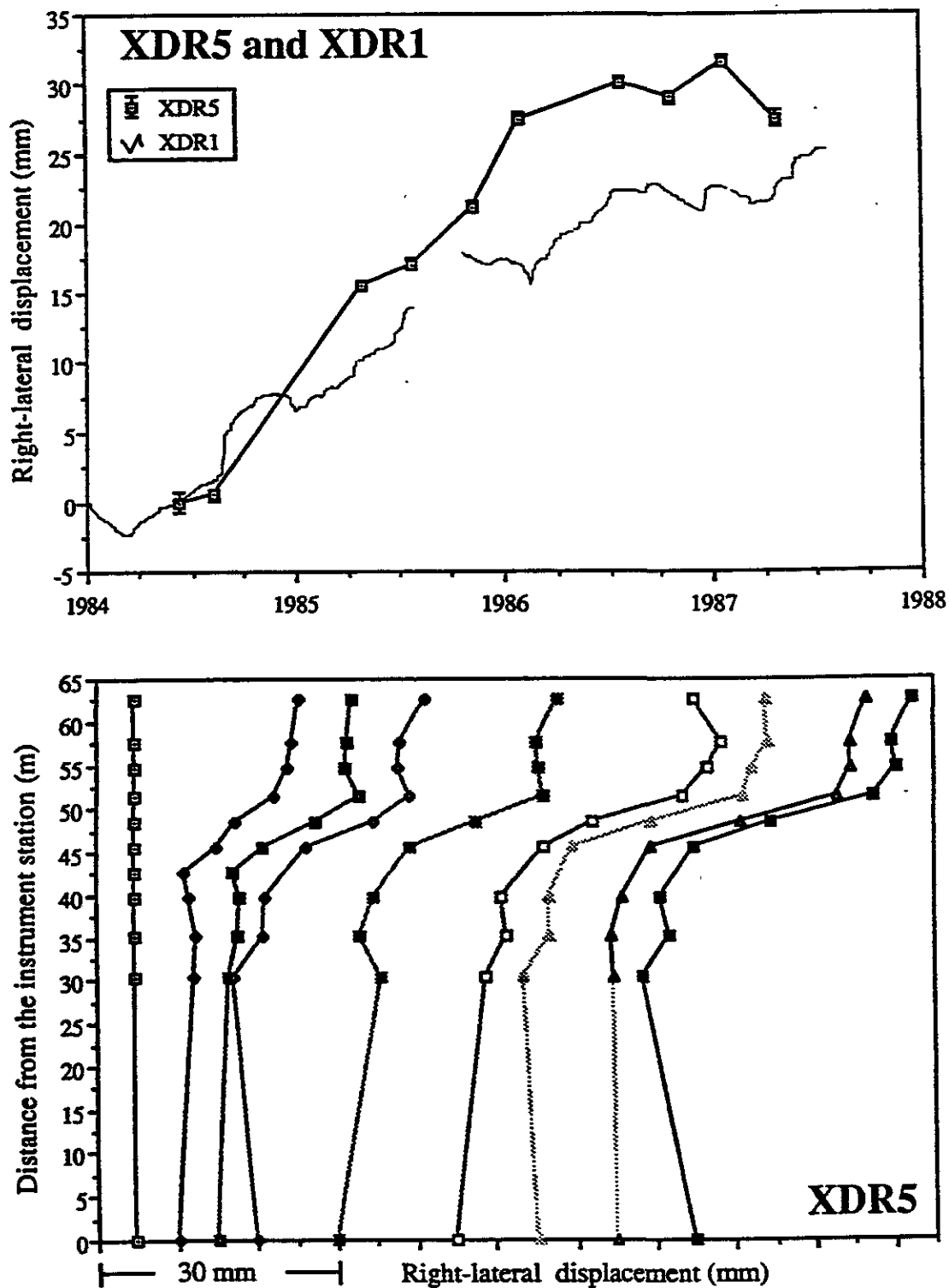


Figure 50. XDR5 Data Plots.

Site Description

Station Code HST4 Name Hearst North County Monterey
 Quad Parkfield Latitude 35° 52.4' Longitude 120° 24.1'
 ES1/OS1 101°45' 11.7"

To Reach: From Paso Robles, take California State Highway 46 east approximately 25 miles and turn north on the Parkfield-Cholame Valley Road. Travel 11.8 miles to the array, ~50 meters before the creek crossing.

General Description: The IS is about 2 meters east of the dirt road. ES is atop a ridge near the creepmeter vault. The OS is north of the IS between the road and the fence near the shed. The ES and deflection stations are embedded in cement on the ground surface. The IS and OS are subsurface monuments.

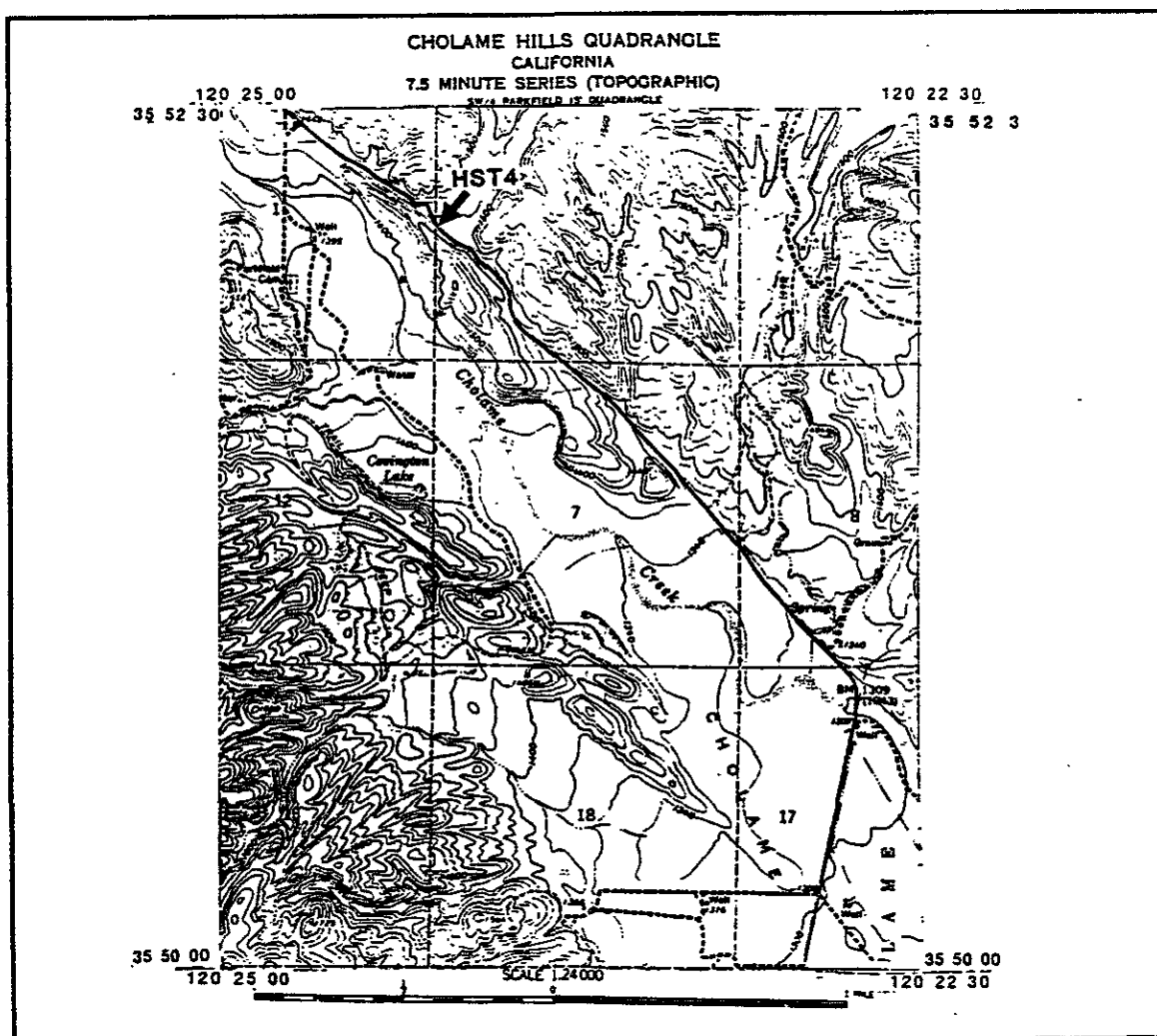


Figure 51. HST4 Site Description.

Site Map

U.S.G.S. : HEARST NORTH ALINEMENT ARRAY

(HST4) 11/22/86

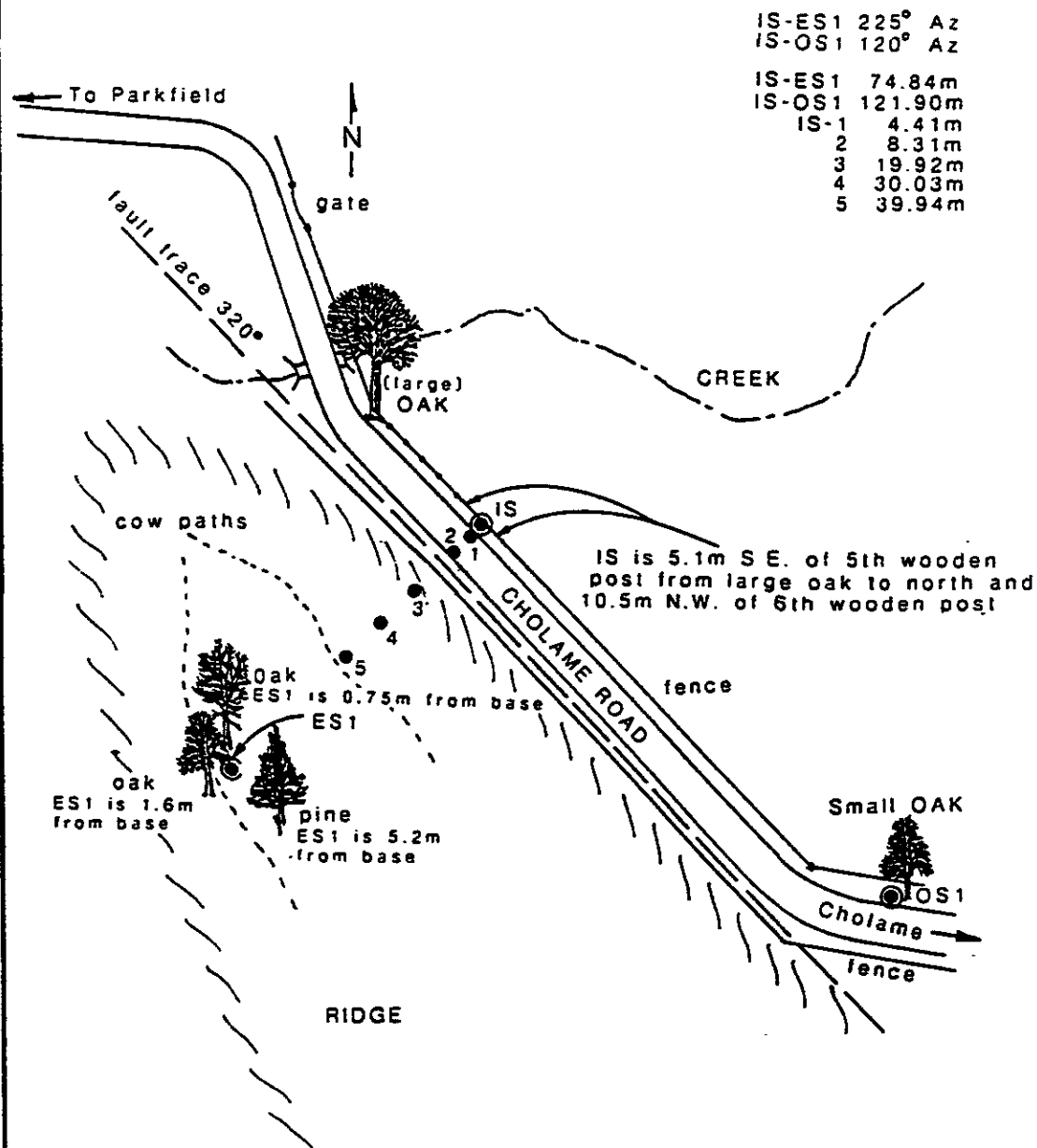


Figure 52. HST4 Site Map.

Data Plots

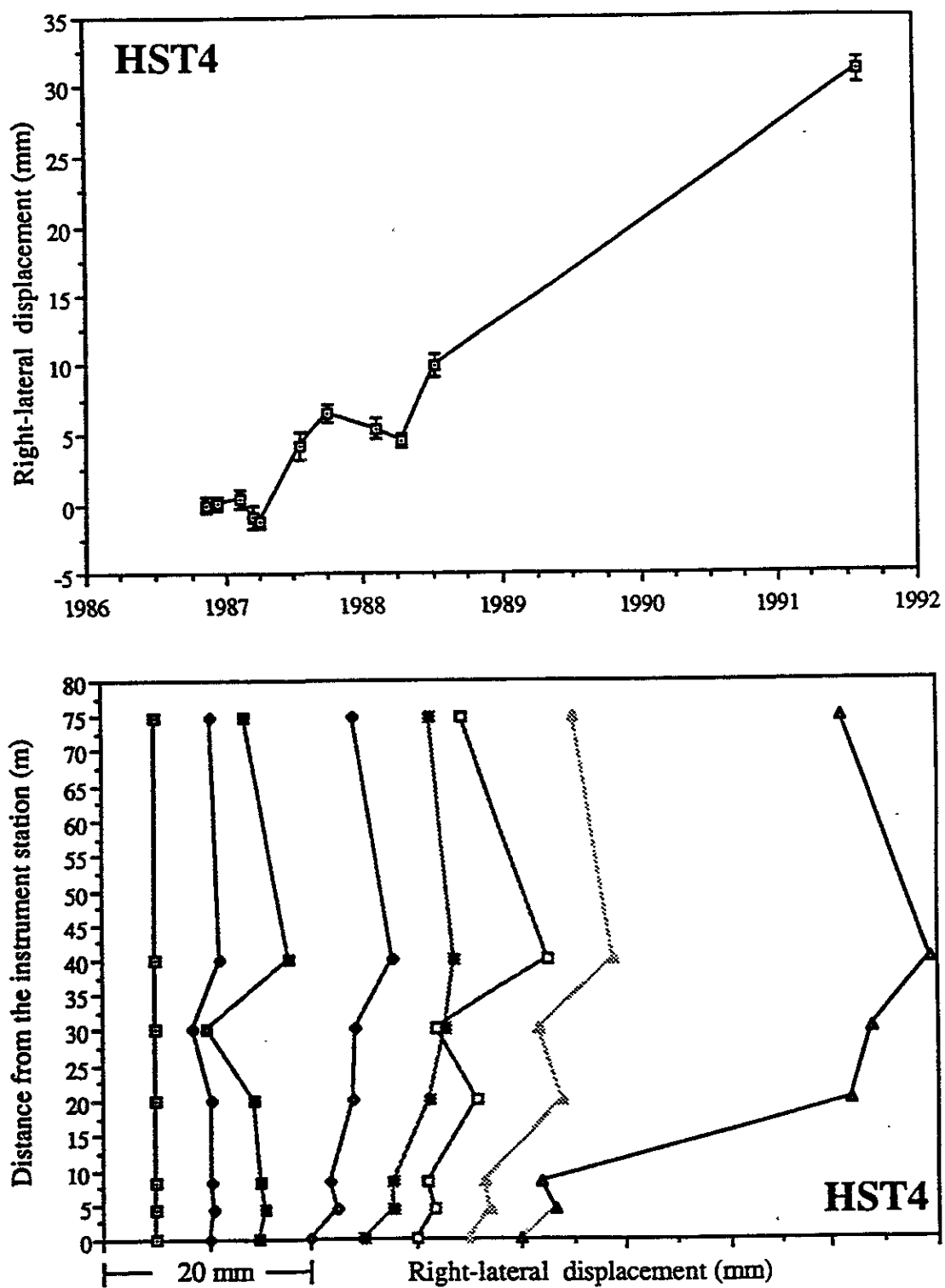


Figure 53. HST4 Data Plots.

Station Code HSW4 Name Hearst Southwest County Monterey
 Quad Cholame Hills Latitude 35° 51.8' Longitude 120° 25.3'
 ES1/OS1 89° 58' 19.3"

To Reach: From Paso Robles, take California State Highway 46 east approximately 25 miles and turn north on the Parkfield-Cholame Valley Road. Travel 12.4 miles and turn west onto Parkfield Cemetery Road. Cross Cholame Creek, pass the ranch and turn left just before the corral. The passes next to a house and through a gate. Turn right and go a 1/4 mile and turn right at the gate. Cross the creek, staying to the right, pass a fork in the road, cross the creek again, another fork and turn right into the pasture.

General Description: The monuments are all subsurface and covered with rocks. DS 3 is just off the trail to the northeast. The IS is ~50 meters southwest of DS 3. ES1 is 5 meters to the southeast of a Digger pine tree on the same small ridge as the water tank. ES2 is a nail in an oak tree ~160 meters from the IS to the southwest. The OS is near a tree towards the galley to the southeast of the IS.

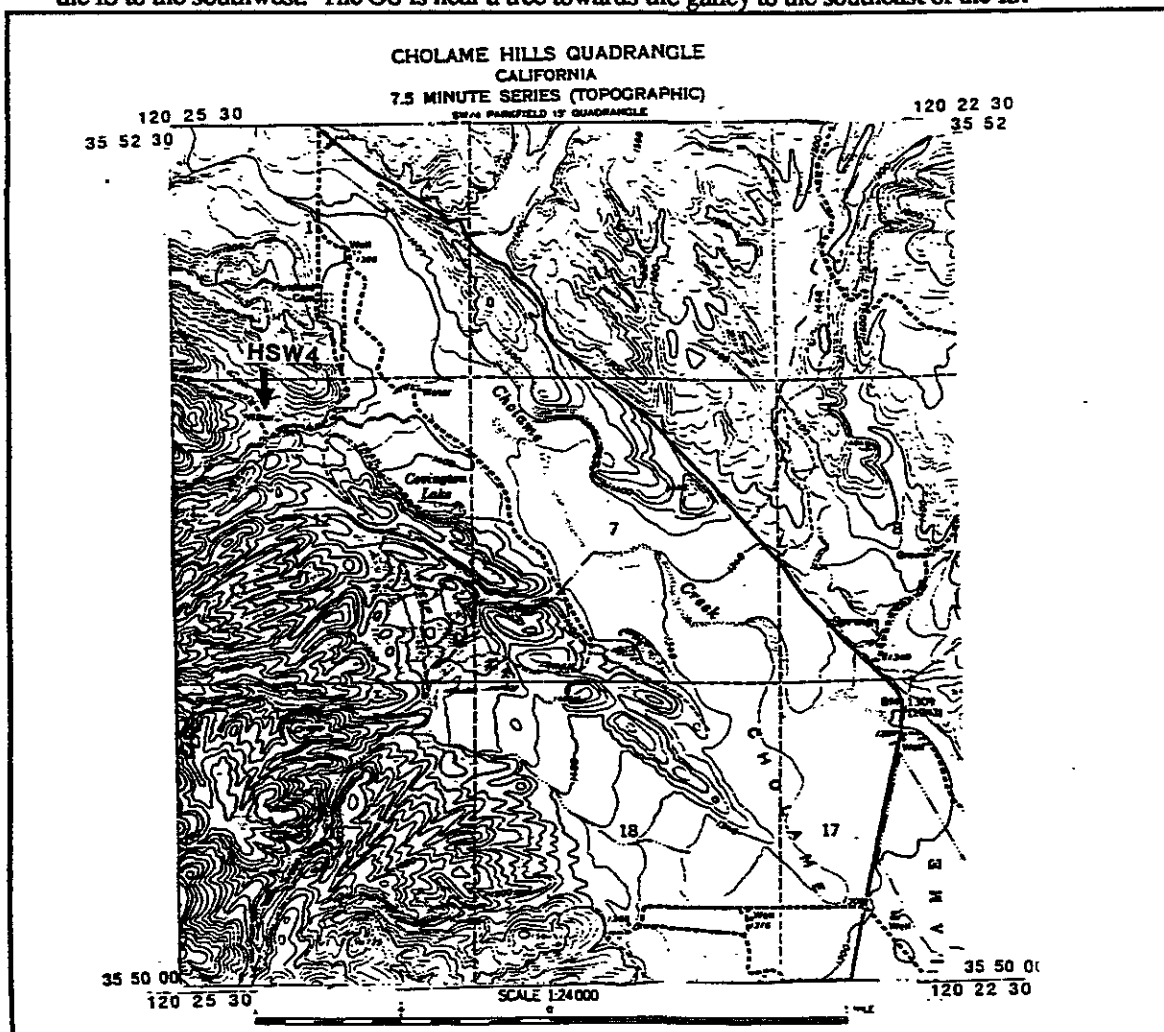


Figure 54. HSW4 Site Description.

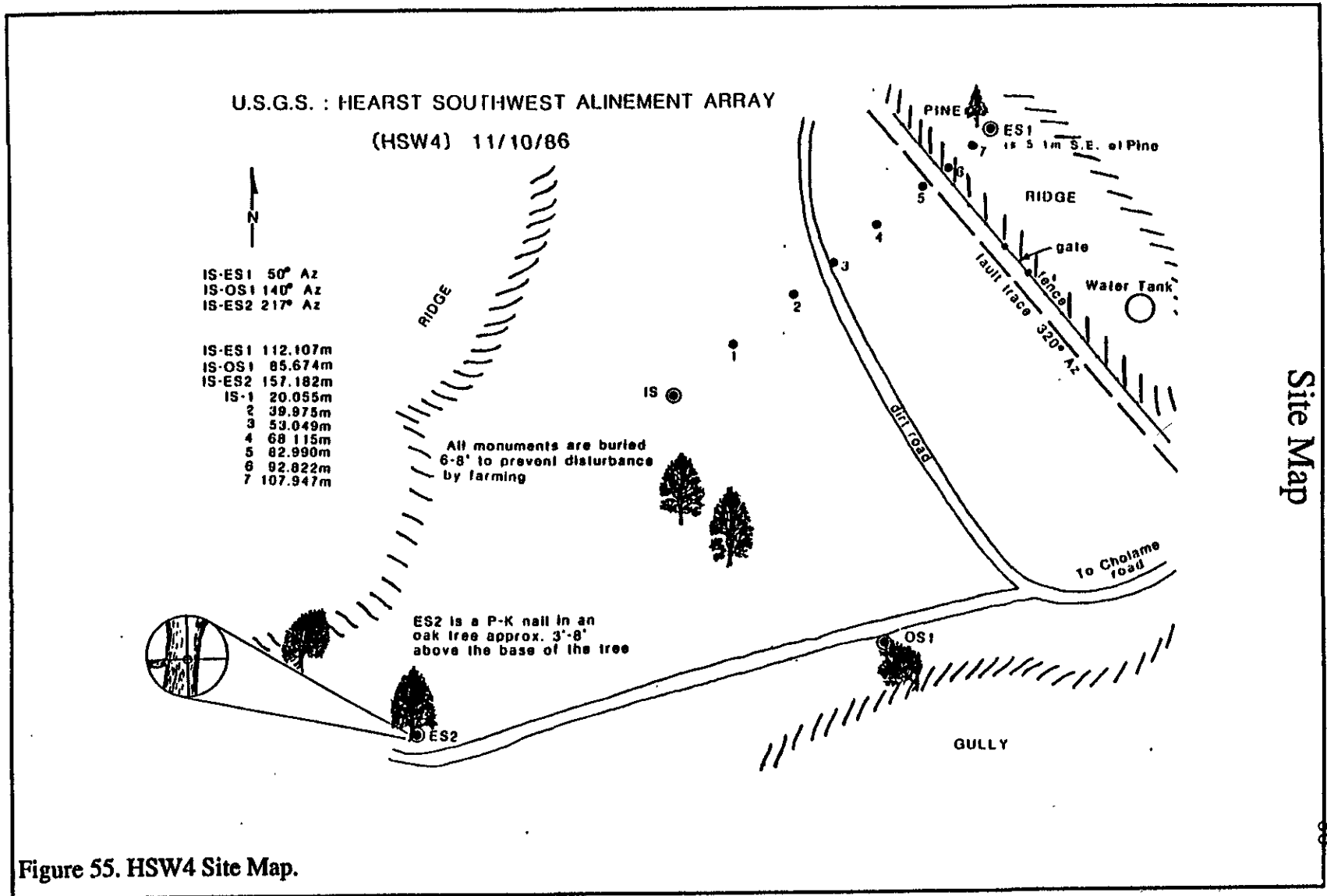


Figure 55. HSW4 Site Map.

Data Plots

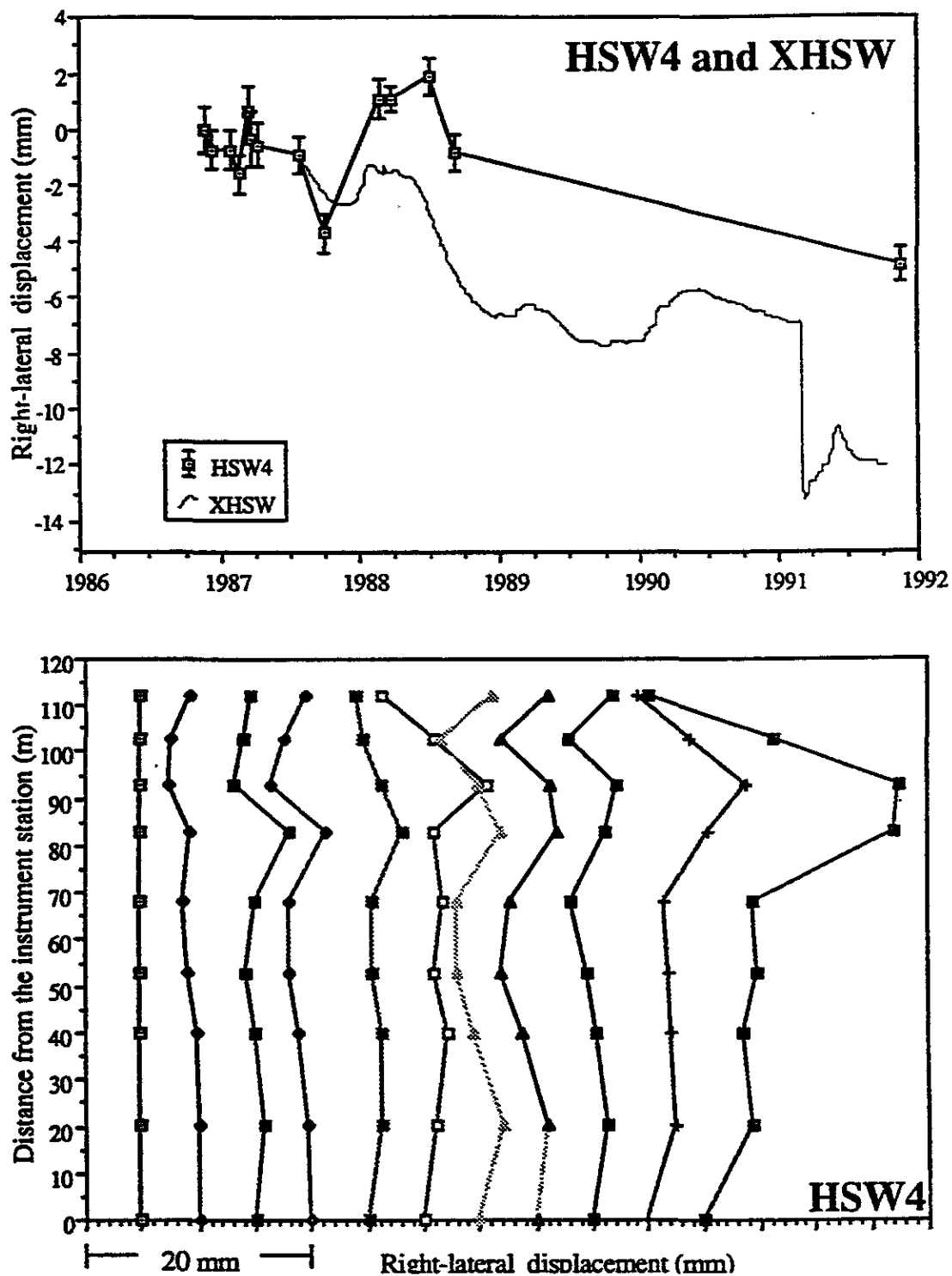


Figure 56. HSW4 Data Plots.

Site Description

88

Station Code WKR4 Name Work Ranch County Monterey
 Quad Cholame Hills Latitude 35° 51.8' Longitude 120° 23.8'
 ES1/OS1 99° 08' 01.9" ES2/OS1 82° 05' 02.5"

To Reach: From Paso Robles, take California State Highway 46 east approximately 25 miles and go north on the Parkfield-Cholame Valley Road 11 miles to the array. It lies about 1/4 mile north of the Work Ranch creepmeter and 30 meters north of the telephone drop pedestal.

General Description: The monuments are all subsurface. The IS is about 5 meters west of the fence to the west of the road. The array is perpendicular to the road.

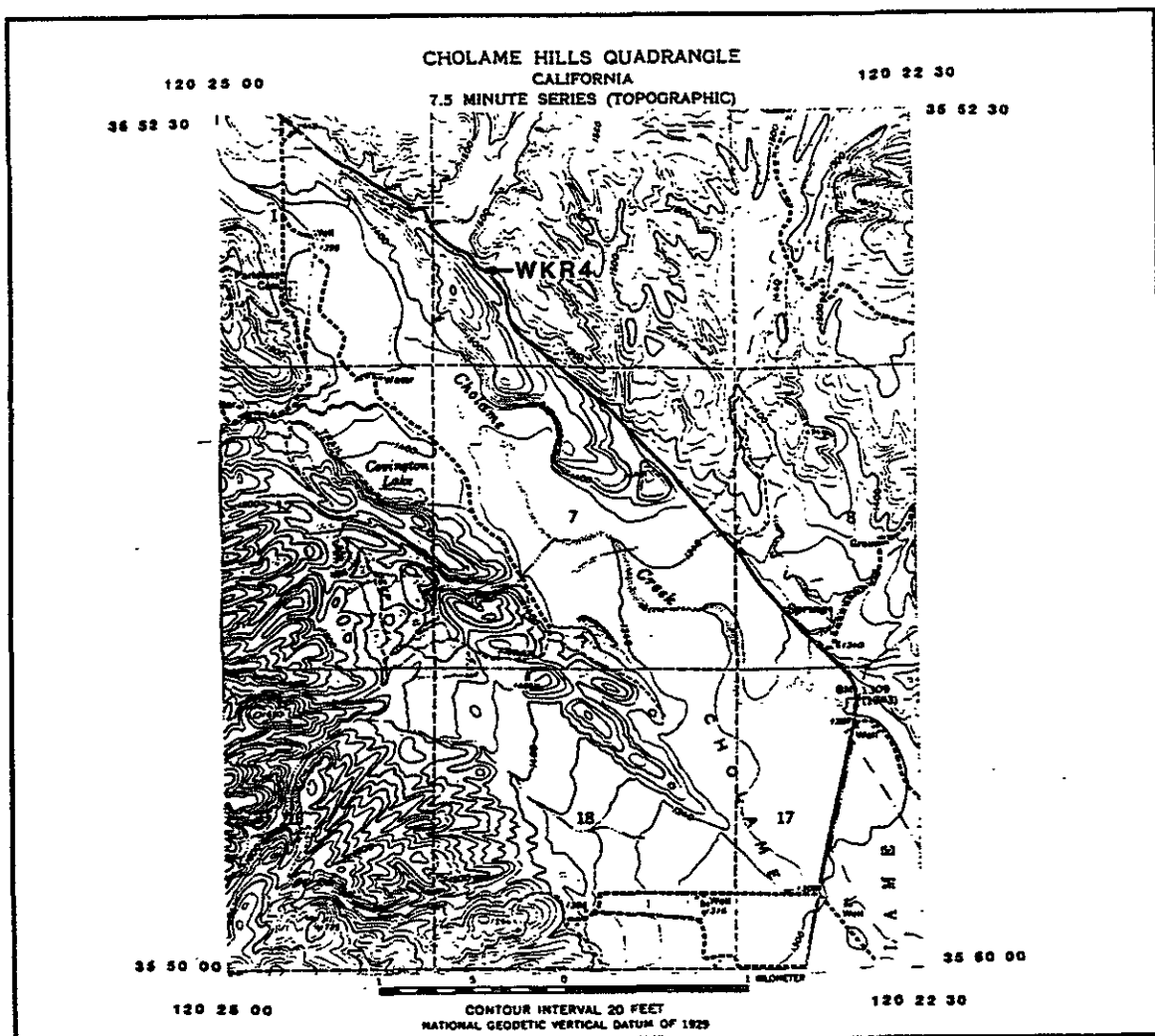


Figure 57. WKR4 Site Description.

Site Map

USGS : WORK RANCH ALINEMENT ARRAY (WKR4) 6/6/84

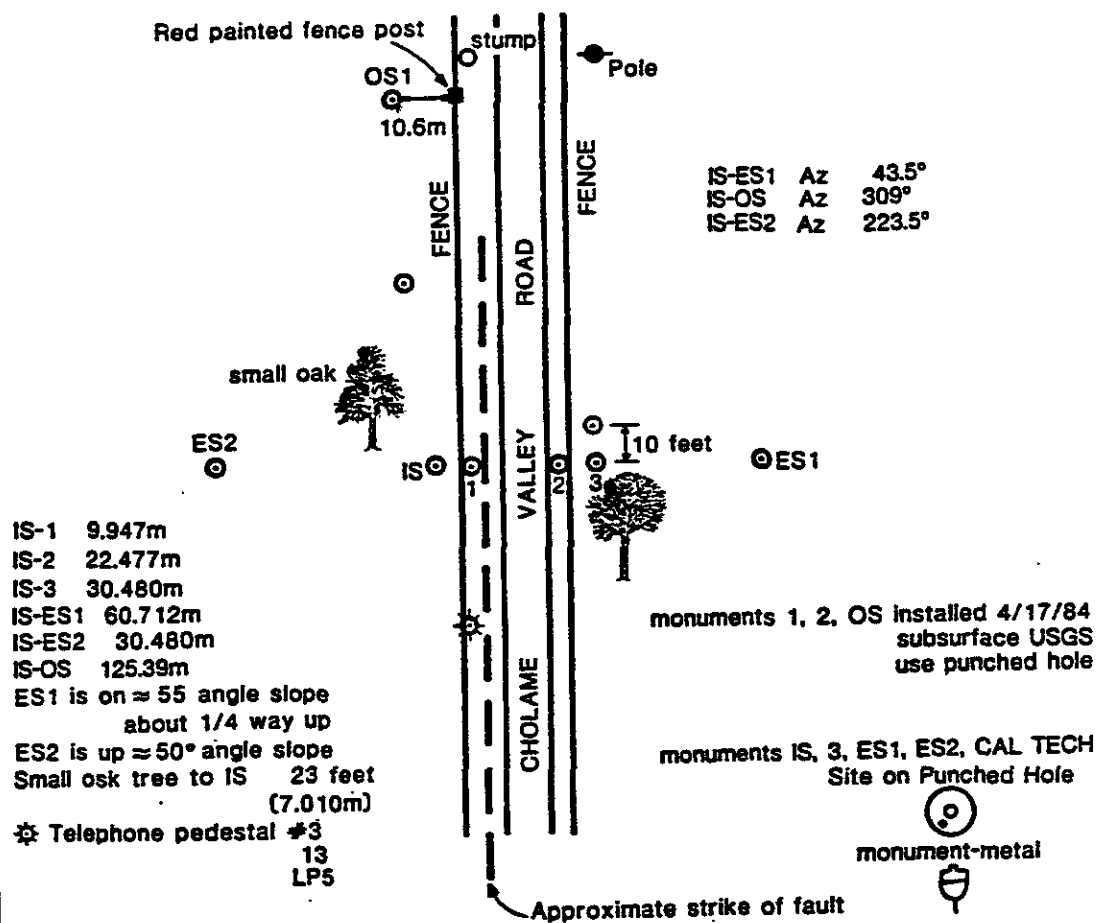


Figure 58. WKR4 Site Map.

Data Plots

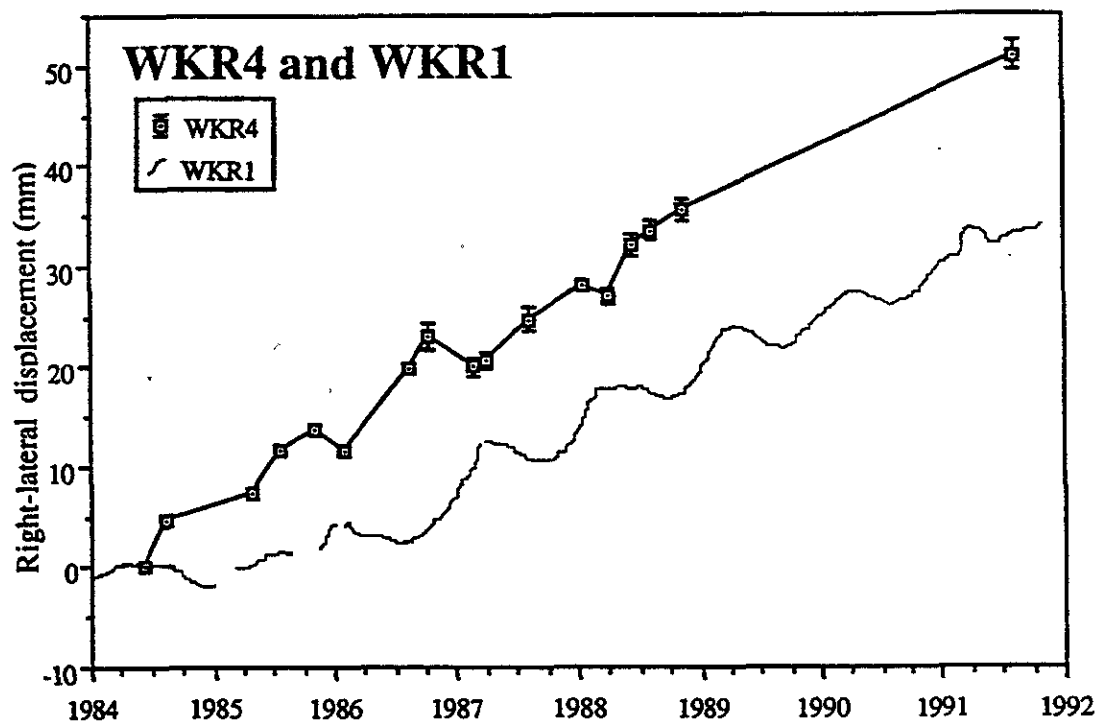


Figure 59. WKR4 Data Plot.

Site Description

91

Station Code KEN5 Name Kennedy Ranch County Monterey
 Quad Cholame Hills Latitude 35° 50.7' Longitude 120° 22.6'
 ESI/OS1 99° 57' 30.2"

To Reach: From Paso Robles, take California State Highway 46 east approximately 25 miles and go north on the Parkfield-Cholame Valley Road. Go 10.36 miles 175 meters past the bridge to the gate on the right hand side of the road. Follow the trail to the top of the escarpment. Turn back north about 100 meters, just past a gully and park.

General Description: The monuments are all subsurface. The IS is at the crest of the scarp approximately 15 meters from the edge. Deflection station 1 is at the edge of the slope. ES1 is near the fence line about 0.75 meters NW of a concrete slab near the road. ES2 is on a ridge 185 meters to the NE from the IS. The OS is next to the dirt road 77 meters SE of the IS.

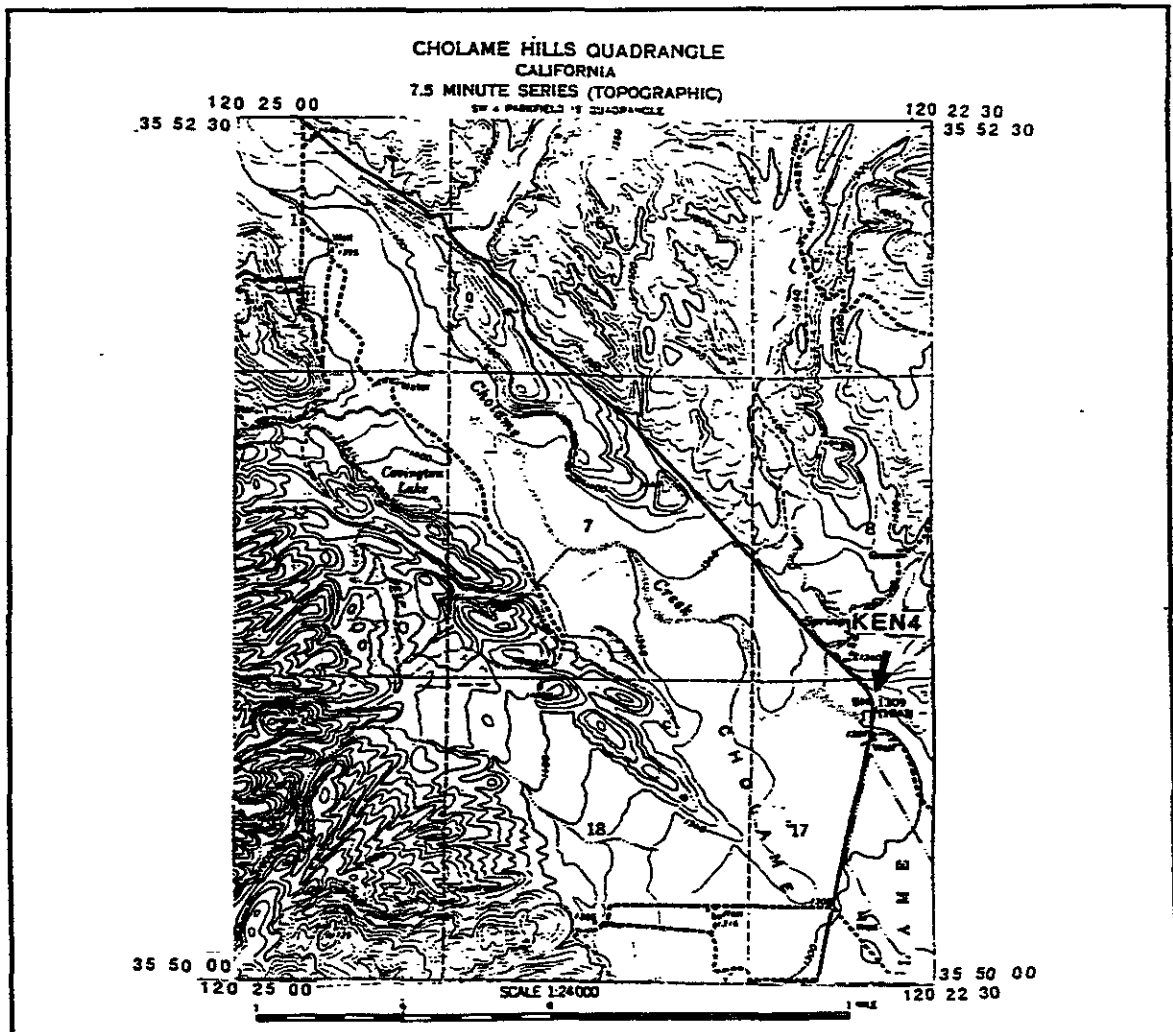


Figure 60. KEN5 Site Description.

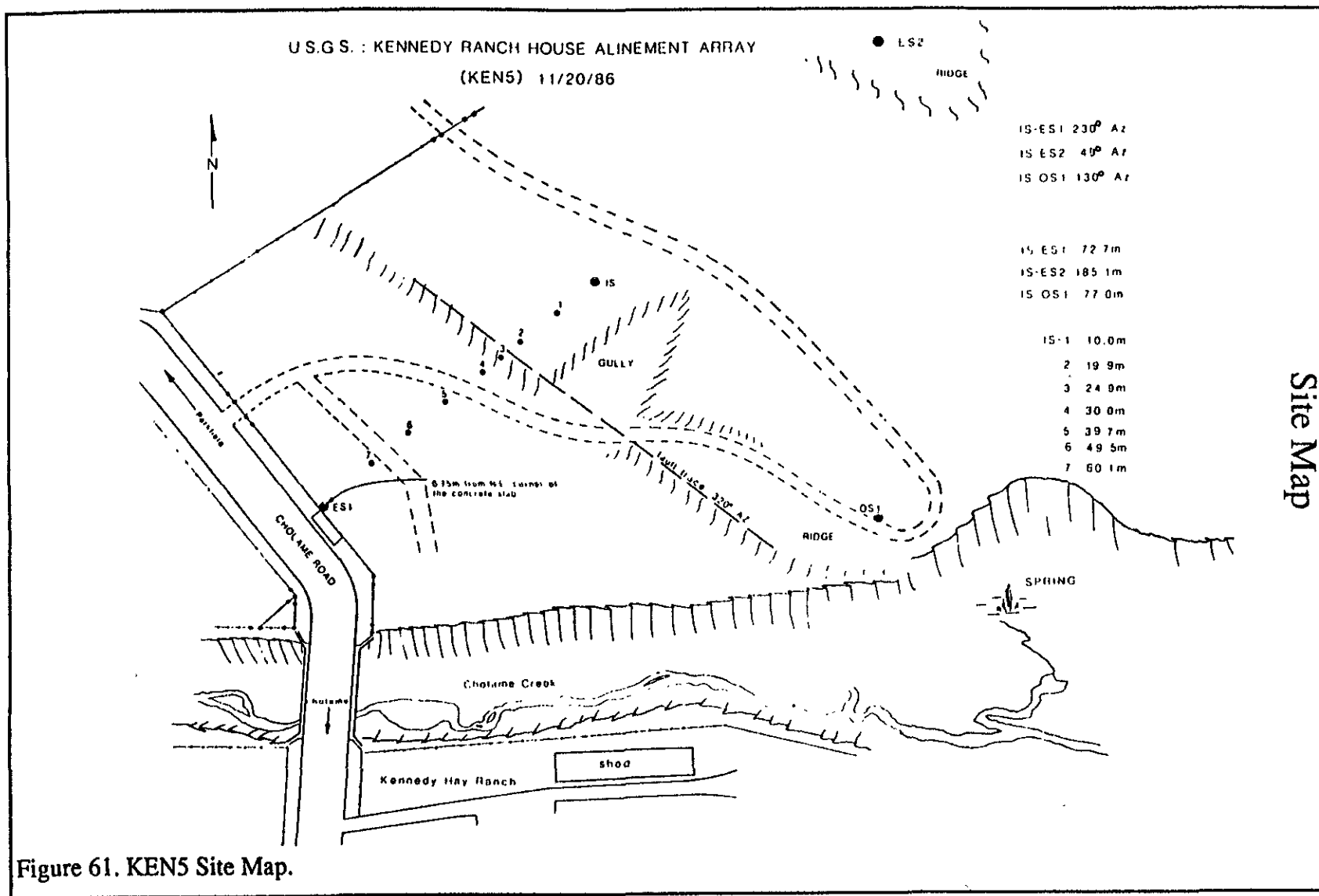


Figure 61. KEN5 Site Map.

Data Plots

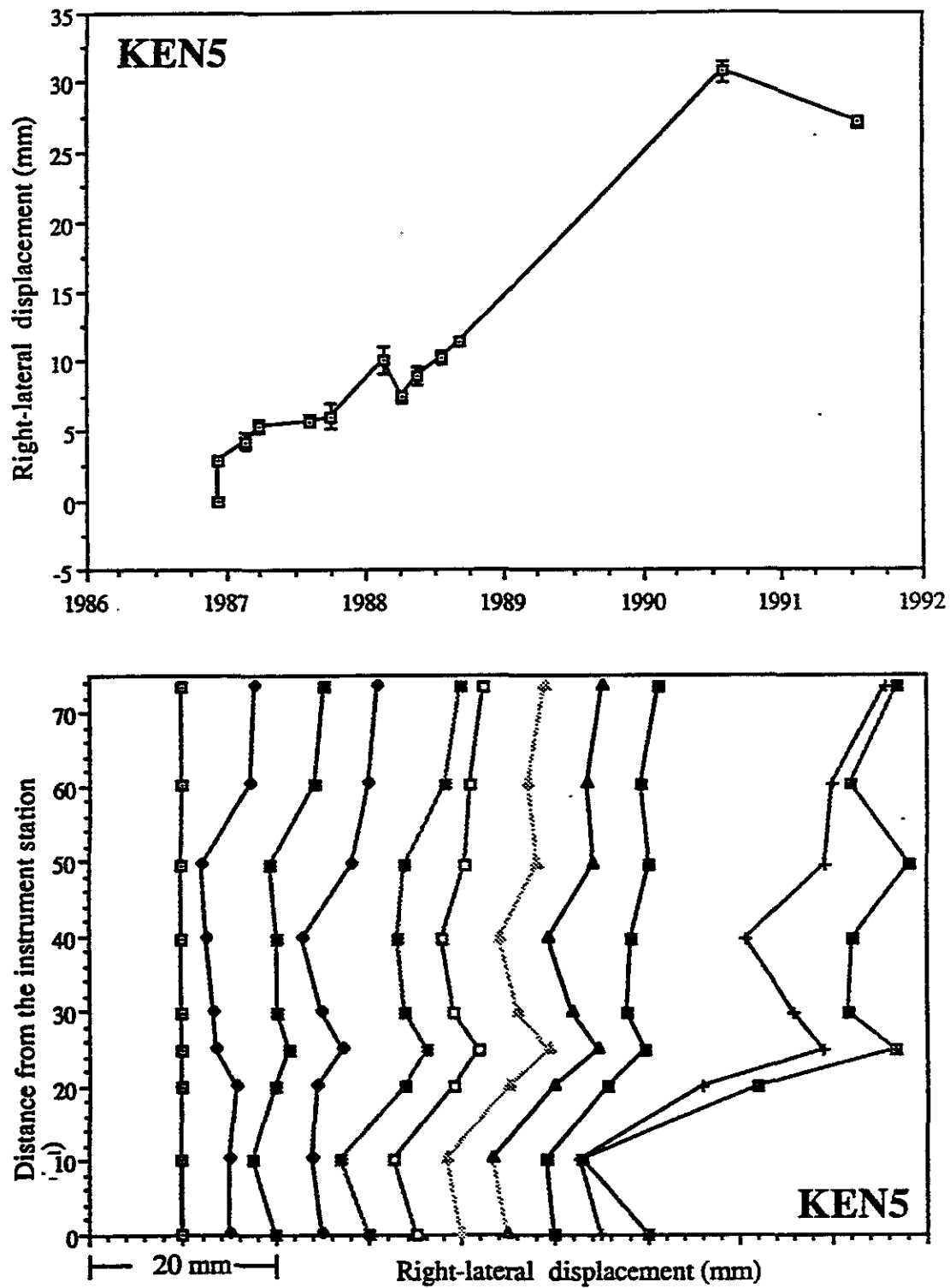


Figure 62. KEN5 Data Plots.

Site Description

Station Code HAR4 Name Harlan Ranch County Monterey
 Quad Cholame Hills Latitude 35° 50.4' Longitude 120° 22.9'
 ES/OS1 121° 55' 08.1"

To Reach: From Paso Robles, take California State Highway 46 east approximately 25 miles and go north on the Parkfield-Cholame Valley Road. Go 10.3 miles to the Harlan Ranch Road to the left. The IS is just inside the gate on the NW corner of the intersection. The array crosses the Parkfield-Cholame Valley Road, with the ES on the east side of the road.

General Description: The IS is equidistant from the telephone pedestal, the telephone pole to the east in the fence line, and the water tank. The ES is on the east side of the road on a small knoll. The OS is the farthest leg of the third set of steel power poles west of the fault. Deflection stations 3, 4, and 5 are P&K nails driven into the pavement of the Parkfield-Cholame Valley Road.

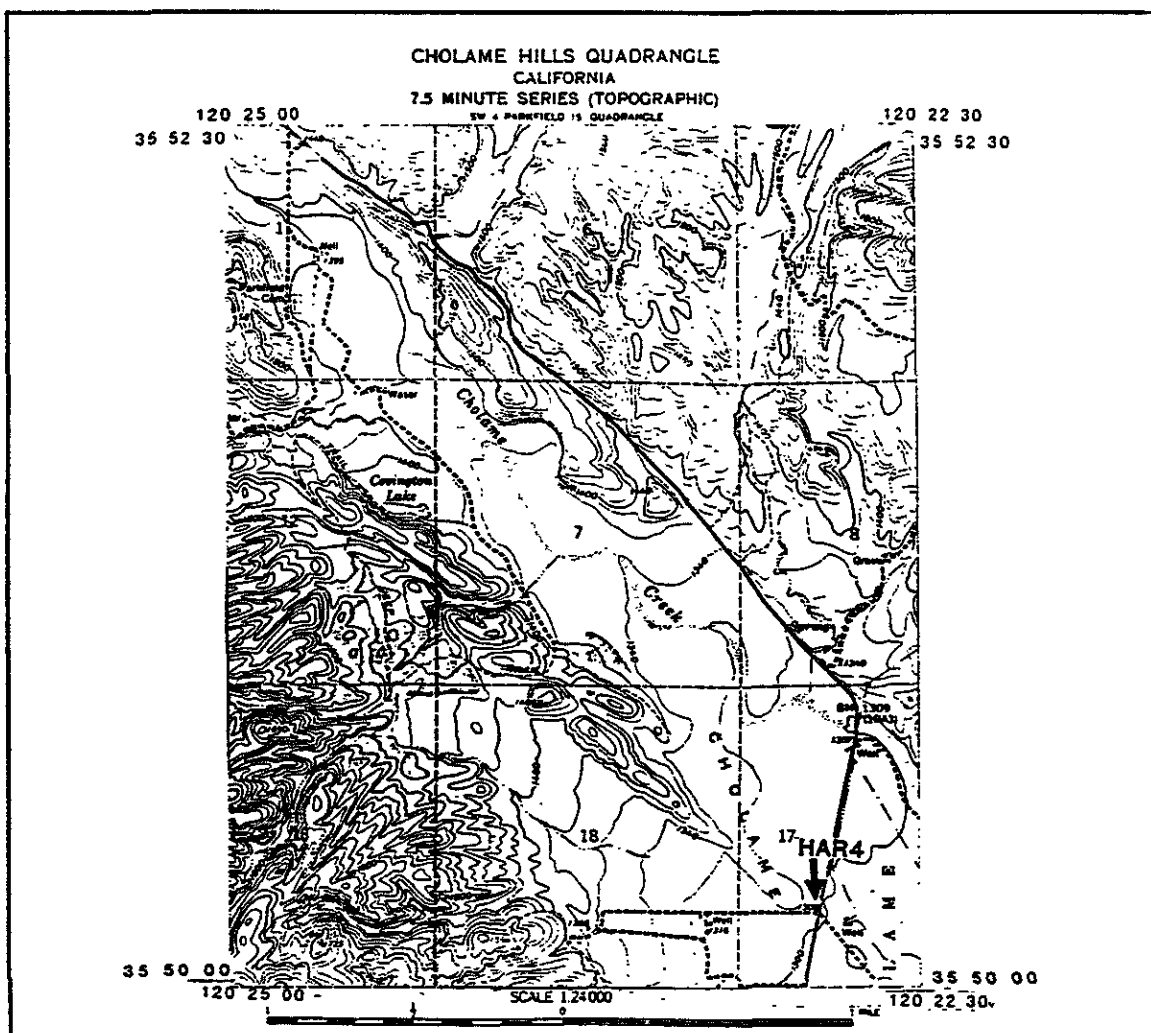


Figure 63. HAR4 Site Description.

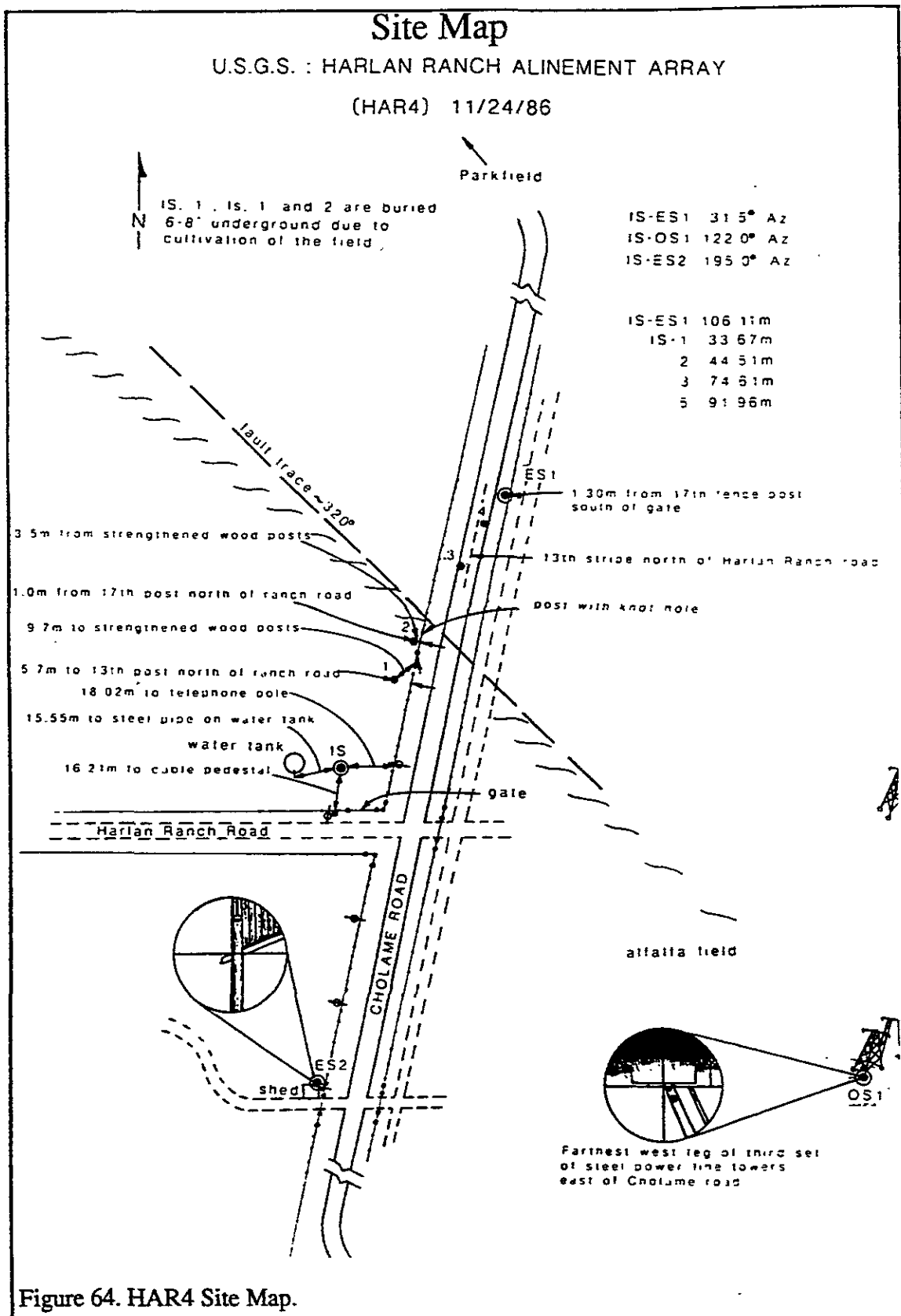


Figure 64. HAR4 Site Map.

Data Plots

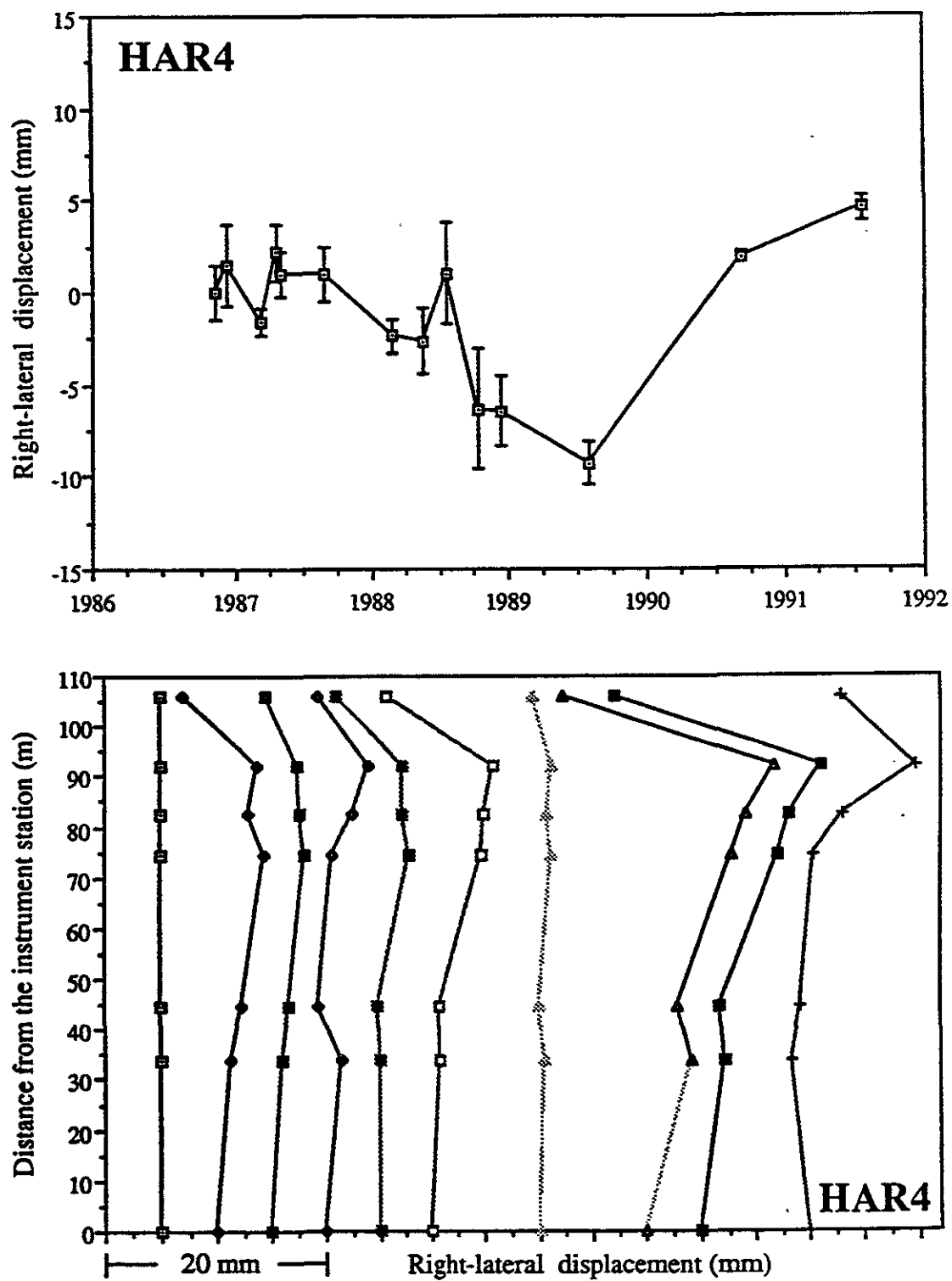


Figure 65. HAR4 Data Plots.

Site Description

97

Station Code CRR4 Name Carr Ranch County Monterey
 Quad Cholame Valley Latitude 35° 50.1' Longitude 120° 21.9'
 ES1/OS1 77° 22' 21.4"

To Reach: From Paso Robles, take California State Highway 46 east approximately 25 miles and go north on the Parkfield-Cholame Road. Travel 10.35 miles, turn into the Jack Ranch Hay Headquarters and go past the ranch house and barns. Drive east on the dirt road along the fence line for 1.1 miles, turn left on trail leading toward the two grain silos. Before reaching the silos, take the first turn to the right. The array crosses the trail just north of the creepmeter vault and solar panel.

General Description: The monuments are all subsurface. Deflection station 2 is approximately 0.75 meters northwest from the creepmeter vault. The ES is near the fence line at an azimuth of 56.5 degrees from station 2. The IS is 25 meters in the opposite direction from station 2. The monuments are buried about 0.5 meters deep to avoid being disturbed by the heavy machinery. A metal detector is necessary to find them. OS is 402 meters southeast of the IS, and 1.3 meters to the east of the 16th fence post south of the high voltage tower.

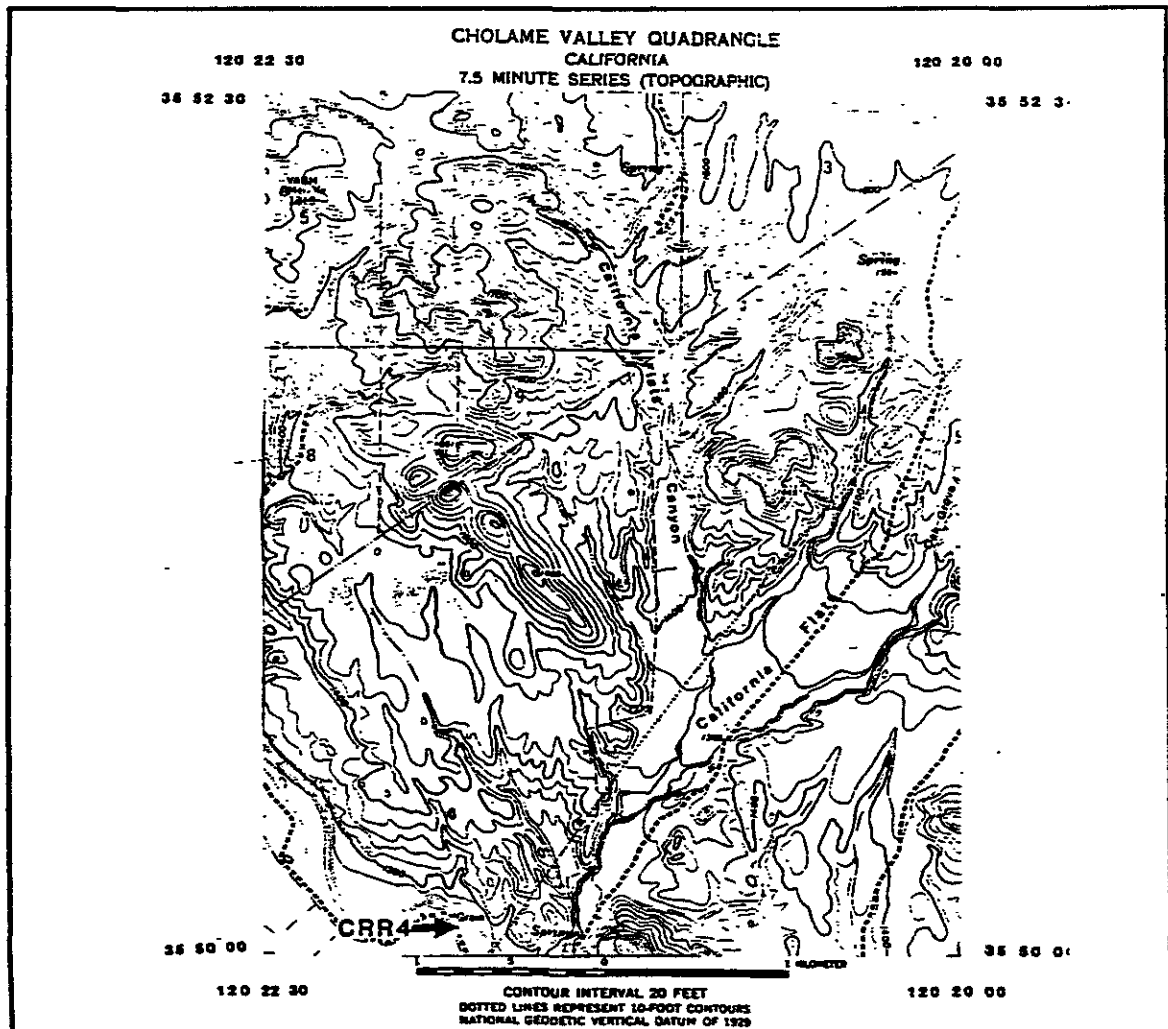


Figure 66. CRR4 Site Description.

USGS : CARR RANCH ALINEMENT ARRAY (CRR4) 1/5/84
(STOP AT RANCH HOUSE PRIOR TO ENTRY)

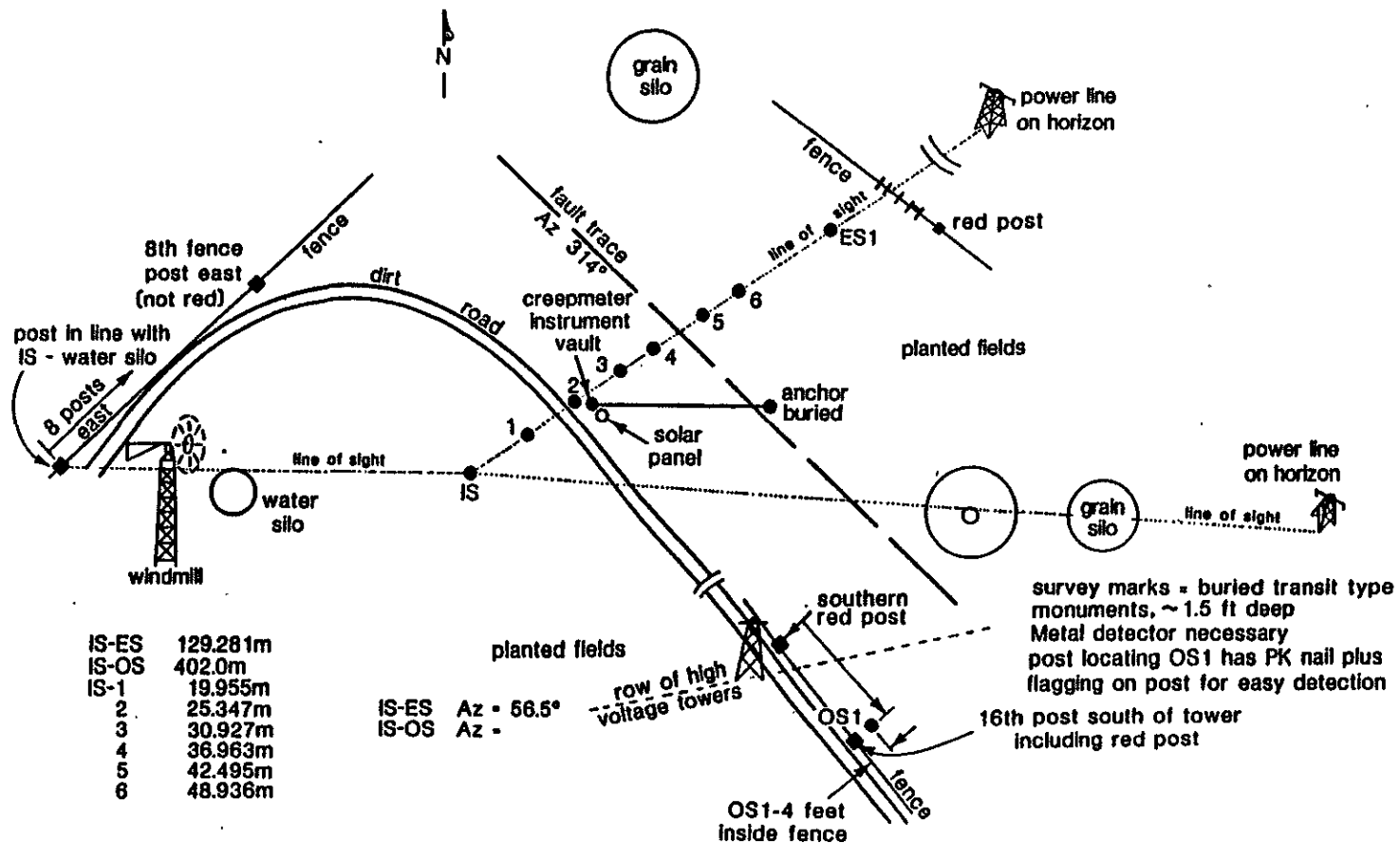


Figure 67. CRR4 Site Map.

Site Map

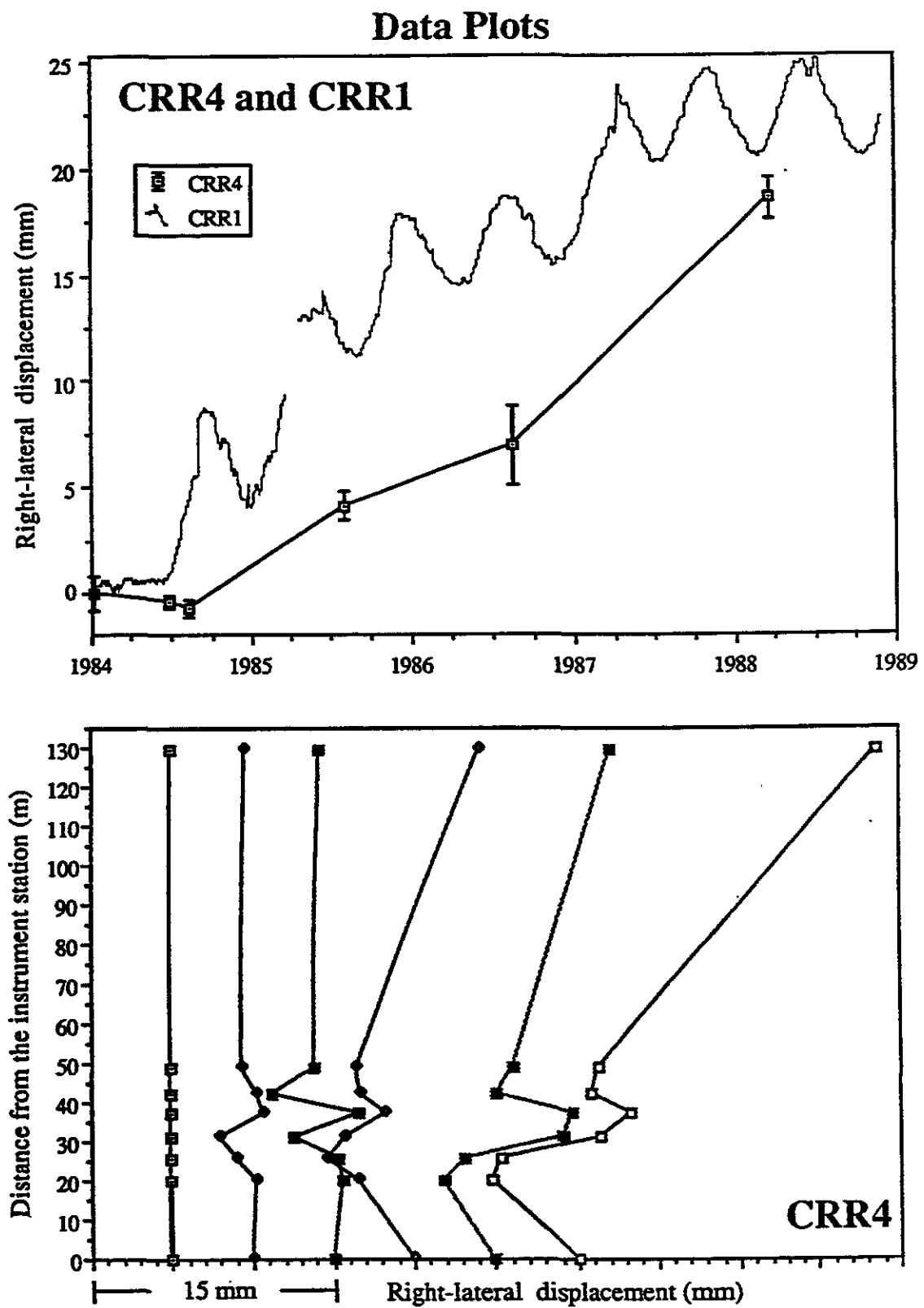


Figure 68. CRR4 Data Plots.

Site Description

Station Code GHG4 Name Gold Hill Gilman County Monterey
 Quad Cholame Hills Latitude 35° 49.1' Longitude 120° 21.0'
 ES1/OS1 118° 21' 28.3"

To Reach: From Paso Robles, take California State Highway 46 east approximately 25 miles and go north on the Parkfield-Cholame Road. Go 6.35 miles to Jack Ranch. Pass the ranch house and cross over to the northeast gate at the horse barn. Go through the gate, cross the stream, pass through the middle gate into the northeast pasture and follow the road along the western base of Gold Hill for 0.3 miles. Look for a white fiberglass creepmeter vault lid approximately 100 meters to the left of the road. The array is just north of the creepmeter.

General Description: OS1 and OS2 are U.S.G.S. subsurface monuments, the others are small metal monuments. The IS is 10.5 meters from the fence line. The ES lies along a cow trail, across the fault from the IS to the northeast. OS1 is southeast of the IS and 19 fence posts south of an exposed underground cable. OS2 is northwest of the IS and 1.1 meters from a post with a nail in its top.

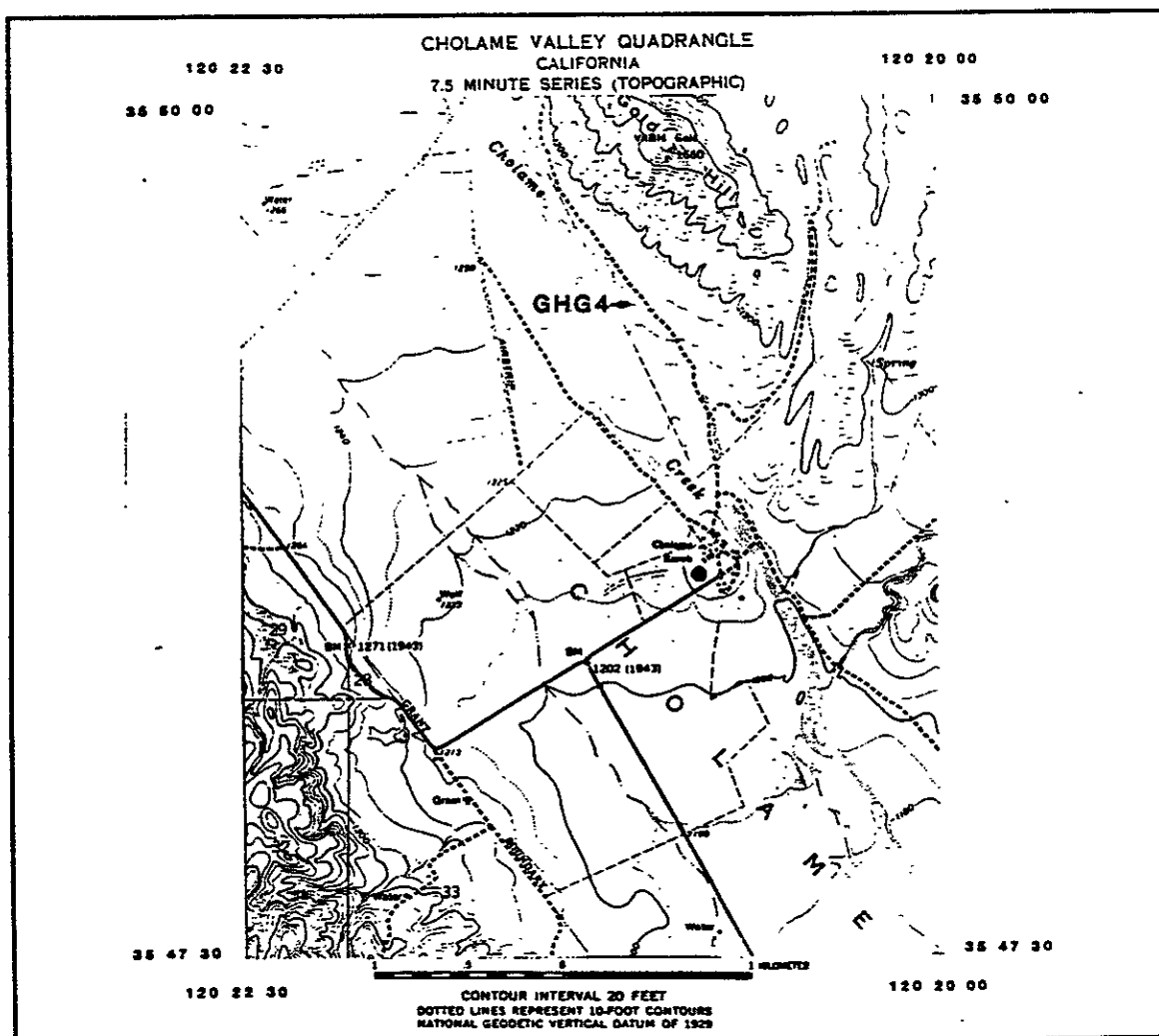


Figure 69. GHG4 Site Description.

Data Plots

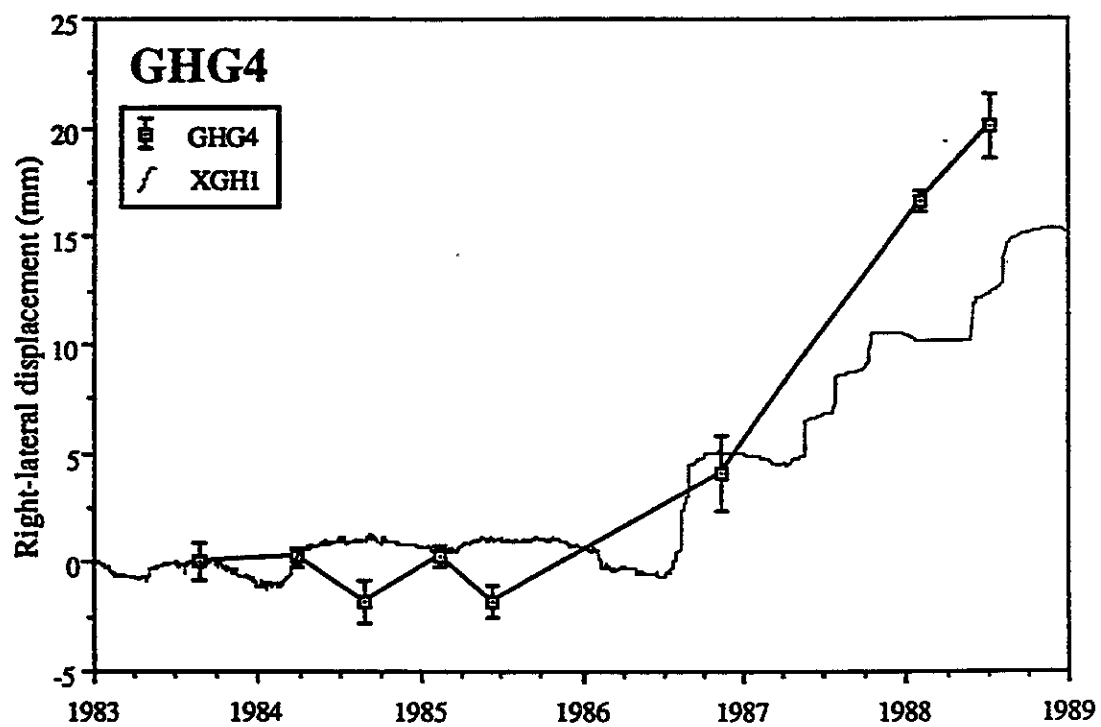
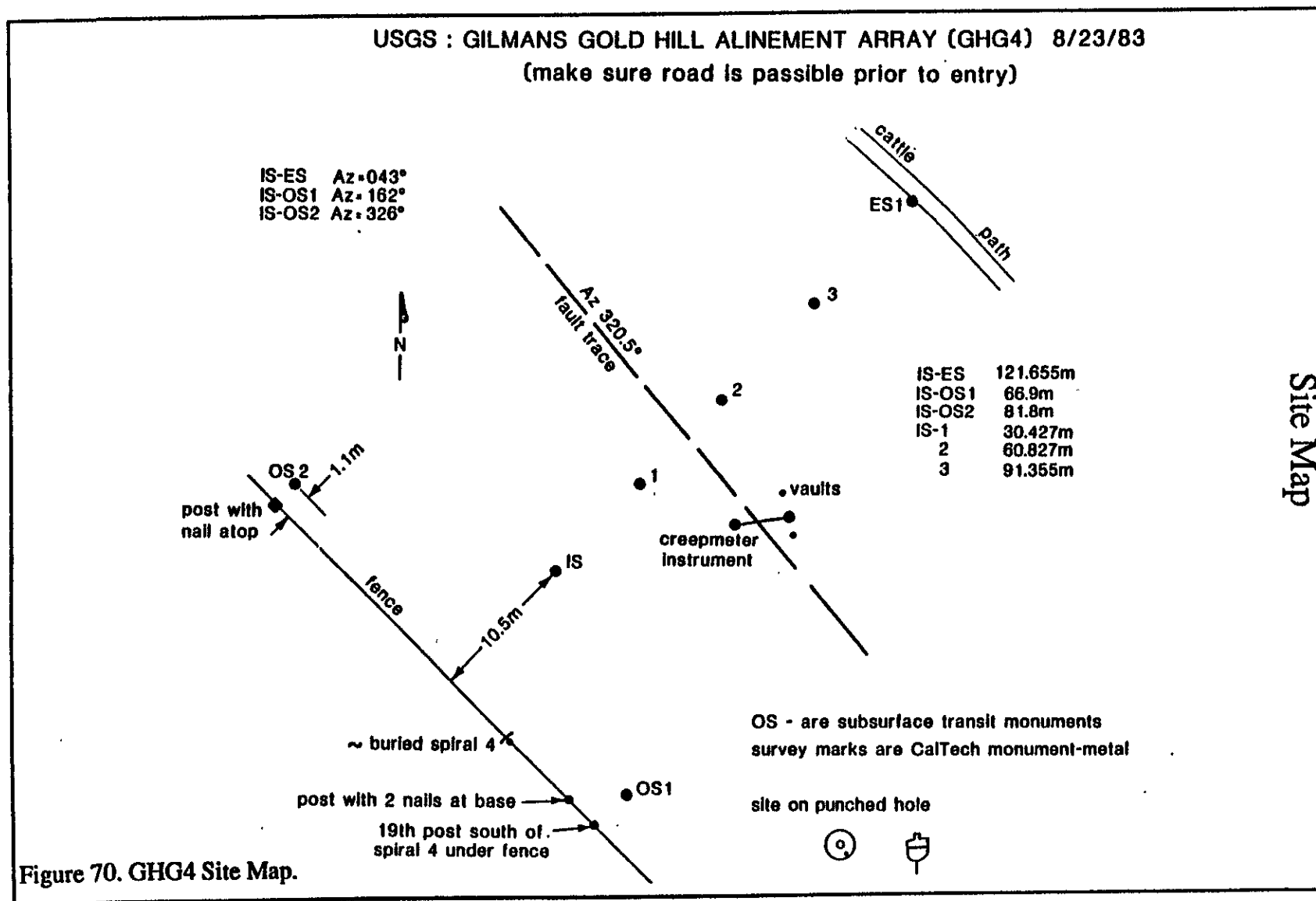


Figure 71. GHG4 Data Plot.



Site Description

Station Code PHG4 Name Gold Hill County Monterey
 Quad Cholame Hills Latitude 35° 49.1' Longitude 120° 21.0'
 ES1/OS1 74° 37' 54.0"

To Reach: From Paso Robles, take California State Highway 46 east approximately 25 miles and go north on the Parkfield-Cholame Road. Go 6.35 miles to Jack Ranch. Pass the ranch house and cross over to the northeast gate at the horse barn. Go through the gate, cross the stream, pass through the middle gate into the northeast pasture and follow the road along the western base of Gold Hill for 0.3 miles. Look for a white fiberglass creepmeter vault lid approximately 100 meters to the left of the road. The array is just south of the creepmeter.

General Description: The monuments are the subsurface type, covered by rocks. The IS is the same monument as OS1 from GHG4, and the OS is the same as OS2 in GHG4. There are nine deflection stations and an unused monument behind the ES. NOTE: Set the ES tripod high so that it may be seen over the ridge from the IS.

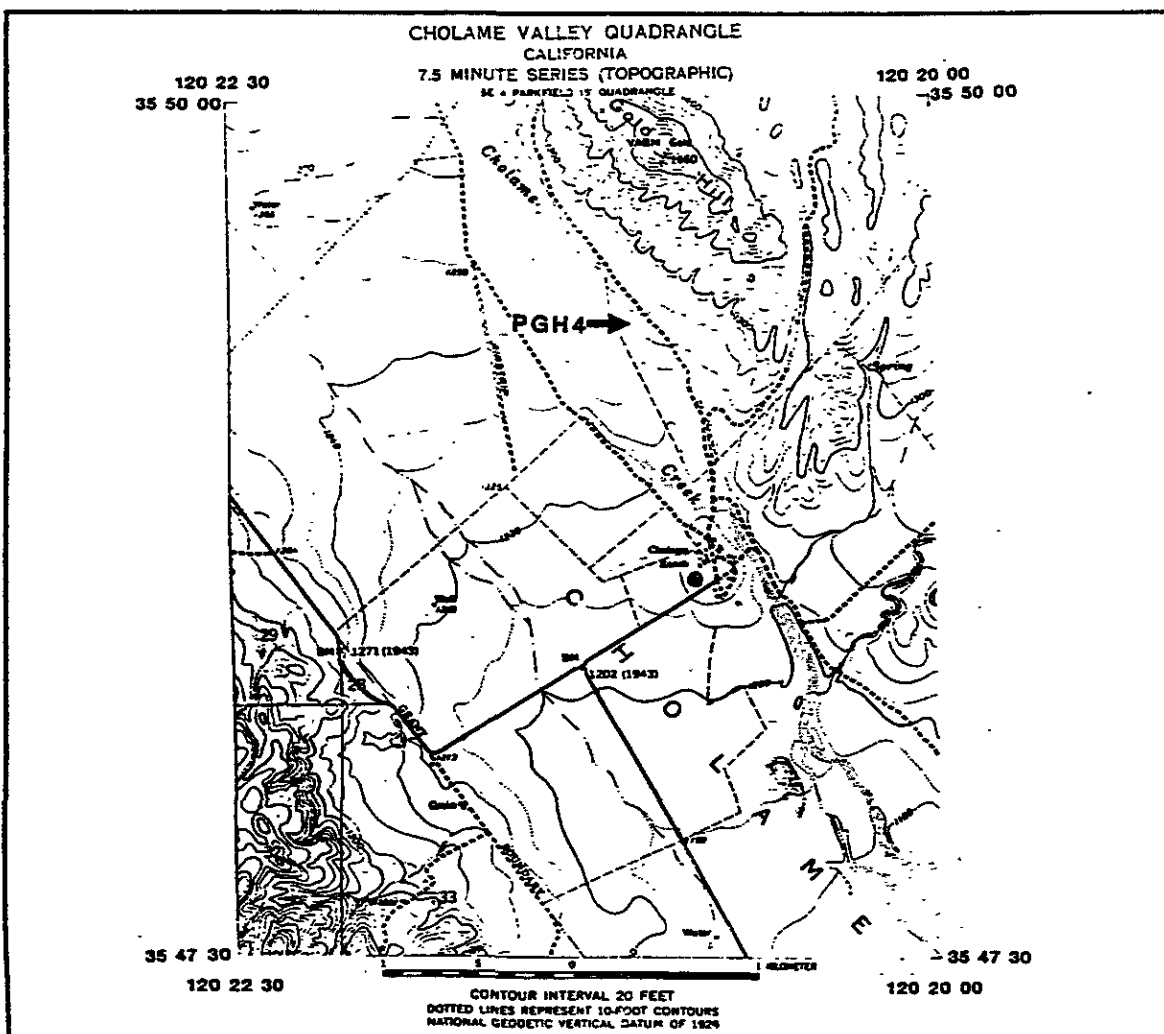


Figure 72. PGH4 Site Description.

Site Map

USGS : GOLDHILL ALINEMENT ARRAY (PGH4) 11/8/83

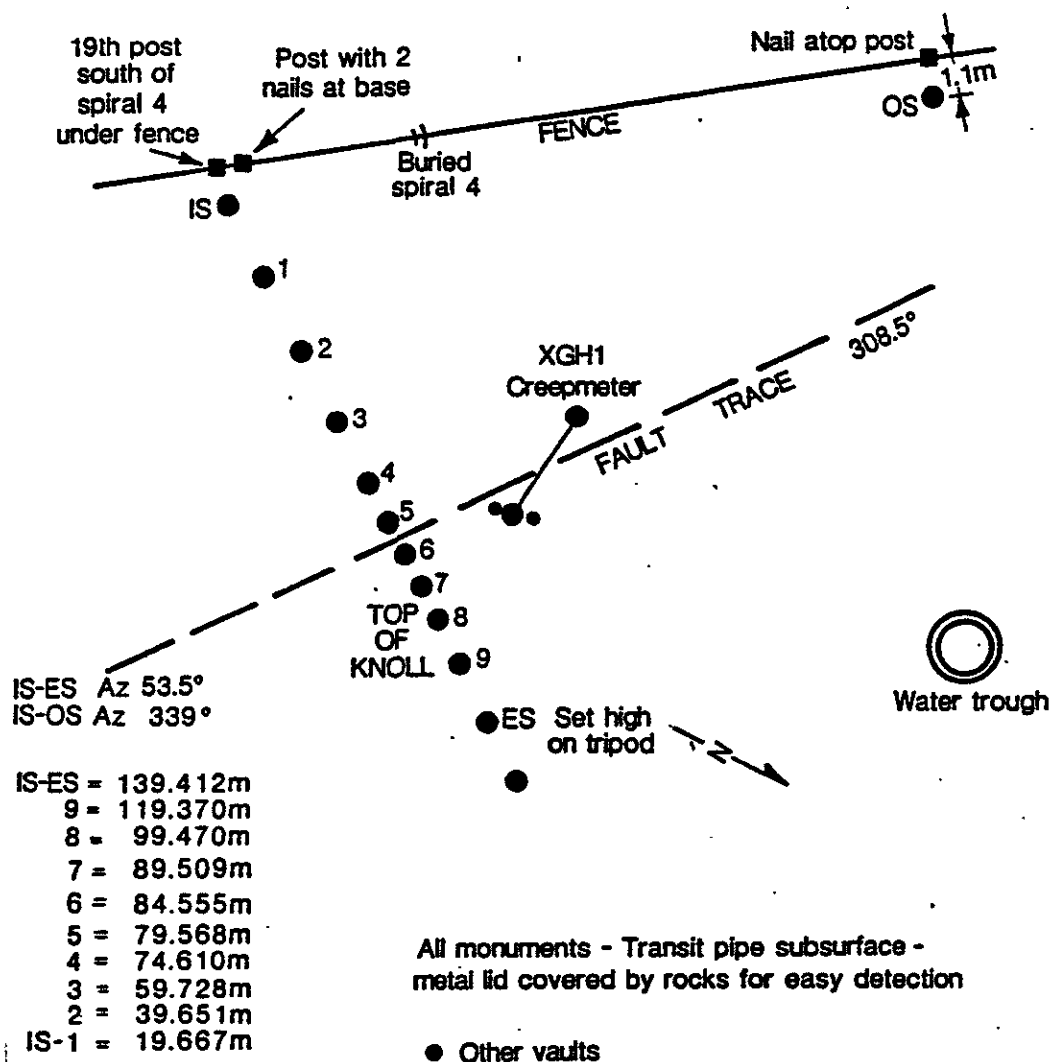


Figure 73. PGH4 Site Map.

Data Plots

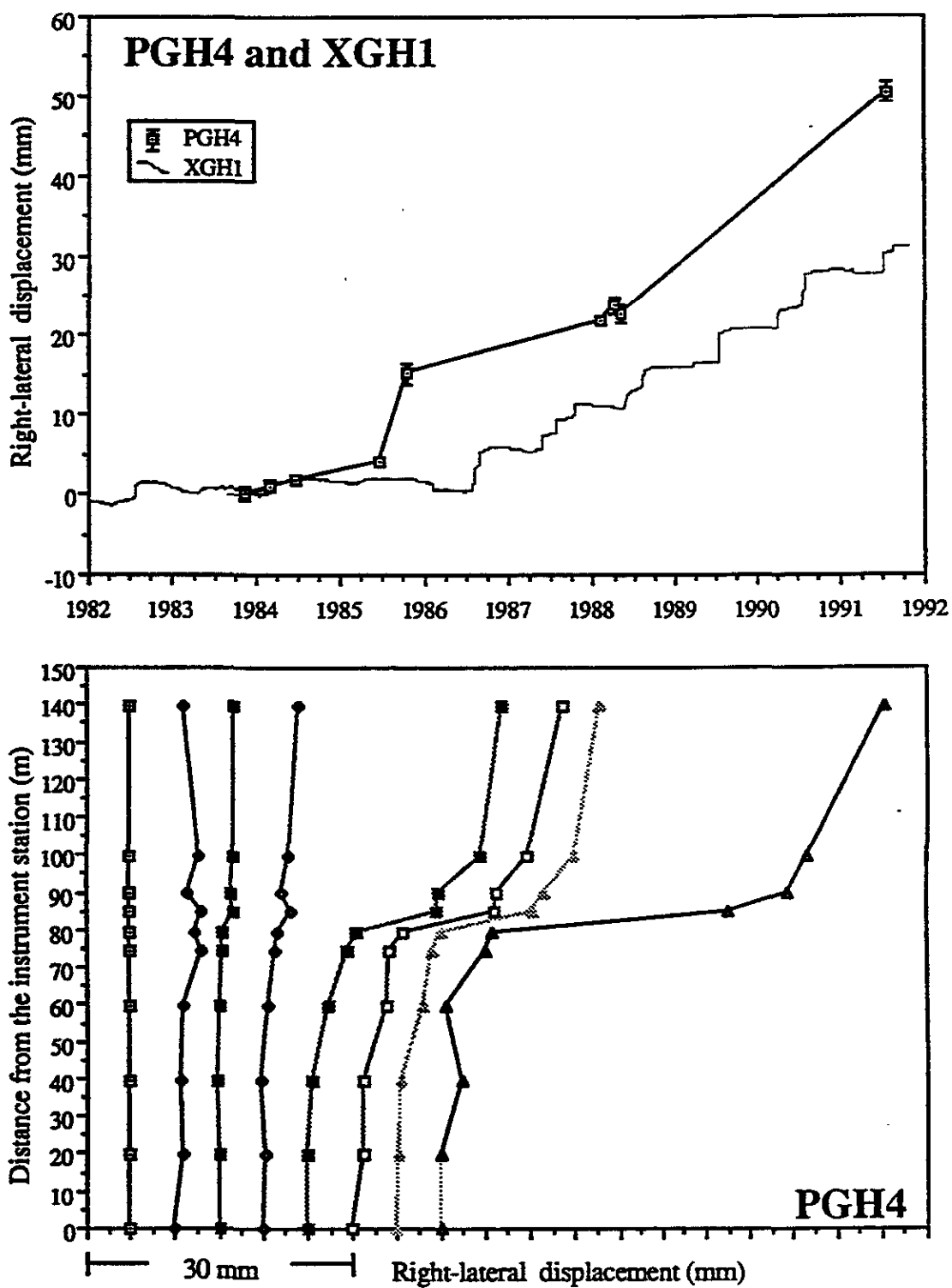


Figure 74. PGH4 Data Plots.

Site Description

Station Code XWT4 Name Water Tank County San Luis Obispo
 Quad Cholame Valley Latitude 35° 45.4' Longitude 120° 18.5'
 ES1/OS1 120° 53' 42.0"

To Reach: From Paso Robles, take California State Highway 46 east approximately 25 miles and go north on the Parkfield-Cholame Road. Travel 1.3 miles and turn west just north of the fence. Cross the fence line at the water tank. The array starts 8 fence posts west of the gate and runs along the fence line to the west.

General Description: All the monuments are brass caps embedded in cement except the OS which is a subsurface monument. The IS is between the 8th and 9th fence posts west of the gate and is covered by rocks. The OS is 5 meters toward the IS from the outside lip of the water tank north of the fence. The deflection stations and the ES are aligned parallel to the fence line toward the northwest.

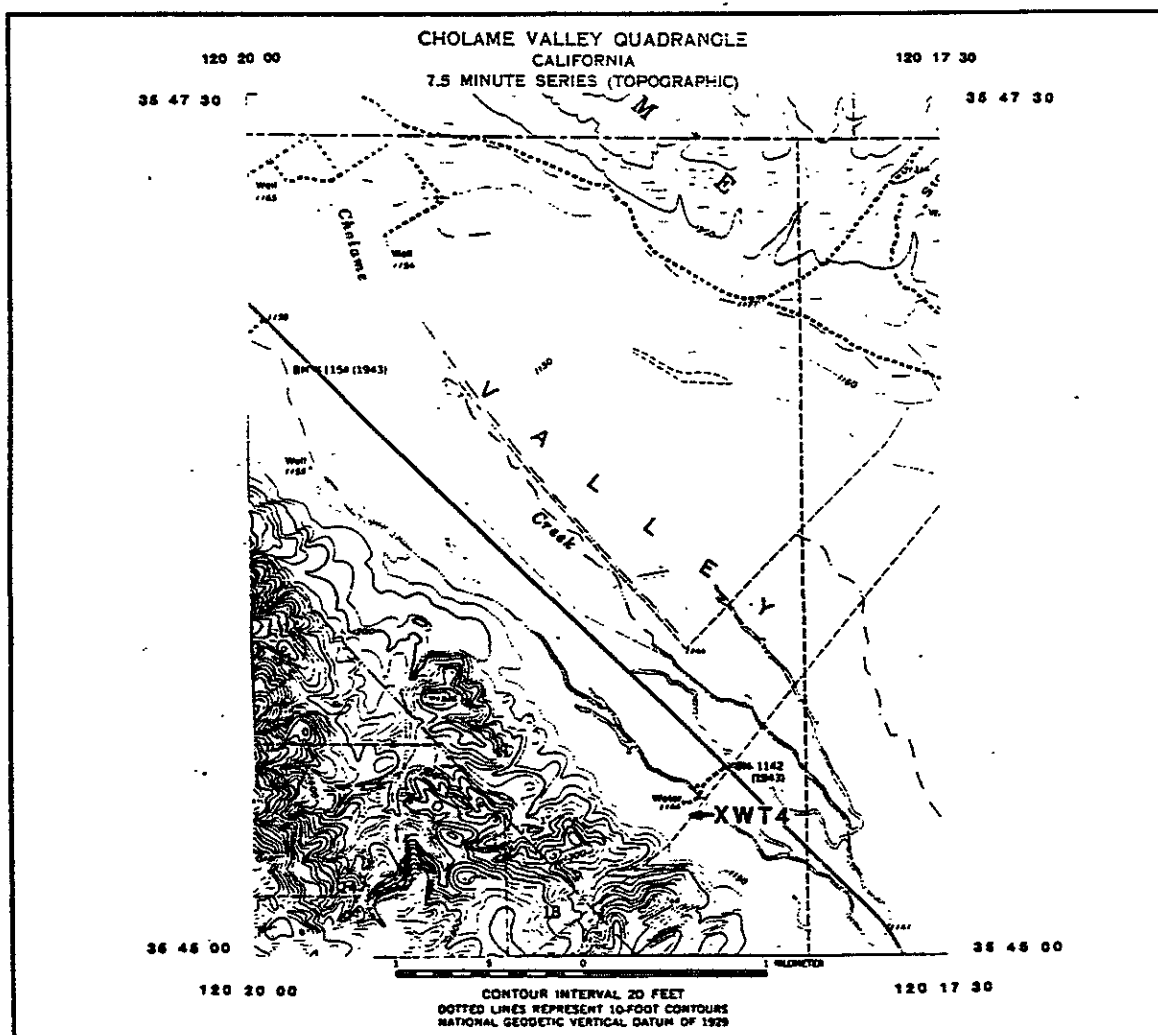


Figure 75. XWT4 Site Description.

Site Map

USGS : WATER TANK ALINEMENT ARRAY (XWT4) 5/19/83

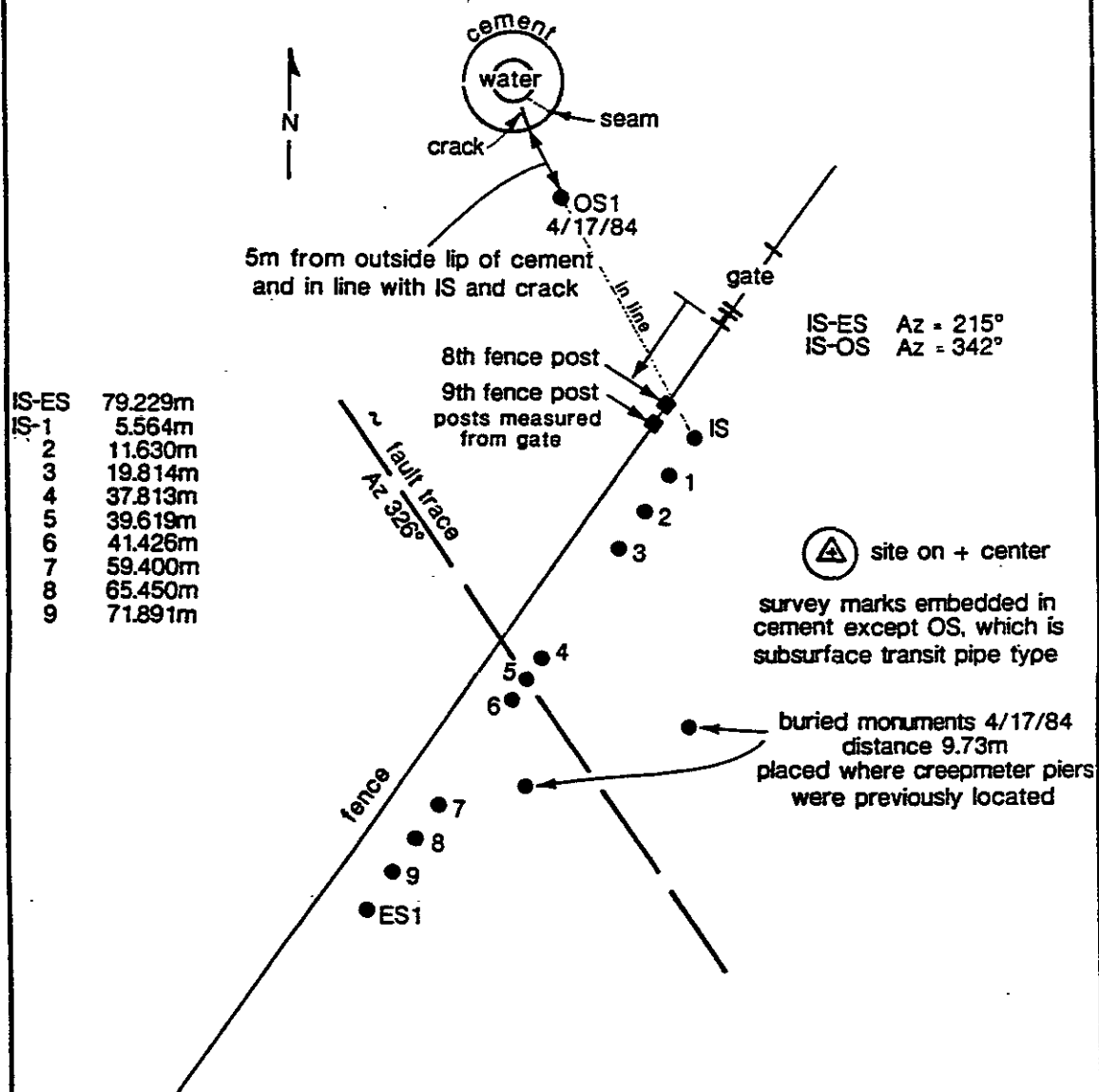


Figure 76. XWT4 Site Map.

Data Plots

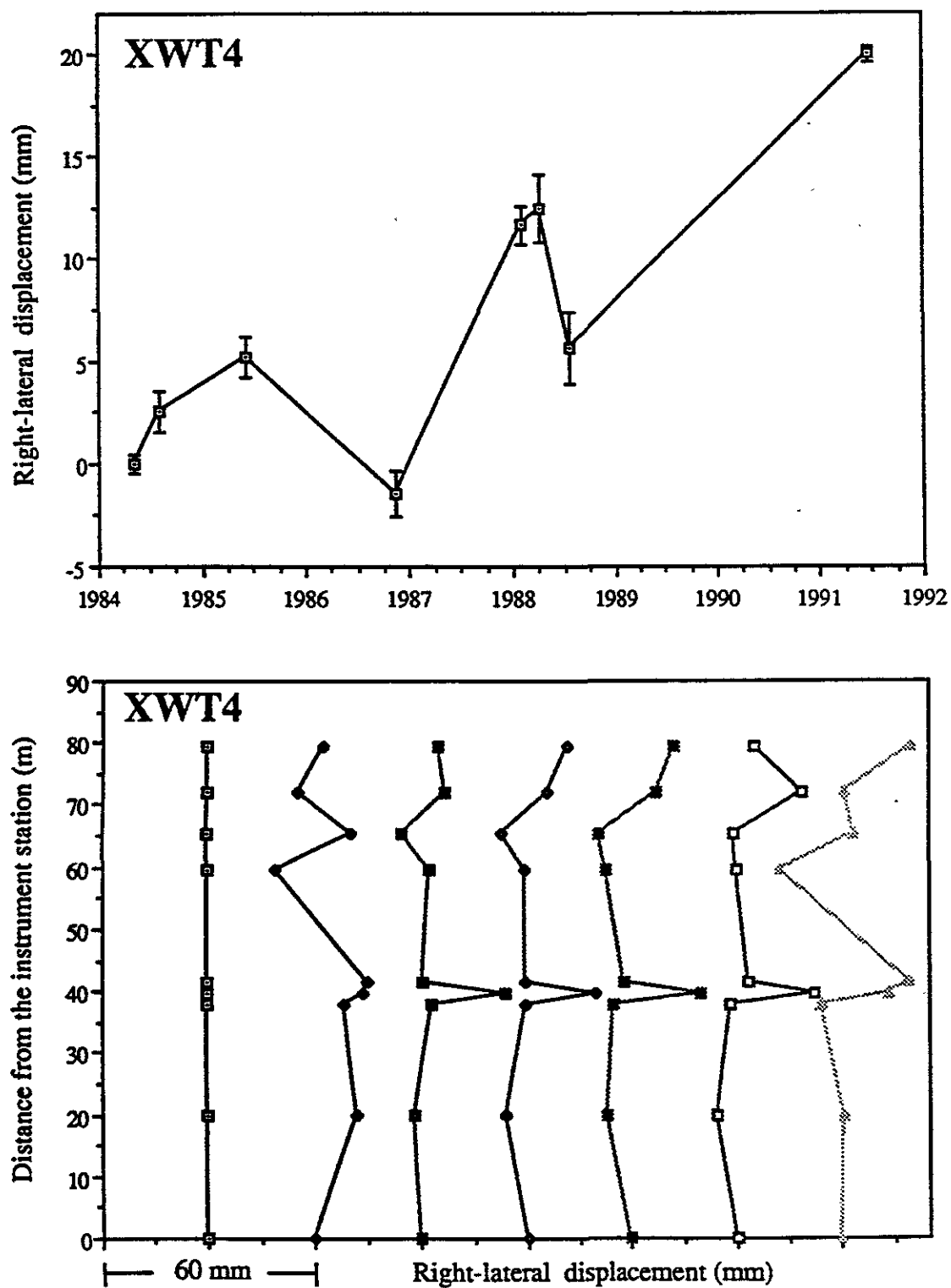


Figure 77. XWT4 Data Plots.

Site Description

Station Code H464 Name Highway 46 County San Luis Obispo
 Quad Cholame Hills Latitude 35° 44.1' Longitude 120° 17.2'
 ESI/OS1 121° 14' 13.6"

To Reach: From Paso Robles, take California State Highway 46 east approximately 25 miles and go north on the Parkfield-Cholame Road. Go about 25 meters and turn onto the field to the west.

General Description: All of the monuments are small metal plugs with hexagonal openings on top except OS1, which is a subsurface monument and OS2 which is a spike driven into a telephone pole. The IS is approximately 100 meters from the road. OS1 is 21 meters from the road and 155 meters further north. The ES is next to the fence beside Highway 46.

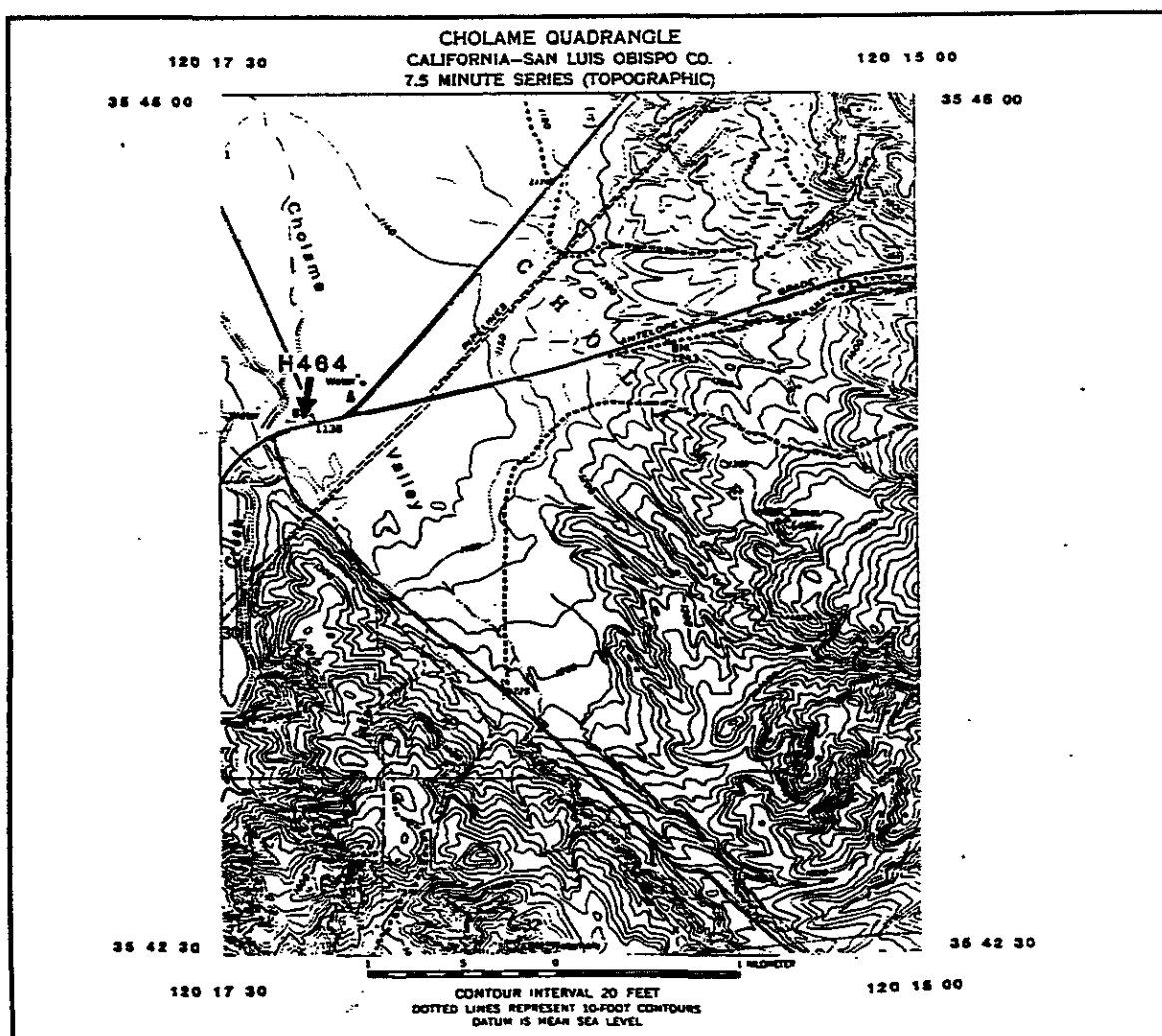
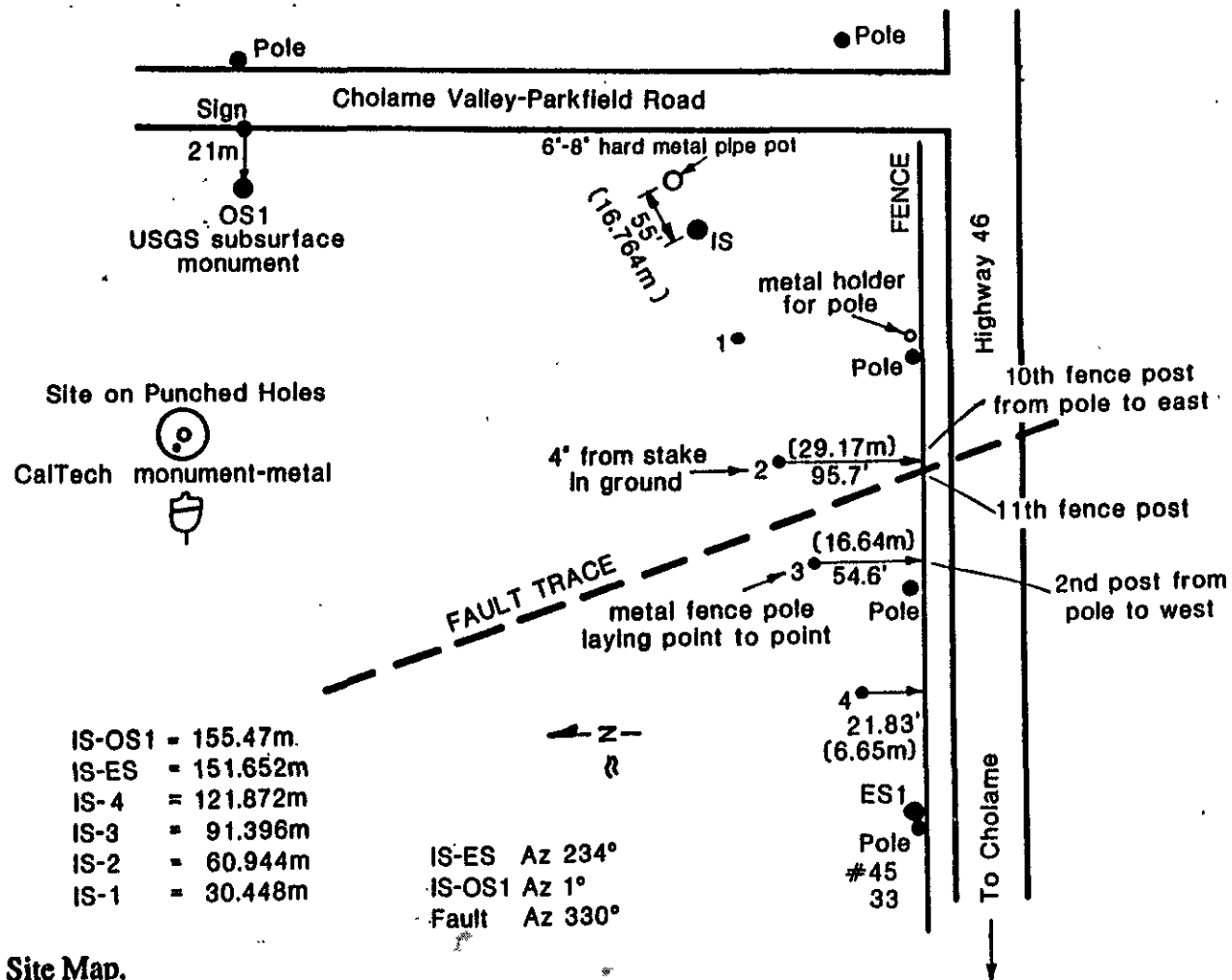


Figure 78. H464 Site Description.

USGS : HIGHWAY 46 - ALINEMENT ARRAY (H464)

8/24/83



Site Map

Figure 79. H464 Site Map.

Data Plots

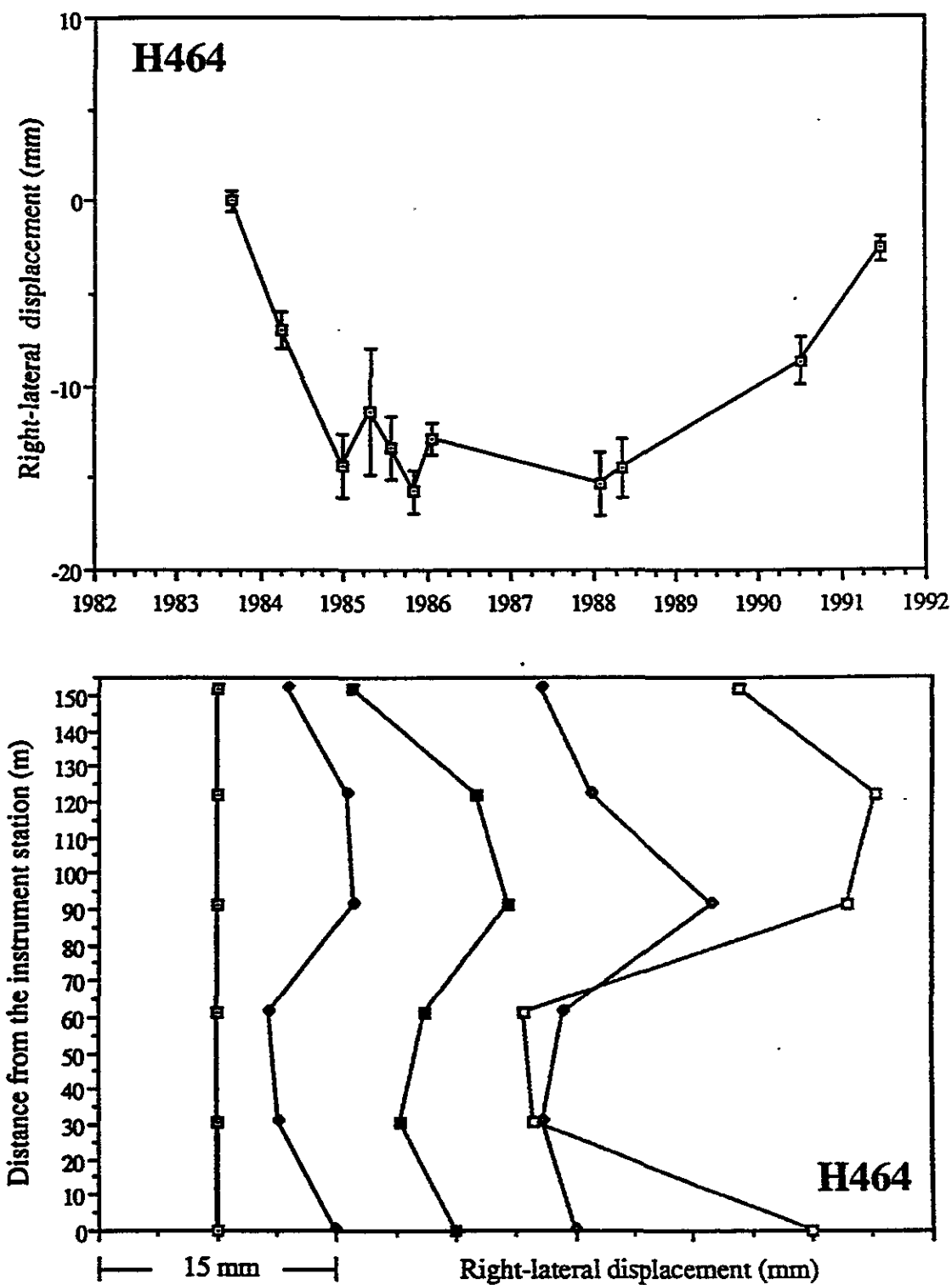


Figure 80. H464 Data Plots.

Site Description

Station Code X464 Name Highway 46 South County San Luis Obispo
 Quad Cholame Latitude 35°43.3' Longitude 120° 16.7'
 ES1/OS1 118° 12' 48.3" ES1/OS2 66° 57' 03.0"

To Reach: From Paso Robles, take California State Highway 46 east approximately 24 miles to Cholame.

Approximately 0.8 miles past Cholame turn right on Davies Road and travel 1.2 miles to a jeep trail on the right side of the road. The trail is 10 meters north of a culvert marked by a red San Luis Obispo road marker. Follow trail about 1/4 mile to the top of the small ridge just past the fault gully.

General Description: The IS is approximately 3 meters north of the jeep trail and follow the top of the ridge on the fault side. The ES (encircled by 3 stakes driven nearly flush with the ground) is 8.5 meters from the center line of Davies Road, approximately 140 meters north of the culvert described above. OS1 is 74 meters at an azimuth of 312° from the IS.

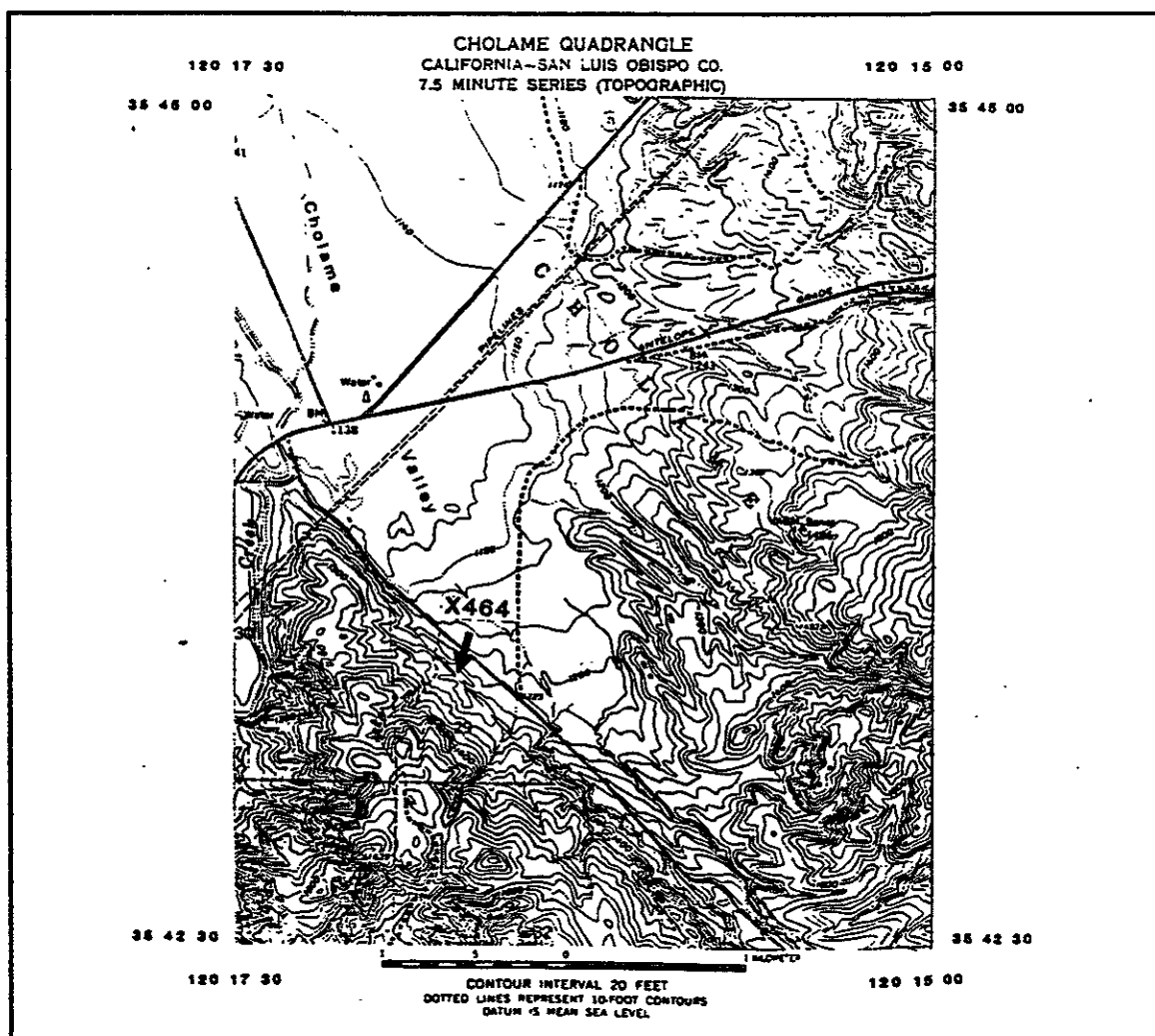
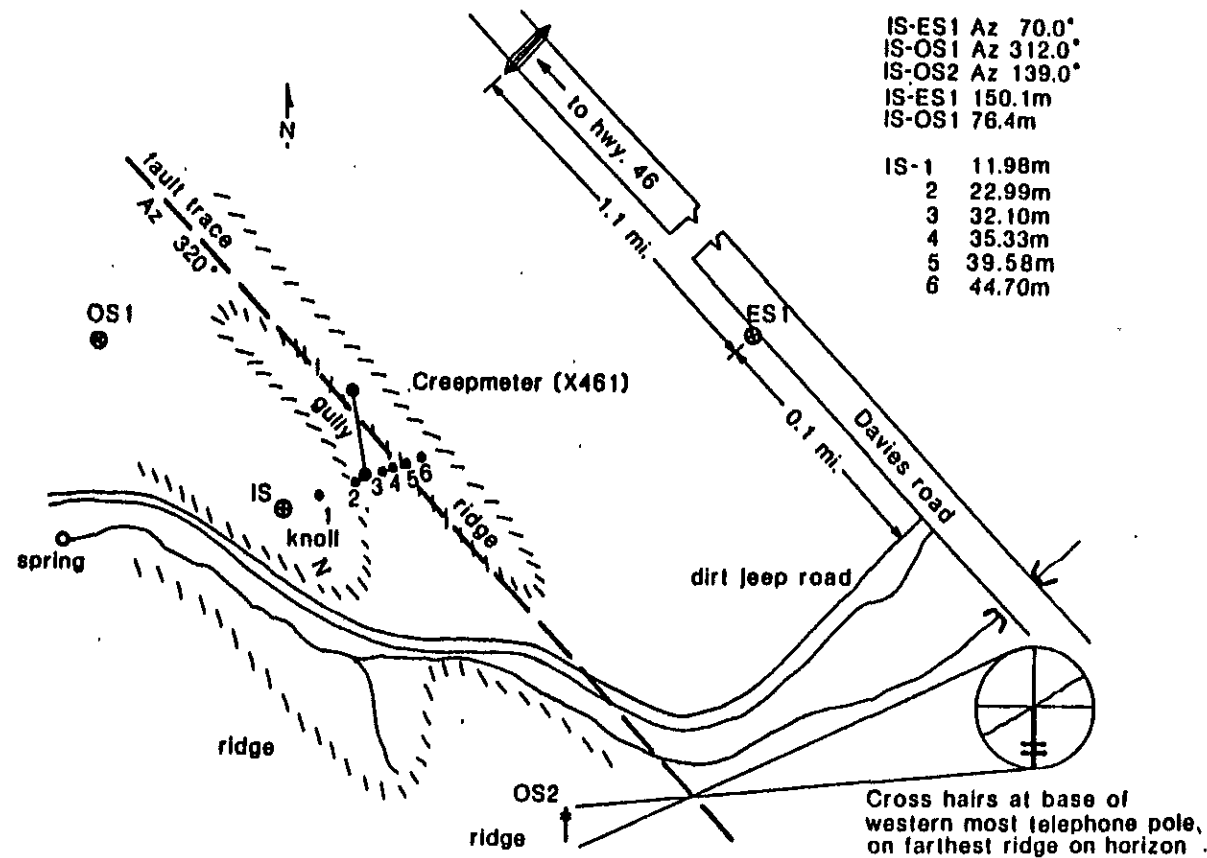


Figure 81. X464 Site Description.

USGS : HIGHWAY 46 SOUTH ALINEMENT ARRAY
(X464) 6/12/86



Site Map

Figure 82. X464 Site Map.

Data Plots

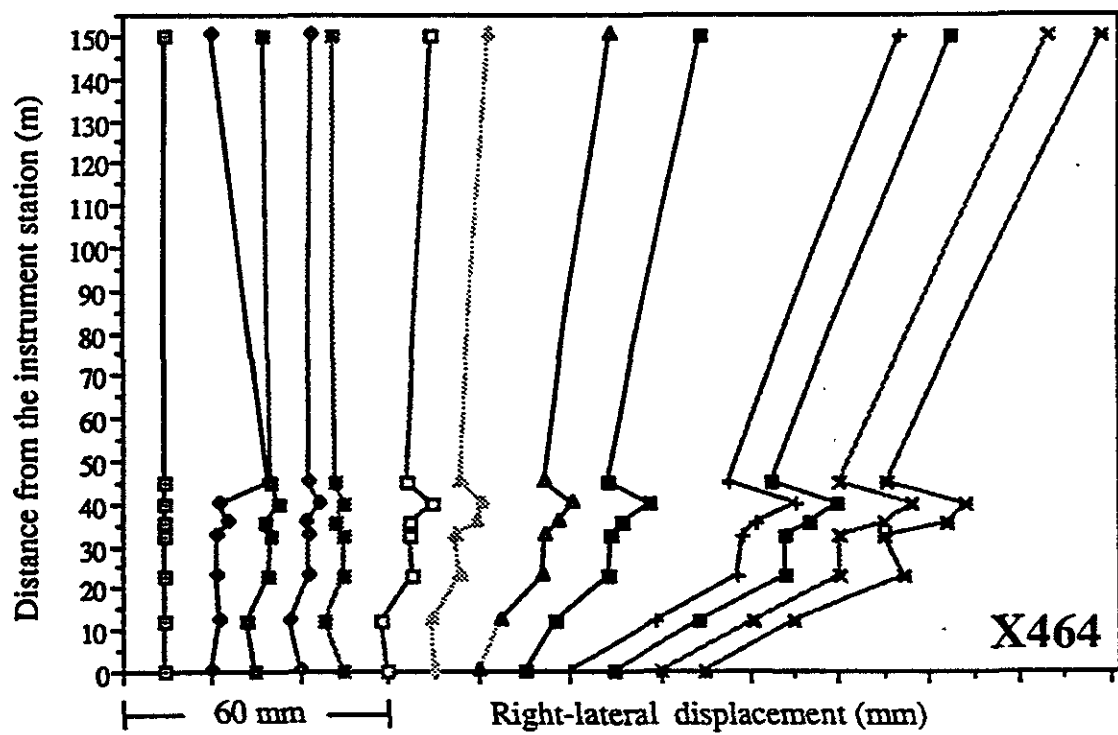
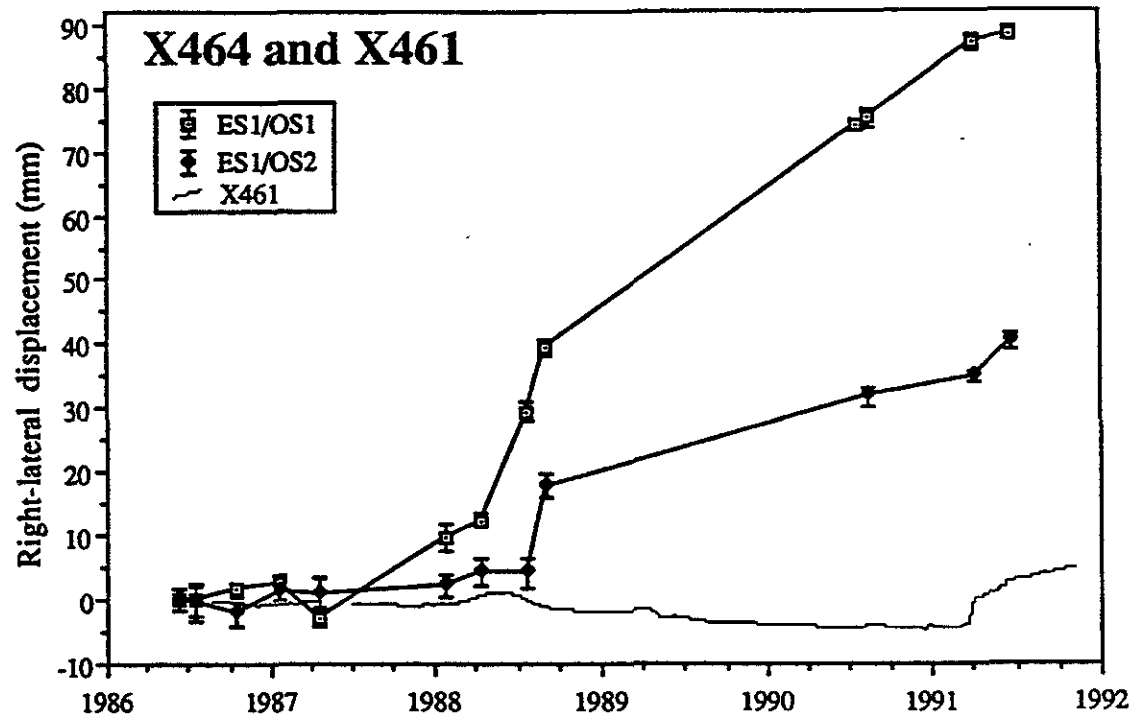


Figure 83. X464 Data Plots.

Site Description

Station Code PPP4 Name Palo Prieto Pass County San Luis Obispo
 Quad Cholame Latitude 35°43.3' Longitude 120° 16.7'
 ES1/OS1 79° 59' 54.4" ES1/OS2 89° 15' 51.6"

To Reach: From Paso Robles, take California State Highway 46 east approximately 24 miles to Cholame.

Approximately 0.8 miles past Cholame turn right on Davies Road and travel 1.2 miles to a jeep trail on the right side of the road. The trail is 10 meters north of a culvert marked by a red San Luis Obispo road marker. Follow trail about 1/4 mile to the top of the small ridge just past the fault gully.

General Description: The IS is approximately 3 meters north of the jeep trail and follow the top of the ridge on the fault side. The ES (encircled by 3 stakes driven nearly flush with the ground) is 8.5 meters from the center line of Davies Road, approximately 140 meters north of the culvert described above. OS1 is 74 meters at an azimuth of 312° from the IS.

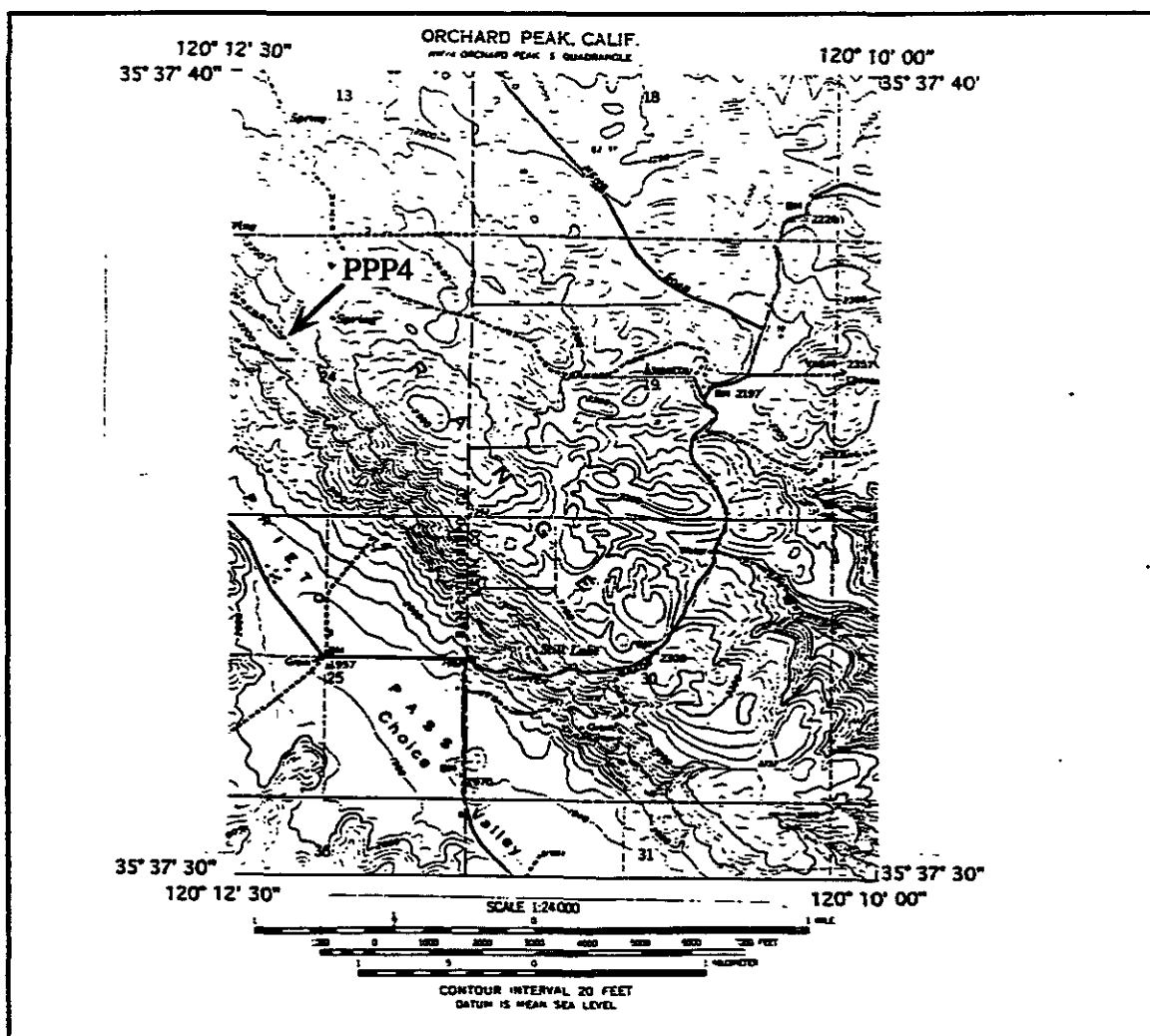
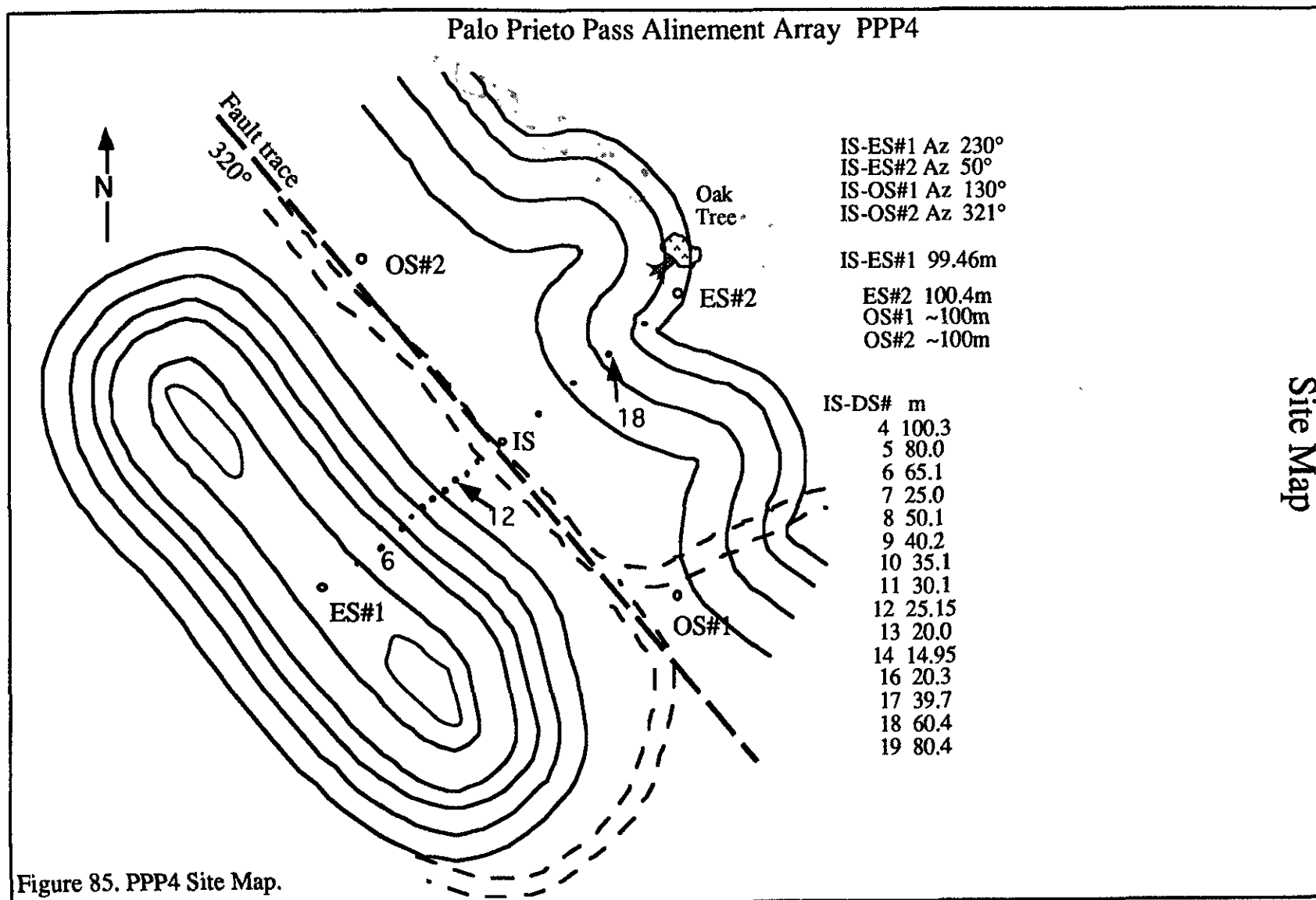


Figure 84. PPP4 Site Description.



Site Map

Data Plots

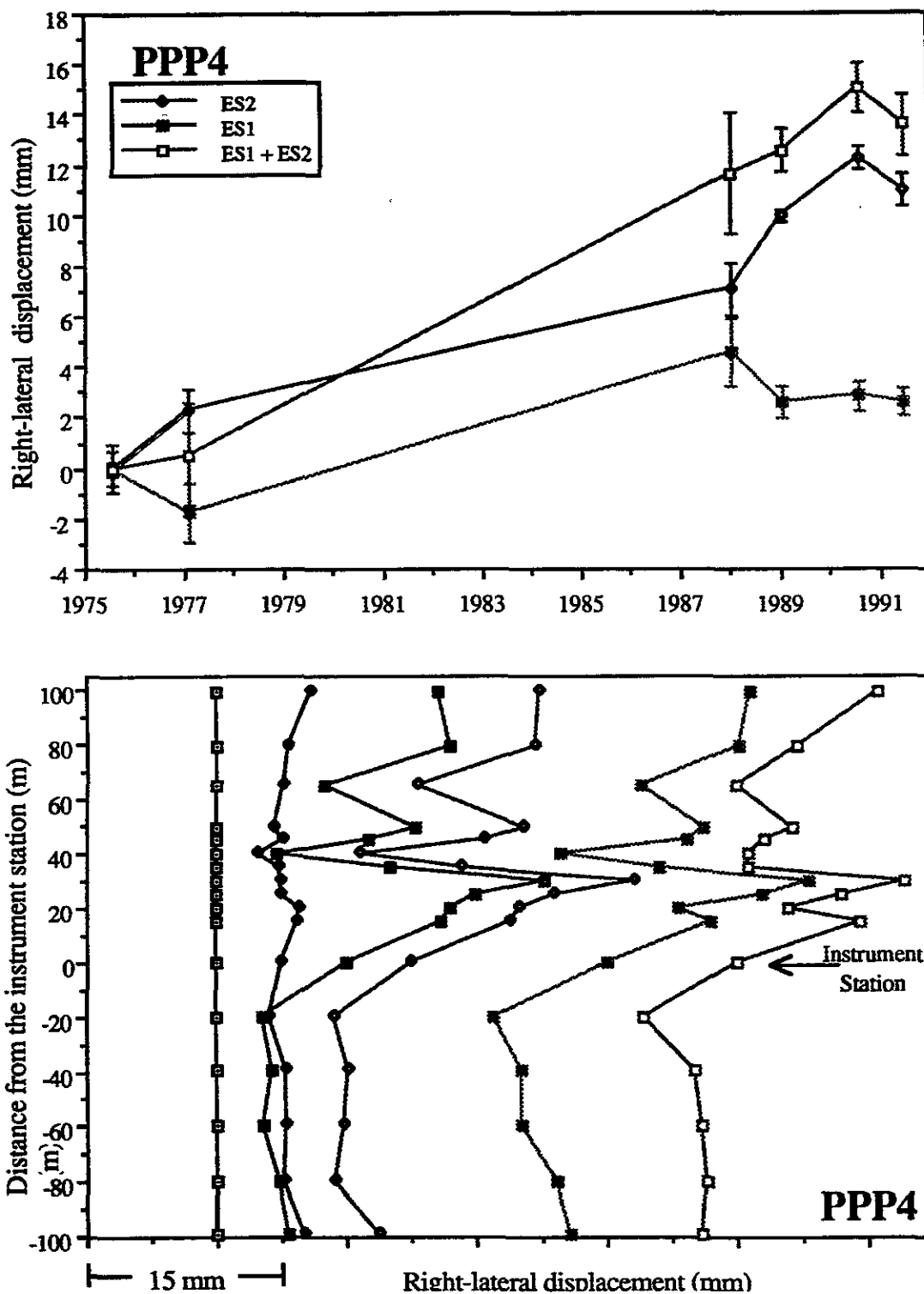


Figure 86. PPP4 Data Plots.